



Michigan Technological University
Create the Future Digital Commons @ Michigan Tech

Dissertations, Master's Theses and Master's
Reports - Open


Dissertations, Master's Theses and Master's
Reports

2013

HIGH VOLTAGE ELECTROPHORETIC DEPOSITION FOR ELECTROCHEMICAL ENERGY STORAGE AND OTHER APPLICATIONS

Sunand Santhanagopalan
Michigan Technological University

Follow this and additional works at: <https://digitalcommons.mtu.edu/etds>


 Part of the [Mechanical Engineering Commons](#), [Nanoscience and Nanotechnology Commons](#), and the [Power and Energy Commons](#)

Copyright 2013 Sunand Santhanagopalan

Recommended Citation

Santhanagopalan, Sunand, "HIGH VOLTAGE ELECTROPHORETIC DEPOSITION FOR ELECTROCHEMICAL ENERGY STORAGE AND OTHER APPLICATIONS", Dissertation, Michigan Technological University, 2013.
<https://doi.org/10.37099/mtu.dc.etds/653>

Follow this and additional works at: <https://digitalcommons.mtu.edu/etds>

 Part of the [Mechanical Engineering Commons](#), [Nanoscience and Nanotechnology Commons](#), and the [Power and Energy Commons](#)

HIGH VOLTAGE ELECTROPHORETIC DEPOSITION FOR ELECTROCHEMICAL
ENERGY STORAGE AND OTHER APPLICATIONS

By

Sunand Santhanagopalan

A DISSERTATION

Submitted in partial fulfillment of the requirements for the degree of

DOCTOR OF PHILOSOPHY

In Mechanical Engineering – Engineering Mechanics

MICHIGAN TECHNOLOGICAL UNIVERSITY

2013

© 2013 Sunand Santhanagopalan

This dissertation has been approved in partial fulfillment of the requirements for the Degree of DOCTOR OF PHILOSOPHY in Mechanical Engineering – Engineering Mechanics.

Department of Mechanical Engineering – Engineering Mechanics

Dissertation Advisor: *Dr. Dennis Desheng Meng.*

Committee Member: *Dr. Craig Friedrich.*

Committee Member: *Dr. Reza Shahbazian-Yassar.*

Committee Member: *Dr. Yu Wang.*

Department Chair: *Dr. William W Predebon.*

TABLE OF CONTENTS

TABLE OF CONTENTS.....	3
LIST OF FIGURES	8
PREFACE.....	13
ACKNOWLEDGEMENTS.....	14
ABSTRACT.....	15
Chapter 1. Introduction	17
1.1. Significance of electrochemical energy in today’s world.....	17
1.2. Role of nanomaterials	19
1.3. Outline of chapters.....	22
Chapter 2. Introduction to electrophoretic deposition	27
2.1. Electrophoretic deposition	27
2.2. Particle polarization during EPD	29
Chapter 3. High Voltage Electrophoretic Deposition for Vertically-Aligned Forests of One-Dimensional Nanoparticles.....	31
3.1. Introduction.....	31
3.2. Working Mechanism.....	34
3.3. Experimental Section.....	35
3.4. Results and discussions.....	38
3.4.1. <i>Impact of Parameters on HVEPD</i>	38
3.4.1.1. Deposition Voltage:	38

3.4.1.2. Deposition Time:	41
3.4.1.3. Concentration of MWCNTs:.....	42
3.4.1.4. Concentration of $\text{Mg}(\text{NO}_3)_2$:.....	43
3.4.2. <i>Final Parameters Chosen for HVEPD</i>	45
3.4.3. <i>Other characterizations of alignment</i>	45
3.4.3.1. Contact Angle Measurement:	45
3.4.3.2. Electrical Contact Measurement:.....	46
3.4.3.3. Electrochemical Testing:	48
3.4.4. <i>Versatility of HVEPD Process.</i>	48
3.5. Conclusions.....	50
Chapter 4. High Voltage Electrophoretic Deposition of Aligned Nanoforests for Scalable Nanomanufacturing of Electrochemical Energy Storage Devices.....	
4.1. Introduction.....	52
4.2. Working Mechanism.....	53
4.3. Experimental Methods	56
4.4. Results and discussions.....	57
4.4.1. <i>FESEM visualization:</i>	57
4.4.2. <i>Electrochemical testing:</i>	58
4.4.3. <i>FESEM visualization of continuous HVEPD sample on long strips:</i>	59
4.4.4. <i>Electrochemical testing of continuous HVEPD sample on long strips:</i>	60
4.5. Conclusions.....	61

Chapter 5. Scalable High-Power Redox Capacitors with Aligned Nanoforests of Crystalline MnO ₂ Nanorods by High Voltage Electrophoretic Deposition.....	62
5.1. Introduction.....	62
5.2. Experimental methods	66
5.2.1. Chemicals:	66
5.2.2. Hydrothermal synthesis of α -MnO ₂ nanorods:	66
5.2.3. Material Characterization:.....	66
5.2.4. High voltage electrophoretic deposition:	67
5.2.5. Electrochemical characterization:.....	68
5.2.6. Continuous HVEPD:.....	68
5.3. Results and discussions.....	69
5.3.1. Hydrothermal synthesis of α -MnO ₂ nanorods:	69
5.3.2. High voltage electrophoretic deposition:	70
5.3.3. Electrochemical characterization:.....	73
5.3.4. Continuous HVEPD:.....	82
5.4. Conclusions.....	85
Chapter 6. Further Improvements of Electrochemical Performance and Alignment Quality.....	87
6.1. Hybrid deposition for improved electrochemical performance	87
6.2. AC/DC pulsed deposition for improved alignment quality	88
Chapter 7. Conclusions	92
Chapter 8. Recommendations for Future Work.....	94

8.1. Field Emission	94
8.2. Dopamine detection for neural applications	95
8.3. Three-dimensional (3D) structures	96
References.....	97
Appendix A: Water based HVEPD	112
A1. Introduction.....	112
A2. Experimental Methods.....	113
A3. Results and Discussions	115
<i>A3.1. Effect of concentration of CNTs and salt</i>	<i>117</i>
<i>A3.2. Effect of voltage and time of deposition</i>	<i>117</i>
<i>A3.3. Electrical and Electrochemical testing</i>	<i>118</i>
A4. Conclusions.....	120
Appendix B: Supporting Information for Chapter 3.....	121
B1. Characterization of as-purchased multi-walled carbon nanotubes.....	121
B2. Preparation and characterization of β -MnO ₂ nanorods.....	122
B3. Variation of deposition voltage.....	123
B4. Variation of deposition time.....	125
B5. Variation of Mg salt concentration	125
B6. Electrical contact measurements - setup for electrical bridging method and results of linear sweep to measure electric resistance while contacting	126
B7. Setup for electrochemical characterization	128
B8. Cyclic voltammograms of MWCNT-deposited samples	129

B9. Cyclic voltammograms of nanorod-deposited samples	130
Appendix C. Continuous roll printing setup	131
Appendix D. Copyright Permissions	132
D1. Copyright Permission for Figure 1.1.	132
D2. Copyright Permission for Chapter 3 and Appendix B	135
D3. Copyright Permission for Chapter 4	136
D4. Copyright Permission for Chapter 5	138
D5. Copyright Permission for Appendix A	139

LIST OF FIGURES

Figure 1.1. Ragone plot of various energy devices ⁹ (Reprinted with permission from Woodbanks Communications Ltd.)	18
Figure 2.1. Schematic illustration of anodic and cathodic EPD	28
Figure 2.2. Schematic of alignment process of an individual 1D nanoparticle under the influence of the electric field	29
Figure 3.1. Schematic of HVEPD mechanism: 1D nanoparticles (NPs) are dispersed in liquid together with the precursor of holding layer added. The 1D NPs are polarized and aligned by the strong electric field. Their relatively low concentration prevents them from aggregation before deposition so as to avoid bundle formation. A thin holding layer is simultaneously co-deposited to keep the deposited 1D NPs upright and help them to survive the washing and drying process to follow.	35
Figure 3.2. FESEM images showing variation of voltage and time of deposition	41
Figure 3.3. FESEM images showing variation of concentrations of MWCNTs and $\text{Mg}(\text{NO}_3)_2$	43
Figure 3.4. Further verification and characterization of alignment: Top-view (a, b) and side-view (c, d) FESEM images of a horizontal CNT film by low-voltage EPD (a, c) and an aligned CNT forest by HVEPD (b, d). The water contact angle measurement shown in the inserts of a, b indicate superhydrophobicity of the aligned CNT forest after PTFE-coating. (e) The electric contact to a parallel plate electrode with increasing gap measurement (f) Charge-discharge curves of a horizontal CNT film and an aligned CNT forest.	47

Figure 3.5. Versatility of the HVEPD technology: FESEM images of a random MnO ₂ -nanorod film obtained by LVEPD (a) and an aligned MnO ₂ -nanorod forest by HVEPD (b) are compared. Their charge-discharge curves are shown in (c). Aligned CNT forests were also deposited on flexible (d) and transparent substrates (e).....	50
Figure 4.1. Schematic of continuous HVEPD	54
Figure 4.2. Flow configuration	55
Figure 4.3. FESEM images of aligned MWCNT forests achieved by HVEPD (a) with non-conductive (Mg(OH) ₂) holding layer, (b) with conductive (Ni) holding layer.	58
Figure 4.4. (a) Cyclic voltammograms and (b) galvanometric charge-discharge curves for small SS substrates (2 x 2.54 cm ²) with aligned MWCNT forests.	59
Figure 4.5. Aligned MWCNT forests on a long strip	60
Figure 4.6. (a) Cyclic voltammograms and (b) galvanometric charge-discharge curves for a section of long strip with aligned MWCNT forests	61
Figure 5.1. FESEM image and XRD analysis of α -MnO ₂ nanorods synthesized by hydrothermal synthesis.	70
Figure 5.2. Schematic and working mechanism of continuous HVEPD setup.....	71
Figure 5.3. FESEM images of aligned nanoforests of α -MnO ₂ nanorods with different holding layers.....	73
Figure 5.4. (a) Cyclic voltammetry curves at 20 mV/s for the three types of samples defined in Table 5.1 and (b) cyclic voltammetry curves at different scan rates for sample I showing high rate stability.	75

Figure 5.5. (a) Galvanostatic charge discharge curves at 0.25 mA/cm ² current for the three types of samples defined in Table 5.1 and (b) Variation of device capacitance with increasing current density for sample I showing high rate stability.	77
Figure 5.6. Electrochemical impedance spectroscopy at 0V DC bias with small 10 mV AC excitation from 10 mHz to 100 kHz for the three types of samples defined in Table 5.1.	78
Figure 5.7. Drop of device capacitance over 2000 cycles for the three types of samples defined in Table 5.1.	79
Figure 5.8. Ragone plot for the three types of samples defined in Table 5.1, as compared with a few examples of the highest performance achieved with MnO ₂ nanostructures and their composites in the most recent literature. The 340 kW/kg attainable power density obtained in this work is about 3 times of that reported in ¹⁵¹ and more than 1 order of magnitude higher than the typical values with MnO ₂ -based systems. ¹⁵³⁻¹⁵⁵ The power density achieved is also significantly higher than that of a typical CNT-based EDLC (room temperature). ¹⁵⁶	81
Figure 5.9. (a) Aligned nanoforests of α -MnO ₂ nanorods deposited on a long flexible strip (b) FESEM image of part of the long strip (c) Galvanostatic charge discharge curves of part of the long strip compared to the small rigid substrate.....	84
Figure 5.10. Deposition current during continuous HVEPD	85
Figure 6.1. Ragone plot of structured hybrid deposits obtained by HVEPD.....	88
Figure 6.2. Variation of capacitance and IR drop with number of AC/DC pulsed deposition cycles.....	90

Figure 8.1. CV curve of CNT film in aCSF with dopamine + ascorbic acid electrolyte.	95
Figure A1. Schematic of HVEPD process for VACNT.....	113
Figure A2. Setup to test the electrochemical properties of the obtained VACNT forest for its application in micro-supercapacitor.	115
Figure A3. EDS spectrum of holding layer determining its composition to be MgO. ..	116
Figure A4. SEM images of the VACNT forests (a-c) and the control experiments (d-i).	117
Figure A5. Electrical resistance vs distance from a reference steel plate.	119
Figure A6. Cyclic Voltammetry (C-V) curves of devices prepared by the VACNT forest and control samples.....	119
Figure B1. FESEM image of the as-purchased MWCNTs.....	121
Figure B2. FESEM image (a) and XRD pattern of the as-prepared β -MnO ₂ nanorods	122
Figure B3. FESEM images of deposited sample under varied voltage	123
Figure B4. FESEM images of deposited sample with varied deposition time	125
Figure B5. FESEM images shows the morphology of holding layer deposited with salt solution of different concentrations	126
Figure B6a. The setup of electrical bridging method for verification of vertical alignment.....	127
Figure B6b. I-V curves to characterize the electric resistance	128
Figure B7. Schematic of the setup used for electrochemical characterization.	128
Figure B8. CV curves of horizontal CNT film obtained by LVEPD and the aligned CNT forest obtained by HVEPD	129

Figure B9. CV curves for EPD of MnO ₂ nanorods.....	130
Figure C1. Setup for continuous HVEPD.....	131

PREFACE

The following document has been formatted as an electronic thesis or dissertation (ETD). Hyperlinks are intended to facilitate navigation from the table of contents, list of figures and tables to main text within the main document as well as the supplementary appendix sections.

The publications presented in this document are the research conducted as part of my PhD at Michigan Technological University. This work investigates the efficient use of one-dimensional nanomaterials for electrochemical energy storage applications.

Chapter 3 introduces the high voltage electrophoretic (HVEPD) technique to obtain vertically aligned one-dimensional nanomaterials. Mr. Sunand designed and conducted the different experiments in this work. Dr. Fei Teng provided the β -MnO₂ nanorods produced in-house in the same laboratory.

Chapter 4 presents the scalable fabrication approach for supercapacitor electrodes using roll-printing HVEPD. The work also investigates the improvement of electrochemical performance of such electrodes by reducing internal resistance. Experiments were designed and conducted by Mr. Sunand. Mr. Anirudh Balram, Mr. Franco Marcano and Mr. Evan Lucas helped with the design, machining and assembly of the continuous roll-printing HVEPD setup.

Chapter 5 presents the development of scalable high power redox capacitors using aligned forests of highly crystalline α -MnO₂ nanorods. The work also investigates the roles of crystallinity and internal resistance in achieving high power electrodes for redox capacitors. All experiments were designed and conducted by Mr. Sunand. Mr. Anirudh Balram helped with continuous roll-printing HVEPD process to obtain large-scale electrodes.

ACKNOWLEDGEMENTS

I would like to thank Michigan Technological University for the opportunity to study and conduct research at this esteemed university. I gratefully acknowledge the financial support from the Department of Mechanical Engineering – Engineering Mechanics. I also want to thank the National Science Foundation for their financial support of the research at our laboratory at Michigan Technological University.

I sincerely express thanks to Owen Mills of the Material Sciences Department for his patient help with scanning electron microscopy. I also thank the staff of the Mechanical Engineering - Engineering Mechanics Department, especially Joanne Stimac, for all the help with the rules and paper work of the graduate program.

I express my deepest gratitude to Nate Kroodsmma, Pragnesh Patel, Xiaobao Geng, Ryan Lemmens, Dr. Fei Teng, Anirudh Balram, Yiping Feng and all other team members in Multi Scale Energy Systems (MuSES) laboratory for the great working atmosphere, support and regular inputs that have helped me during my research at Michigan Technological University.

I thank Dr. Craig Friedrich, Dr. Reza Shahbazian-Yassar and Dr. Yu Wang for their inputs as part of my committee.

My greatest appreciation goes to my academic advisor, Dr. Dennis Meng. He took me in as a graduate student, giving me the opportunity to work on exciting and innovative research projects. He has always been there as a valuable mentor and guide. This work would not have been possible without his constant support, encouragement and invaluable contribution to my life at a professional and personal level.

Lastly, I am thankful to my parents and my wife for their love and support through every stage of my life.

ABSTRACT

High voltage electrophoretic deposition (HVEPD) has been developed as a novel technique to obtain vertically aligned forests of one-dimensional nanomaterials for efficient energy storage. The ability to control and manipulate nanomaterials is critical for their effective usage in a variety of applications. Oriented structures of one-dimensional nanomaterials provide a unique opportunity to take full advantage of their excellent mechanical and electrochemical properties. However, it is still a significant challenge to obtain such oriented structures with great process flexibility, ease of processing under mild conditions and the capability to scale up, especially in context of efficient device fabrication and system packaging. This work presents HVEPD as a simple, versatile and generic technique to obtain vertically aligned forests of different one-dimensional nanomaterials on flexible, transparent and scalable substrates. Improvements on material chemistry and reduction of contact resistance have enabled the fabrication of high power supercapacitor electrodes using the HVEPD method. The investigations have also paved the way for further enhancements of performance by employing hybrid material systems and AC/DC pulsed deposition.

Multi-walled carbon nanotubes (MWCNTs) were used as the starting material to demonstrate the HVEPD technique. A comprehensive study of the key parameters was conducted to better understand the working mechanism of the HVEPD process. It has been confirmed that HVEPD was enabled by three key factors: high deposition voltage for alignment, low dispersion concentration to avoid aggregation and simultaneous formation of holding layer by electrodeposition for reinforcement of nanoforests. A set of suitable parameters were found to obtain vertically aligned forests of MWCNTs. Compared with their randomly oriented counterparts, the aligned MWCNT forests showed better electrochemical performance, lower electrical resistance and a capability to achieve superhydrophobicity, indicating their potential in a broad range of applications. The versatile and generic nature of the HVEPD process has been demonstrated by achieving deposition on flexible and transparent substrates, as well as aligned forests of manganese dioxide (MnO_2) nanorods.

A continuous roll-printing HVEPD approach was then developed to obtain aligned MWCNT forest with low contact resistance on large, flexible substrates. Such large-scale electrodes showed no deterioration in electrochemical performance and paved the way for practical device fabrication. The effect of a holding layer on the contact resistance between aligned MWCNT forests and the substrate was studied to improve electrochemical performance of such electrodes. It was found that a suitable precursor salt like nickel chloride could be used to achieve a conductive holding layer which helped to significantly reduce the contact resistance. This in turn enhanced the electrochemical performance of the electrodes.

High-power scalable redox capacitors were then prepared using HVEPD. Very high power/energy densities and excellent cyclability have been achieved by synergistically combining hydrothermally synthesized, highly crystalline α -MnO₂ nanorods, vertically aligned forests and reduced contact resistance.

To further improve the performance, hybrid electrodes have been prepared in the form of vertically aligned forest of MWCNTs with branches of α -MnO₂ nanorods on them. Large-scale electrodes with such hybrid structures were manufactured using continuous HVEPD and characterized, showing further improved power and energy densities. The alignment quality and density of MWCNT forests were also improved by using an AC/DC pulsed deposition technique. In this case, AC voltage was first used to align the MWCNTs, followed by immediate DC voltage to deposit the aligned MWCNTs along with the conductive holding layer. Decoupling of alignment from deposition was proven to result in better alignment quality and higher electrochemical performance.

Chapter 1. Introduction

1.1. Significance of electrochemical energy in today's world

The twenty-first century has seen the advent of great technological progress. From small, smart electronics to efficient hybrid vehicles, major developments in every field are being achieved at a rapid pace. This ever-increasing role of technology, though, has brought with it a surge of energy requirements and calls for an equally rapid development in the field of energy conversion and storage. With depleting natural resources, the need for low-cost, smart energy devices are developed to fulfill the exponentially growing demands. The worldwide energy consumption was estimated to be 13 trillion watts in 2008. However, 80% of this energy consumed currently comes from fossil fuels, with other energy sources like nuclear, biomass and hydropower sharing the rest of the energy load.¹ Constant population expansion indicates that energy requirements will only increase and smarter means to harvest, store and supply energy will have to be realized.

Researchers around the world have recognized this grave need for development in the field of energy devices and are continually investigating alternate technologies. In recently years, substantial progresses have been made in renewable energy technologies like solar cells, wind and biofuels *etc.* Meanwhile, in addition to significant improvement in performance and reduction in cost, the spatial and temporal variations of renewable energy sources also call for better energy storage devices. On the other hand, electrochemical devices, such as batteries, supercapacitors and fuel cells have been recognized as promising alternatives to current energy storage and conversion methods. Advancement in the chemistry of materials has been a most important route to current strides in the field of energy storage and conversion. At the same time, the attention has also been increasingly placed on morphology control, process flexibility, system construction, and scalability, which will be reflected in this work.

Any energy storage/conversion device needs to provide the capability to both carry sufficient energy and quickly transfer energy (often in form of charges) in and out of the device. The two characteristics are commonly quantified as energy and power densities

and represented as Ragone plot shown in Figure.1 with the range of some typical devices exemplified. Fuel cells lie in the region of high energy density and low power density. They have the capacity to store a large amount of energy, yet have to release them relatively slowly. Quick refilling, although not captured in the Ragone plot, can be considered a great advantage of fuel cells. On the other hand, batteries tend to provide well-balanced energy density and power density, positioning them well in term of market readiness for many applications. Supercapacitors, located in the high power density region of the Ragone Plot, are known for their very fast charge discharge capabilities. They are traditionally viewed as excellent surge power providers in hybrid systems. In recently years, improvements on energy density and specific capacitance of supercapacitors, in additional to their long cycle life, great reversibility and high power density, has made them a feasible/preferable choice of primary energy storage approach for many applications, such as energy harvesters, microelectromechanical systems (MEMS), portable electronics and even electric vehicles.²⁻⁵ At the same time, supercapacitors remain as a perfect choice to provide the required peak power load when coupled with a fuel cell or battery in hybrid systems.⁶⁻⁸

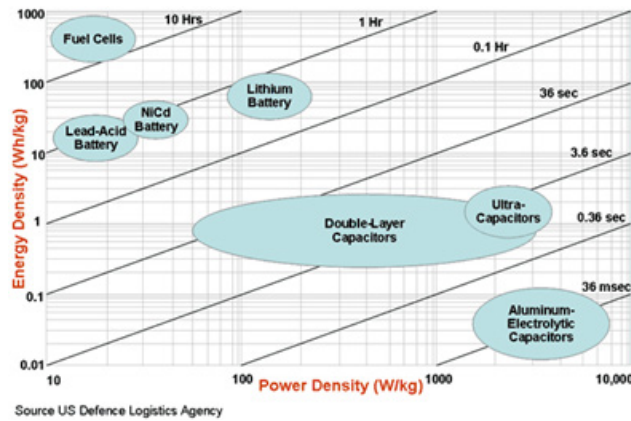


Figure 1.1. Ragone plot of various energy devices⁹ (Reprinted with permission from Woodbanks Communications Ltd.)

1.2. Role of nanomaterials

The use of nanoscale materials has been prevalent for quite a long time. Even before the advent of nanotechnology as a scientific and engineering venture, metal or metal oxide particles supported on ceramics were being used for crude oil refinement and now these can be classified as nanoparticles.¹⁰ However, the discovery of carbon nanotubes by Iijima in 1991 marks the initiation of significant advancements in this field.¹¹ Nanostructured materials are known to exhibit differed behavior from their bulk counterparts due to the increasing effect of scaling. Their mechanical, electrical and chemical properties are often altered owing to the more active atoms on the large surface area available at the interfaces.¹¹⁻¹² In many cases, quantum effects, the wavelike behavior of electrons and interactions between atoms start to emerge and affect the material properties.¹¹⁻¹² The unique properties and phenomena in the "small world" have been motivating the researchers to control, manipulate and develop various nanomaterials for the exploitation of desirable properties. The intensive research on deliberate manufacturing and property control at the nanoscale over the last a few decades has resulted in many practical applications in fields of electronics and computers, photonics, sensors, bioelectrical systems, energy storage etc.¹⁰ Nanomaterials have especially shown great promise in the field of power generation and energy storage. With the increasing influence of technology on our lives, the importance of finding cheaper and more efficient energy storage systems is ever increasing.

One-dimensional (1D) nanomaterial has a unique role in the development of nanotechnology. Ever since the discovery of carbon nanotubes, several other 1D nanostructures, such as nanorods and nanowires of oxides like MnO₂, TiO₂, ZnO, SiO₂ and alloys like BN, GaP etc. have been synthesized and used for various applications.¹¹ For example, metal alloy nanomaterials like Al, Sn, Si with lithium have high lithium storage capacities and have been investigated as anode materials for lithium-ion batteries.¹³⁻¹⁵ Other nanomaterials comprising of Si-C, Sn-Fe-C, SnO-based glasses, Sn-Mn-C,¹⁶⁻²⁰ TiO₂-B nanowires as host for lithium ions²¹ have also been suggested for the same purpose. Especially, silicon has exceptionally high lithium ion storage capacities

and thus highest energy densities in all known anode materials. However, the volumetric expansion can pulverize the silicon electrode easily after a few cycles. Use of 1D Si nanowire pillars has been shown to help reduce fracture and thus retain high capacity retention for longer cycle life.^{13-14, 19, 22-23} 1D nanomaterials also have a shorter diffusion path for the ion and electron exchange and larger electrochemically active area for higher charge/discharge rates, both of which may considerably enhance the performance of batteries.^{13, 22} On the other hand, platinum nanoparticles loaded on carbon black or carbon nanotubes have been used to enhance the catalytic properties and reduce the expensive platinum loading in fuel cells.^{13, 24} Fuel cells have been envisioned as next-generation power sources for automobiles and personal electronics. However, their economic commercialization is still to be fully realized. The reduced usage and replacement of the costly platinum catalyst without significantly sacrificing the oxygen reduction capability has motivated research on alternative materials and methods of fabrication. Transition metals alloyed with platinum like Pt-Fe, Pt-Cr have shown high oxygen reduction capabilities and are seen as a possible alternative.²⁵⁻²⁷ Nitrogen as a doping or alloy material with carbon nanomaterials is also said to have high oxygen reduction rates and could be potential catalysts in future fuel cells.²⁸⁻³¹ Nanomaterials like TiO₂ nanowires, Si nanowires etc. have also been investigated for photovoltaic applications.³²⁻³³

Supercapacitor devices have tremendous use for nanostructures as they provide high specific capacitance due to the high surface area available for capacitive energy storage. Porous carbon was first observed to exhibit very high capacitance in 1957.³⁴ The phenomenon was identified as supercapacitance due to the formation of an electric double layer. It was in the 1970s that the first commercial supercapacitor was introduced in the market.³⁴⁻³⁵ Further research has led to the development of two kinds of supercapacitors known as electric double layer capacitors (EDLCs) and reduction-oxidation (redox) supercapacitors based on pseudo-capacitance. Carbon nanotubes have been investigated as potential electrodes in EDLCs due to their high surface area and well-controlled, appropriate pore size for electrolyte access.^{13, 36-38} Redox supercapacitors employ Faradaic reaction to enhance charge storage capability or specific capacitance,

which is usually referred as pseudo-capacitance. The electrode material can be transition metal oxides, e.g., RuO₂, MnO₂, ZnO or conducting polymers, typically in form of nanostructures, such as nanorods and nanotubes. Many of those pseudo-capacitor materials, especially transition metal oxides, suffer from low electrical conductivity as a major limitation on attainable capacitance.^{13, 39} Therefore, efforts are being made to create hybrid systems by combining pseudo-capacitor materials with electrically conductive carbon nanotubes to give high power and energy densities.⁴⁰⁻⁴²

The fabrication of various nanomaterials with desirable chemistry and morphology is thus a key factor in the development of nanotechnologies. For example, most of the above mentioned applications can benefit from an ordered array of 1D nanomaterials rather than a randomly oriented layer.^{11, 43} An ordered array of vertically aligned one carbon nanotubes (CNTs) would provide better electron conductivity through their axes instead of relying on contact with each other, which typically results in significant loss of energy.⁴⁴ Furthermore, in case of battery or supercapacitor electrodes, a regular vertical array would provide a higher interfacial area for ion and electron exchange as well as more space for electrolyte to access the electrochemically active material. Similarly, in fuel cells, the oxygen reduction activity would improve with higher surface area available in an ordered vertically aligned array. Higher electron conductivity, an open framework and the ease to access individual 1D nanoparticles make the vertical alignment extremely desirable.

Traditionally such vertical arrays have to be obtained during the synthesis of the nanomaterial itself. Carbon nanotubes have been grown to form vertically aligned forests (VACNT) using catalytic-chemical vapor deposition (C-CVD) using a suitable catalyst to initiate growth in the required direction. The C-CVD process involves high temperature, typically close to 1000°C, which is not compatible most other device fabrication steps. Post-growth methods to align nanotubes/nanowires under mild condition have thus become an area of great interest for the convenient economic fabrication of many devices. Carbon nanotube alignment has been in the forefront of such work. Many attempts have been made to obtain VACNT forests by wet chemical self-assembly,⁴⁵

using magnetic fields and a binder,⁴⁶ filtration through hydrophilic membranes,²⁴ electrochemical polymerization of a binder along with electrophoretic deposition of nanotubes,⁴⁷ and polymer assisted alignment using a template,⁴⁸ to name a few. These methods have provided significant insight and shown progress in achieving vertical alignment of carbon nanotubes. However, most of them have faced problems like bundle formation, additional material on the nanotubes, lack of good alignment or control over the density and alignment angles etc. There are still many challenges in obtaining a well separated, dense array of vertically aligned 1D nanoparticles (nanoforests) with facile, precisely controlled process. There has been even less work reported on post-growth alignment methods of other 1D nanomaterials than CNTs.

Above analyses of current research trends on nanomaterials for energy applications have indicated that 1D nanomaterials possess excellent electrical, mechanical, optical and chemical properties, due to the combined effect of bulk and surface properties on their behavior. They have shown great promise in applications such as electrode materials of supercapacitors and batteries, catalyst support for fuel cells. Similarly, 1D nanoparticles, including CNTs, have shown great potentials in field emitters, photovoltaic devices, electrochemical probes, ultrafiltration membranes and many other applications. Oriented morphology can take great advantage of the superior properties at the nanoscale. The key for further development depends on both improvements on the synthesis of the nanoparticles and facile methods to achieve oriented structures and scale-up production, which are both challenging and exciting tasks in the adventure of nanotechnology for practical applications.

1.3. Outline of chapters

Oriented one-dimensional nanomaterials can take great advantage of the superior properties at the nanoscale. It is well known that one-dimensional nanomaterials exhibit several superior properties like large surface areas, short diffusion paths and modified electrochemical properties over their bulk counterparts.^{13, 49} Ordered structures with vertically-aligned forests of such 1D nanostructures provide additional advantages like

greater packing density, ballistic electron transport along the vertical axis, better electrolyte access and better electrical contact that are extremely useful in electrochemical energy applications.^{1, 50} This work presents a novel technique, namely, high voltage electrophoretic deposition (HVEPD) to obtain such ordered structures with great flexibility and ease of processing. The performance of such structures in energy storage applications is explored and demonstrated with the fabrication and characterization of high performance supercapacitor devices.

Chapter 1 discusses the background and motivation behind this research. The discussion observes the growing demand for energy and explores the significance of electrochemical energy applications. The role of nanomaterials in developing efficient energy technologies is investigated and challenges for further progress are identified. Chapter 2 introduces the concept of the electrophoretic deposition technique. It also provides an overview of the basic working principle of the HVEPD method.

The HVEPD technique is first demonstrated in Chapter 3. Deposition of aligned forests of 1D nanoparticles (carbon nanotubes and MnO₂ nanorods) on conductive substrates was achieved at room temperature. A comprehensive study of the deposition voltage, deposition time, concentration of MWCNTs and precursor salt was conducted to better understand the working mechanism. The HVEPD process was seen to be enabled by high deposition voltage for alignment, low dispersion concentration of the nanoparticles to avoid aggregation, and simultaneous formation of a holding layer by electrodeposition. The effect of deposition medium was also understood in this work. The elimination of bubble formation due to electrolysis of water was avoided with an organic solvent. Use of an organic deposition medium greatly improved the alignment as compared to when water was used in the previous work discussed in Appendix A. Visualization by scanning electron microscopy clearly showed vertically aligned forests by HVEPD as compared to horizontal nanomaterial films achieved by traditional electrophoretic deposition with lower voltage. Alignment was further confirmed by comparing the contact angle, electrochemical performance, and capability to electrically connect two separated electrodes for the two samples. Teflon-coated aligned MWCNT

forests displayed superhydrophobicity which was not possible to achieve with the horizontal MWCNT film. Aligned MWCNT forests also displayed significantly higher electrochemical capacitance of $512 \mu\text{F}/\text{cm}^2$ than their horizontal counterparts ($157 \mu\text{F}/\text{cm}^2$) and lower electrical resistance. The versatile and generic nature of the process was then demonstrated by deposition of aligned forests on transparent and flexible substrates and by obtaining aligned forests of $\beta\text{-MnO}_2$ nanorods. The vertically aligned orientation achieved by HVEPD made it possible to extract better performance characteristics from the same set of materials implying their potential in a broad range of applications. The process flexibility of HVEPD has been demonstrated with flexible and transparent substrates, which eventually lead to scale-up fabrication to be discussed in chapters 4-6. The route to device fabrication was sought by trying to achieve scalable electrodes by using a continuous roll-printing approach. At the same time, improvement in electrochemical performance was pursued by reducing the high contact resistance associated with the non-conductive holding layer used in chapter 3.

Chapter 4 introduces the roll-printing method for scalable fabrication and investigates the role of the holding layer in improving electrochemical performance. HVEPD was used to obtain forests of aligned multi-walled carbon nanotubes (MWCNTs) on long strips of flexible, conductive substrates. Successful design and integration of a continuous HVEPD setup enabled scalable fabrication of electrodes for electrochemical energy storage. The mechanism of continuous HVEPD was investigated to ensure appropriate alignment. Well-aligned forests of MWCNTs were obtained using a conductive holding layer which helped reduce internal resistance and enhance the electrochemical performance of the electrodes. It was also verified that scaling-up introduced no detrimental effect on the performance as compared to nanoforests on small, rigid substrates.

HVEPD is then applied to fabricate high power redox capacitors in Chapter 5 to synergistically combine high crystallinity and alignment. It is commonly believed that such capacitors that exhibit pseudo-capacitance have to compromise the charge/discharge rate, power density and cyclability to achieve higher energy density than carbon-based

electric double layer capacitors. This chapter explores the synergetic advantages of combining the high crystallinity of hydrothermally-synthesized α -MnO₂ nanorods with the process versatility of high voltage electrophoretic deposition (HVEPD) for high performance redox capacitors with vertically-aligned nanoforests. The scalable nanomanufacturing process was demonstrated by roll-printing an aligned forest of α -MnO₂ nanorods on a large flexible substrate (1 inch by 1 foot). The electrodes showed very high power density (340 kW/kg at an energy density of 4.7 Wh/kg) and excellent cyclability (over 92% capacitance retention over 2000 cycles). Pretreatment of substrate and use of a conductive holding layer was seen to significantly reduce the contact resistance between the aligned nanoforests and the substrates. High areal specific capacitances of around 8500 μ F/cm² were obtained for each electrode with two-electrode device configuration. Over 93% capacitance retention was observed when the cycling current densities were increased from 0.25 mA/cm² to 10 mA/cm², indicating high rate capabilities of the fabricated electrodes and resulting in the very high attainable power density. The high performance of the electrodes is attributed to the crystallographic structure, 1D morphology, aligned orientation and low contact resistance.

Further improvement of electrochemical performance was sought and investigated in Chapter 6. Hybrid deposition of MWCNTs with branches of highly crystalline α -MnO₂ nanorods were prepared by using HVEPD co-deposition. The advantages of high conductivity and pseudo-capacitance were combined herein^{42, 51} to achieve supercapacitor electrodes with even higher power and energy densities. Control experiments were conducted to comparatively study a structured hybrid configuration. High areal capacitances of 20 mF/cm² were found at the optimal HVEPD parameters. With the combination of highly crystalline MnO₂ nanorods, conductive MWCNTs, low contact resistance and a structured film with aligned branched structures, it was possible to achieve a power density as high as ~850 kW/kg with an energy density of ~11 Wh/kg. Such structures retained almost 97% of their original capacitance over 2000 cycles. The high power/energy densities were enabled by the excellent capacitance retention of 96% over an increase of cycling current densities from 0.25 mA/cm² to 10 mA/cm². Electrodes with such hybrid deposits were also scaled up by using the roll printing

technique discussed earlier. A simple way of setting up a supercapacitor device was explored by assembling and characterizing a rolled up high performance supercapacitor. The improvement of alignment quality was also achieved by an AC/DC pulsed deposition technique. MWCNTs were first subjected to high-frequency AC voltage which was immediately followed by the application of a strong DC pulse. The alignment and deposition functionalities were thus decoupled in this approach. The AC field at high enough frequency allowed for the MWCNTs to be aligned without actually depositing on the electrode surface. The following DC field achieved the deposition of the aligned MWCNTs. Multiple cycles of AC/DC pulsed deposition allowed for improvement in alignment density. Better quality of alignment resulted in almost doubling the capacitance than that had achieved by HVEPD discussed in chapter 3.

The work is concluded in chapter 7 followed by recommendations of future works on field emission and dopamine detection in chapter 8.

Chapter 2. Introduction to electrophoretic deposition

2.1. Electrophoretic deposition

Electrophoretic deposition (EPD) has been regarded as a simple, economical and reliable room-temperature process to form thin films of micro and nanoparticles on any conductive substrate.^{44, 52-53} Figure 2.1 shows a schematic of the EPD working mechanism, which can be either cathodic or anodic. Prior to EPD, solid particles to be deposited should be dispersed in a suitable liquid deposition medium, e.g., water or alcohol. It is well known that when a solid is in contact with a liquid, it attracts a first layer of co-ions due to surface interactions, selective ion absorption and other mechanisms. This layer of co-ions attracts a second layer of counter-ions with the opposite polarity. The combination of these two layers constitutes the electric double layer (EDL). The first layer, called the stern layer, is strongly bound and cannot be easily displaced from the surface, which is considered as net charges introduced to the particles. The electrostatic repulsive force thus keeps the particles from aggregation. As a result, the particles in the dispersion are charged to form a stable colloid due to the electrostatic repulsion among them. An electric field is then applied to move the charged solid particles towards one of the electrodes, which is subsequently deposited with a layer of the solid particles due to surface-particle interactions.^{44, 54} The charges on these particles can be conveniently tuned by adding a suitable charging agent to alter the deposition kinetics and control the electrode on which deposition is required. Since suitable combination of deposition medium and charging agent can be found for almost any solid material, EPD is a very generic approach, which makes it a desirable process for the manipulation of various nanomaterials and their combination (e.g., by codeposition).^{41, 55-}

60

As for the deposition of 1D nanoparticles, EPD of entangled CNT films has been extensively studied.^{44, 61} Efforts were also made to control the orientation of CNTs deposited by EPD. For example, patterned polysilane films were used as a template to align CNTs during EPD.⁶² A template was also formed by pre-coating (sometimes

followed by cracking) a layer of metal hydroxide/oxide⁶³⁻⁶⁴. Co-deposition of conductive polymer was shown to allow part of the CNTs to protrude from the substrate surface.⁶⁵ Ultrasonic agitation was also used to reassemble the EPD-deposited short CNTs into vertically-aligned bundles.⁶⁶ Currently, like other post-synthesis methods, the EPD forests of vertical CNTs are still suffering from far inferior quality than their C-CVD counterparts. However, great potential exists in their high productivity, low cost, scalability, and mild process condition (e.g., room temperature, atmosphere and non-corrosive, non-toxic liquid). Moreover, as a generic method, EPD has the capability to handle various materials either simultaneously or sequentially to form composite or hybrid structures.⁶⁷⁻⁶⁹

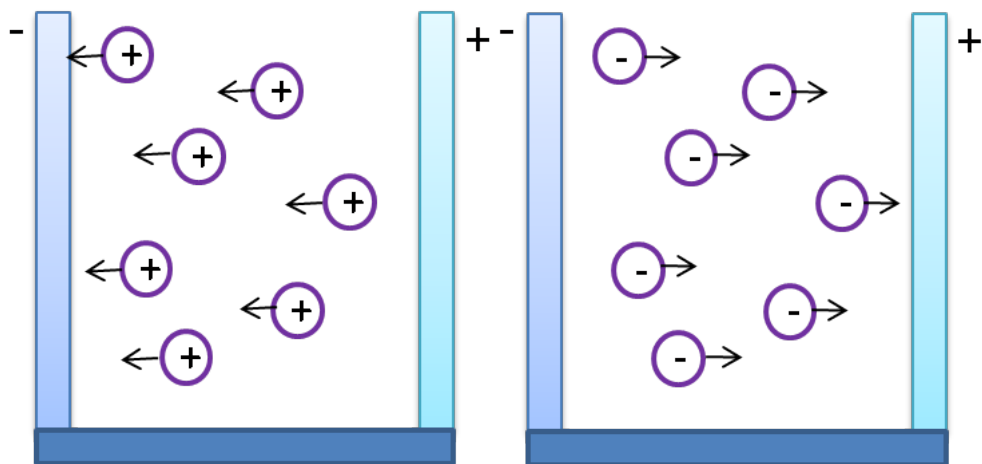


Figure 2.1. Schematic illustration of anodic and cathodic EPD

At the same time, it has been suggested that at high voltages the charged particles in a dispersion would align themselves along the direction of the electric field due to polarization, although they form bundles and do not maintain their orientation after the removal of the field.^{61, 70}

2.2. Particle polarization during EPD

The electric field used during EPD tends to polarize individual 1D nanomaterials.⁶¹ If the field is large enough it can generate a torque on the individual nanoparticle and cause it to align along the electric field direction. Figure 2.2 shows a schematic of how this process unfolds.

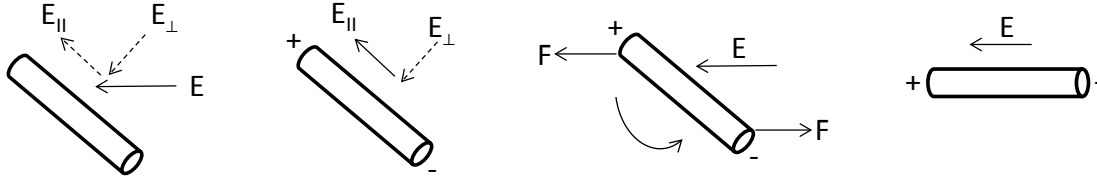


Figure 2.2. Schematic of alignment process of an individual 1D nanoparticle under the influence of the electric field

The applied electric field will have two resolved components in the parallel and perpendicular directions respectively. The parallel component will largely contribute to polarization of the nanoparticle, resulting in a dipole along the longitudinal axis.^{61, 70} The polarization itself has two components in the radial and parallel direction, the magnitudes of which depend on the polarizability tensor of the nanoparticle.⁶¹ With oppositely charged ends of the nanoparticle being pulled toward opposite directions, a torque is created. If this torque is greater than the Brownian force acting on the nanoparticle, they tend to align along the direction of the electric field.⁷⁰⁻⁷¹

For deliberate manipulation and alignment of 1D nanoparticles, the applied electric field has to induce a torque large enough to overcome the Brownian motion. This concept forms the basic premise of the HVEPD process. The use of a strong field to cause alignment is only part of the solution. Under strong electric field, the oppositely polarized ends of 1D nanoparticles tend to attract each other to form bundles,⁷⁰ which is undesirable for most applications previously discussed. A third major issue is to maintain the aligned orientation of the nanomaterials because alignment achieved by the strong electric field can be lost when the field is removed, causing the nanomaterials to be randomly oriented again.

HVEPD is thus designed to achieve vertically aligned nanoforests by solving the aforementioned issues. The key parameters involved in the working mechanism of the HVEPD process are discussed in chapter 3.

Chapter 3. High Voltage Electrophoretic Deposition for Vertically-Aligned Forests of One-Dimensional Nanoparticles*

3.1. Introduction

Controlling the orientation of nanomaterials lies behind the fundamental capability to tailor their macroscopic properties and synthesize them with optimal atom- and energy-efficiency.⁷² Many previous studies have pointed out that the vertically-oriented forest is an optimal configuration to enjoy the advantages of 1D nanoparticles, mainly due to the well-defined structural anisotropy and maximization of packing density.⁷³⁻⁷⁵ Shortly after the discovery of carbon nanotubes (CNTs) in early 1990's,^{50, 76} their aligned forests (ACNT forests)⁷⁷⁻⁷⁸ started to attract the attention of a broad scientific community due to their unique characteristics and promising applications, such as, excellent field-emission properties for flat panel displays,⁷⁹ adjustable wettability from superhydrophobic to hydrophilic for microfluidic applications,⁸⁰⁻⁸¹ and large electrochemical interface for supercapacitors.^{75, 82} Since then, many impressive properties and new applications of ACNT forests have been reported. The recent examples include the directional "dry glue" effect of heretically-branching ACNT forests inspired by gecko feet⁸³ and the exciting catalytic activity for oxygen reduction in alkaline fuel cells by nitrogen-doped ACNT forests.²⁸ Following the advent of carbon nanotubes, 1D nanoparticles (e.g., nanotubes, nanowires, nanofibers, nanorods, and nanobelts) of numerous materials have been synthesized and characterized. In spite of the huge variety of material and morphology, aligned forests of 1D nanoparticles continue to show great advantages and promising applications. Many excellent reviews on this topic can be found in the literature.^{50, 73, 78, 84-85}

* The material contained in this chapter was previously published in *Langmuir*. (Reprinted with permission from Santhanagopalan, S.; Teng, F.; Meng, D. D., *Langmuir* 2010, 27 (2), 561-569. Copyright 2010, American Chemical Society.)

A significant challenge for the practical applications of nanoforests is the compatibility with the fabrication processes of complementary metal–oxide–semiconductor (CMOS) integrated circuits and microelectromechanical systems (MEMS). The challenge of process compatibility arises from the often demanding conditions to prepare nanoforests *in-situ*. For example, the vapor-liquid-solid (VLS) mechanism has been widely adopted to grow very dense and uniform nanoforests of CNTs, ZnO nanowires, and Si nanowires, etc. However, high process temperature is the major limiting factor on their compatibility and cost. Significant efforts have been devoted to lower the VLS process temperature of ACNT forests to a range compatible with CMOS fabrication (e.g., 400-450°C or below).⁸⁶ However, the state of the art is still lingering around 500°C or above, which seriously limits their choice of conductive,⁸⁶⁻⁸⁷ flexible⁸⁸⁻⁸⁹ transparent⁹⁰⁻⁹¹ and stretchable⁹²⁻⁹³ substrates to accommodate the trends of next-generation electronics.

Therefore, post-growth methods to align 1D nanomaterial have attracted great interests for the successful integration of nanoforests into devices. Alignment of CNTs has been in the forefront of such efforts.^{44-45, 48, 94} Encouraging progress has been made to achieve vertical alignment in much milder process conditions than that of VLS methods. However, most of them have faced problems like bundle formation, low density, low alignment angle, lack of control, poor uniformity, and difficulty to scale up. Little work has been reported on post-growth deposition of other materials than CNTs to form nanoforests.

Among all the post-growth deposition methods, electrophoretic deposition (EPD)⁹⁵ deserves special attention. EPD has been known as a simple, low-cost, generic and reliable room-temperature method to deposit virtually any solid particles on a conductive surface.^{54, 96} To start an EPD process, solid particles are first dispersed in a liquid solution. The surface of the solid particles selectively adsorbs the ions in the solution. They are thus charged to form a stable colloid due to the electrostatic repulsion among them. An electric field is then applied to move the charged solid particles towards one of the electrodes, which is subsequently deposited with a layer of the solid particles due to

surface-particle interactions.^{44, 54} As for the deposition of 1D nanoparticles, EPD of entangled CNT films has been extensively studied.^{44, 61} Efforts were also made to control the orientation of CNTs deposited by EPD. For example, patterned polysilane films were used as a template to align CNTs during EPD.⁶² A template was also formed by pre-coating (sometimes followed by cracking) a layer of metal hydroxide/oxide.⁶³⁻⁶⁴ Co-deposition of conductive polymer was shown to allow part of the CNTs to protrude from the substrate surface.⁶⁵ Ultrasonic agitation was also used to reassemble the EPD-deposited short CNTs into vertically-aligned bundles.⁶⁶ Currently, like other post-synthesis methods, the EPD forests of vertical CNTs are still suffering from far inferior quality than their VLS counterparts. However, great potential exists in their high productivity, low cost, scalability, and mild process condition (e.g., room temperature, atmosphere and non-corrosive, non-toxic liquid). Moreover, as a generic method, EPD has the capability to handle various materials either simultaneously or sequentially to form composites or hybrid structures.^{67, 69, 97}

In this work, we show that high voltage (i.e., strong electrical field) during EPD can be employed to obtain well-aligned dense nanoforests of 1D nanoparticles without any template. All of the above mentioned advantages of EPD-based methods, such as room-temperature and mild process conditions, are inherent in such a method, especially its complete compatibility with CMOS and MEMS. It is therefore a very promising method for the integrated fabrication of next-generation nano electromechanical systems (NEMS) with nanoscale components. Moreover, the reported method can be combined with high-yield nanomaterial syntheses, such as laser vaporization⁹⁸ and arc discharge⁷⁶ of CNTs and hydrothermal methods, to boost the productivity and reduce the cost. This novel approach is named high-voltage electrophoretic deposition (HVEPD). The concept is proved by revealing the roles of the important process parameters, such as voltage, deposition time and concentrations of key elements in the dispersion. Multi-walled carbon nanotubes (MWCNTs) are used as an exemplary material for such preliminary study. It is then shown that the deposition can be conducted on flexible and transparent

substrates. To further demonstrate the versatility of the technology, β -MnO₂ nanorods are also deposited into aligned nanoforests by the reported HVEPD method.

3.2. Working Mechanism

As illustrated in Figure 3.1, the proposed HVEPD process relies on three innovations to achieve densely-aligned nanoforests under room temperature: 1) increasing the voltage to align 1D nanoparticles (e.g., CNTs) normally to the electrode surface, 2) decreasing the concentration of 1D nanoparticles to avoid bundle formation during EPD and 3) simultaneously depositing a holding layer to keep the 1D nanoparticles aligned after the electrical field is removed. Although the alignment of liquid-dispersed CNTs under high voltage has been known,⁶¹ such an effect has been previously employed to form large linear bundles instead of CNT forest.⁹⁹ In this work we found that the bundle formation can be effectively suppressed by decreasing the concentration of the dispersion. To prove this concept, 1D nanoparticles (e.g., MWCNTs or β -MnO₂ nanorods) were dispersed in isopropyl alcohol (IPA) with Mg(NO₃)₂·6H₂O salt added. The magnesium salt serves two purposes at the same time. First, the Mg²⁺ ions get adsorbed on the surface of the nanoparticles so as to impart them the positive charges required for these particles to move under an electric field, a very common approach that has been widely used in EPD of CNTs.⁴⁴ Moreover, the magnesium nitrate can be electrochemically reduced and deposited as Mg(OH)₂ on the cathode to hold the 1D nanoparticles according to the following reactions:¹⁰⁰



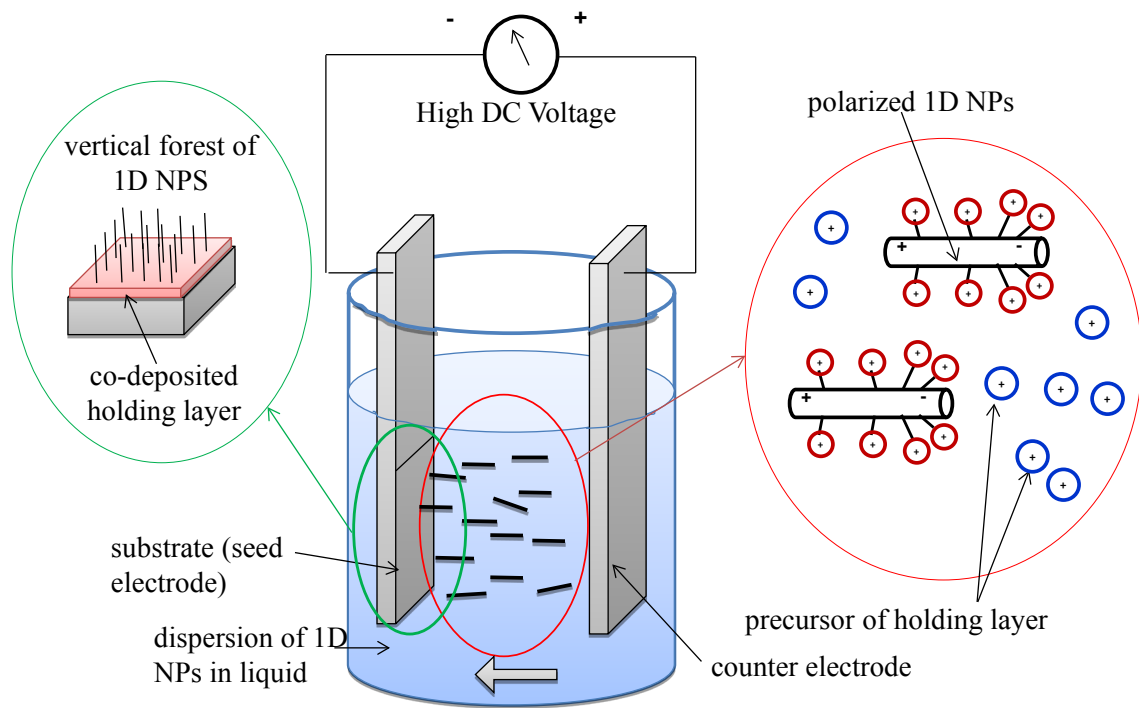


Figure 3.1. Schematic of HVEPD mechanism: 1D nanoparticles (NPs) are dispersed in liquid together with the precursor of holding layer added. The 1D NPs are polarized and aligned by the strong electric field. Their relatively low concentration prevents them from aggregation before deposition so as to avoid bundle formation. A thin holding layer is simultaneously co-deposited to keep the deposited 1D NPs upright and help them to survive the washing and drying process to follow.

3.3. Experimental Section

MWCNTS (MER Corporation, Arizona) were selected as the first exemplary 1D nanoparticle to demonstrate HVEPD, due to their wide availability, broad potential applications and well-characterized properties. The diameter and length of the MWCNTs have been specified as 140 ± 30 nm and 7 ± 5 μ m respectively by the supplier. These dimensions were verified by observing the as-purchased MWCNTs under a Hitachi 6400 FESEM (Appendix B, Figure B1). We have previously reported ACNTs obtained by a similar process with an aqueous dispersion.¹⁰¹ However, the electrolysis of water generated gas bubbles to disturb the deposition which has been identified as a major limitation on the achievable density of the nanoforest deposited on the electrode. In this work, we have switched to IPA, an organic solvent, as the dispersion medium. As a

result, no perceivable gas generation can be observed on the electrodes. Significant improvement on the density of nanoforest has been observed, as will be shown later in this work. A stable dispersion of MWCNTs in IPA was prepared by sonicating their mixture for 30 minutes with a probe sonicator (Sonics and Materials Inc., Connecticut). $\text{Mg}(\text{NO}_3)_2 \cdot 6\text{H}_2\text{O}$ salt (Fisher Scientific, Pennsylvania) was then added to this dispersion which was again sonicated for an additional 15 minutes. The dispersions were stable for at least a couple of weeks. Stainless steel electrodes (McMaster, Illinois) with an exposed area of $2.00 \times 2.54 \text{ cm}^2$ were used in the electrophoretic cell with an electrode gap of 7 mm controlled by a spacer. Care was taken to ensure that the electrodes were parallel to each other. Direct current (DC) voltage was then applied to deposit ACNT forests on the cathode with a controlled deposition time. A voltage amplifier (Tegam, Ohio) was used to provide the high voltages needed for HVEPD. Four parameters were varied to examine their effects on the deposition with FESEM visualization. A set of their optimal values could thus be determined, including the voltage (or electrical field), the deposition time, and the concentrations of the MWCNTs and Mg salt in the dispersion.

After the HVEPD process, the samples were first dried in a desiccator at room temperature for 30 minutes. The drying basically involved the evaporation of the IPA solvent that wets the electrode surface. As a result, the holding layer dried completely to form a strong holding layer in which the CNTs are rooted. We expect that the relatively low surface tension of IPA contributes to better alignment results than our previous work,¹⁰¹ where water with higher surface tension was used as the solvent. After drying, the samples were washed with DI water to remove any CNTs that were loosely adsorbed or deposited on the electrode surface. This step also helps to check the adhesion of HVEPD nanoforests. The samples were again left in the dessicator again for 60 minutes to dry at room temperature. After such a procedure, the HVEPD nanoforests are very robust. Further washing by water or IPA, or mechanical contact with another solid surface, will not perceivably change the characteristics of the nanoforests (e.g., electrochemical capacitance, conductivity, contact angle, etc).

Contact angle measurement, electrical contact, and electrochemical characterizations were then performed to further verify the alignment by HVEPD.

Samples with horizontal CNT films and ACNT forests were first coated with a thin layer of PTFE by solution coating before contact angle measurement was conducted by a setup constructed in house. Water droplets were then dispensed onto the samples using a needle and syringe pump (New Era Pump Systems, Inc., New York). The average of 10 readings for each sample and the standard deviations were taken.

In order to test the electrical contact, the samples were brought into contact with another bare stainless steel plate (counter electrode) to measure the resistance between the sample substrate and the counter electrode through the deposited layer with a multimeter (Omega, Connecticut). The resistance values were taken while the distance between the substrate and counter electrode are gradually increase by 1 μm per step with a 3D stage (Thor labs, New Jersey) until the resistance value become infinite, indicating complete electric disconnection. For comparison, four samples were tested, i.e., ACNT forest, horizontal CNT film, plain stainless steel plate and bare $\text{Mg}(\text{OH})_2$ holding layer. A potentiostat (Princeton Applied Research, Tennessee) has also been employed to measure the resistance between the CNTs and the conductive substrate by a linear voltage sweep.

Electrochemical performance was then tested using a Swagelok-type cell. Two stainless steel plates with either of the two types of deposits were placed parallel to each other and separated by a filter paper (Whatman, New Jersey). The specimen was then immersed in 2M KCl electrolyte to conduct galvanometric charge-discharge and cyclic voltammetry (CV) tests. The charge-discharge curves were scanned with a voltage window of 0V to 1V and current of 2mA. The time was then measured to calculate the capacitance of the samples. CV tests were carried out in the voltage window between -0.5V and 0.5V and at a voltage scan rate of 50 mV/sec.

HVEPD was then used to align $\beta\text{-MnO}_2$ nanorods. The MnO_2 nanorods were produced in house by using a process described in Appendix B, Figure B2. From FESEM

images, the diameter and length of the nanorods were estimated to be about 50 nm and 2-5 μm respectively.

3.4. Results and discussions

3.4.1. Impact of Parameters on HVEPD

3.4.1.1. Deposition Voltage:

Voltage (i.e., electric field) is a major parameter to study because it determines the alignment. It was known that the MWCNTs can be aligned along the direction of a strong electric field,⁹⁹ which can polarize the MWCNTs and induce a dipole moment. Therefore, those MWCNTs originally not aligned along the lines of electric force will then be rotated by a torque induced by the electrical field until they are aligned in the field direction and the torque becomes zero.^{61, 71} The nanotubes have also shown a tendency to form bundles because of the electrostatic attractive forces between the differently-charged ends (poles) due to the polarization.⁹⁹ We conducted experiments to see the morphology of the deposited MWCNTs with various deposition voltages: 30V, 60V, 90V, 120V, 150V, 180V and 200V. For all of those processes, the deposition time was set as 60 seconds and the concentrations of MWCNTs and $\text{Mg}(\text{NO}_3)_2 \cdot 6\text{H}_2\text{O}$ were maintained at 0.05 mg/ml and 0.025 mg/ml respectively. Little alignment was observed at a voltage below 90 V (Figures 3.2a and Appendix B, Figure B3a and b), indicating that the field-induced torque was not enough to align the MWCNTs and deposit them normal to the surface. Alignment started to be observed at 120V (Appendix B, Figure B3c) and reached its optimal morphology at about 150V (Figure 3.2b). Further increasing of the voltage causes the quality of alignment to suffer, with more random arrangement and bundles observed (Figures 3.2c and Appendix B, Figure B3d). Two reasons may account for this inferior alignment at a voltage higher than necessary (e.g., 150V in this case). First, high voltage tends to break down the colloidal dispersion and cause aggregation of CNTs.⁴⁴ Secondly, both the velocity and number of CNTs being deposited increases with the voltage and field strength.⁶¹ Consequently, when more CNTs reach the surface at the same time, there would be higher possibility for them to push each other during

deposition (i.e., flocculation by particle accumulation).⁹⁵ Thus, the CNTs that get deposited first could be pressed down by other following nanotubes. This phenomenon, called crowding effect herein, may negatively impact the alignment during deposition. Further investigation is needed to verify the above hypotheses or provide alternative explanations for the deterioration of alignment at higher voltages than necessary. Our experiments indicated the existence of a window for the optimal deposition voltage. Below the critical alignment voltage shown in Equation 3.4, the nanoparticles cannot be sufficiently aligned. On the other hand, if the voltage is too high, nanoparticles tend to agglomerate and form bundles, which also deteriorate the deposition results. Since a dense forest of MWCNTs was obtained at a voltage of 150 V, it was chosen as the voltage to work with for further tests.

Han and Yang have provided a dimensionless ratio between the tendency to align a rod-like particle by an electrical field and disturb it into random orientation by Brownian motion.⁷¹ By assuming that this ratio is unity, we propose the following equation to calculate critical alignment voltage:

$$V_{cr} = d \cdot \sqrt{\frac{3k_B T}{2\pi\epsilon_0\epsilon_r} \cdot \frac{1}{L \cdot r^2}} \quad (3.4),$$

where d , k_B , T , ϵ_0 , ϵ_r , L and r represents the gap between the EPD electrodes, the Boltzmann constant, the process temperature, the permittivity of free space, the static relative permittivity of solvent, the half-length and radius of the nanoparticles respectively (See Appendix B for details). This V_{cr} estimated by equation 4 corresponds to the transition when the alignment effect induced by the electric field becomes enough to overcome random Brownian disturbance. Consequently, the majority of CNTs would be aligned along the electric field. Using the dimensional data of the MWCNTs from the supplier, the range of alignment voltage was found to be about 120 V – 440 V. The 150V alignment voltage observed in our experiments agrees with this estimation. The voltage required to align nanoparticles of known dimensions can thus be estimated using Equation 3.4. According to this equation, it is easier to align larger nanoparticles due to

easier polarization. However, the nanoparticles close to the surface may not have enough time to be oriented before deposition, as demonstrated in Figure 3.2e & Appendix B, Figure B4a. At the same time, strongly-polarized nanoparticles tend to aggregate. With a longer length, the dispersion is expected to be less stable which will also affect the deposition and alignment result. We expect that such effects will eventually limit the maximum length that can be vertically deposited by HVEPD. On the other hand, small nanoparticles require higher voltages for alignment, which may cause breakdown of the dispersion due to the increased attraction between the oppositely polarized ends. As a result, bundles can be formed and alignment will deteriorate.

The weight yield of the deposit (including the $\text{Mg}(\text{OH})_2$ holding layer) was measured and shown in Figure 3.2d. The weight measurements were repeated for about 4 times to ensure reliability. The results are found to be consistent. For traditional EPD with lower voltage and higher CNT concentration, it has been reported that the weight of the EPD deposit increases linearly with voltage.⁶¹ However, we found an interesting plateau of the total weight yield at 60V, 90V and 120V. It is noted that this voltage range is right below 150V where optimal alignment has been achieved. It is thus suspected that it is related to the alignment process. Further investigation on this interesting phenomenon is still under way and will be reported elsewhere. Nevertheless, our current experimental results and theoretical analysis indicate that this phenomenon is most likely related to the alignment mechanism and can be a signature of the reported HVEPD process.

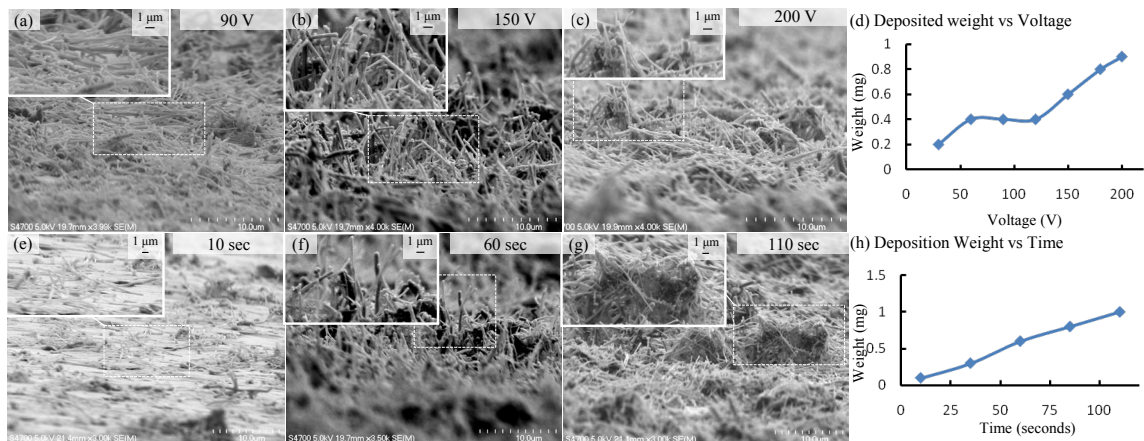


Figure 3.2. FESEM images showing variation of voltage and time of deposition

3.4.1.2. Deposition Time:

In order to reveal the temporal evolution of the MWCNT film, HVEPD was conducted for various deposition times: 10 sec, 35 sec, 60 sec, 85 sec and 110 sec, while the voltage, MWCNT concentration and salt concentration were kept as 150V, 0.05 mg/ml and 0.025 mg/ml respectively. After 10 sec of deposition, some MWCNTs are sparsely laying down on the substrate surface (Figure 3.2e) indicating that those MWCNTs, originally located close to the substrate surface, haven't got the chance to be aligned before their deposition. Certain alignment was observed after 35 sec of deposition with rather low alignment angles (Appendix B, Figure B4a). The lack of alignment in the 10sec and 35 sec samples may also be attributed to the insufficient thickness of holding layer to prevent capillary pulling during drying. This might explain the absence of samples with medium alignment angles. Nicely-aligned nanoforests were observed after 60 sec of deposition (Figure 3.2f). Interestingly, longer deposition of 85 sec and 110 sec (Appendix B, Figure B4 and Figure 3.2g) was seen to result in deterioration of alignment. Two factors may contribute to this phenomenon. First of all, the arrival of excessive MWCNTs after a dense nanoforest is formed can push the previously deposited MWCNTs. The MWCNTs used in this work are especially vulnerable to such a crowding effect because many of them are not ideally straight. The situation has been significantly improved when the rigid and straight β -MnO₂ nanorods are used, as will be demonstrated

later in this work. Secondly, with elongated deposition time, an additional layer of MWCNTs can be coated on top of the nanoforest. However, due to the topology of the nanoforest, the electrical field can be locally distorted. Therefore, the MWCNTs in this additional layer are not well aligned. The weight measurement confirms that the yield of the deposition increases linearly with time (Figure 3.2h), which is typical for EPD of CNTs. It also supports the hypothesis that additional layers can be deposited on top of the forest of MWCNTs. It was therefore concluded that an optimal deposition time exists for the formation of MWCNT forest by HVEPD, which is about 60 sec in our case.

3.4.1.3. Concentration of MWCNTs:

The concentration of MWCNTs holds the key to avoid aggregation, a strong tendency under high voltage. Typically, a CNT concentration of 0.1-1 mg/ml had been previously used for traditional EPD to form a dense film with randomly oriented CNTs.⁴⁴ It has also been shown that discrete linear bundles instead of a continuous film or uniform nanoforest are formed when a CNT dispersion with a concentration of 0.4 mg/ml is subjected to high voltage.⁹⁹ We conjectured that the aggregation of the polarized MWCNTs could be effectively suppressed if their concentration was decreased to reduce their chance of aggregation before they are deposited. This hypothesis has been verified experimentally herein. The deposition results of three different MWCNT concentrations (0.1 mg/ml, 0.05 mg/ml and 0.01 mg/ml) were examined and shown in Figure 3.3, with the voltage, deposition time and $\text{Mg}(\text{NO}_3)_2 \cdot 6\text{H}_2\text{O}$ salt concentration held constant at 150 V, 60 seconds, and 0.025 mg/ml respectively. While bundle formation was observed when the concentration of MWCNTs is 0.1 mg/ml or above (Figure 3.3a), well-separated MWCNTs were uniformly deposited to form a nanoforest when the MWCNT concentration was reduced to 0.05 mg/ml (Figure 3.3b). However, the MWCNTs were again deposited as scarce bundles when its concentration was further reduced to 0.01 mg/ml (Figure 3.3c). The following hypothesis is proposed to explain this phenomenon: at very low concentration, it is presumed that the first-deposited aligned CNTs can form a scarce conductive network on the surface while a majority of the substrate is covered by nonconductive $\text{Mg}(\text{OH})_2$. The electric field can thus be concentrated on those first-

deposited aligned CNTs, causing other nanotubes to get deposited around them instead of on the substrate surface. By contrast, at appropriate concentrations (0.05 mg/ml in our case), a uniform, dense network of aligned CNT forests can be formed before significant distortion of the electric field takes place, as observed in Figure 3.3b.

We also found that the relationship between the yield and MWCNT concentration is not linear (Figure 3.3d), although a linear relationship has been previously reported for traditional EPD.⁶¹ In the case of HVEPD, both CNTs and $\text{Mg}(\text{OH})_2$ are deposited simultaneously. Once the first layer of the nanoforest is deposited and most of substrate surface is covered by the nonconductive $\text{Mg}(\text{OH})_2$, further deposition will only happen on top of the nanoforest. It is possible that relatively higher CNT concentration can lead to bundle formation and nonuniformity in the first deposited layer. The total available area for further EPD is thus reduced, resulting in a lower slope on the yield curve with relatively high CNT concentrations. This explanation is also supported by the observation that the slope of the curve changes at 0.05 mg/ml, the optimal CNT concentration for alignment.

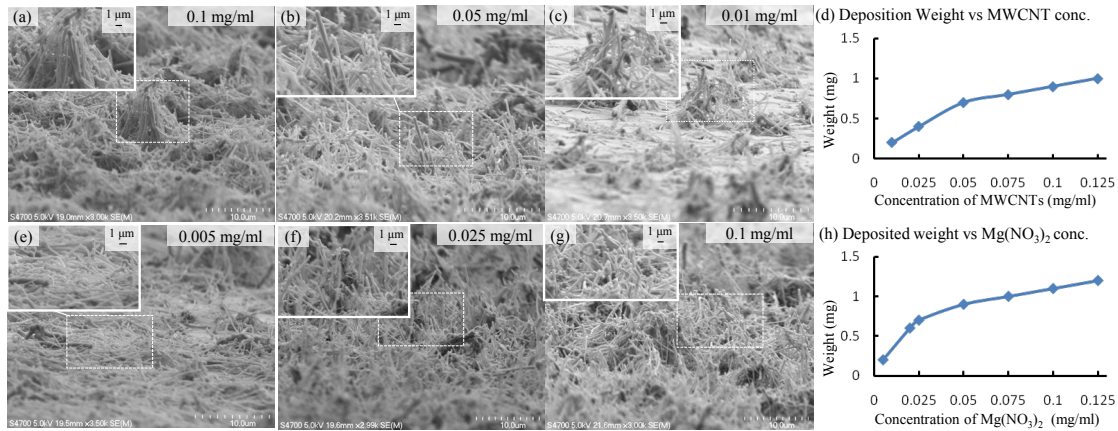


Figure 3.3. FESEM images showing variation of concentrations of MWCNTs and $\text{Mg}(\text{NO}_3)_2$

3.4.1.4. Concentration of $\text{Mg}(\text{NO}_3)_2$:

The concentration of Mg salt is another important parameter worthy of special attention. Conventionally, a very low concentration of Mg salt has been used in EPD

processes to render positive charges to the dispersed solid particles (e.g., CNTs). In the reported HVEPD process, in addition to acting as a charging agent, the Mg salt also serves to form the holding layer, a critical role. Therefore, the concentration of Mg salt was increased accordingly in this work for electrochemical deposition of $\text{Mg}(\text{OH})_2$. Several values of $\text{Mg}(\text{NO}_3)_2 \cdot 6\text{H}_2\text{O}$ salt concentration were examined, including 0.005 mg/ml, 0.025 mg/ml, 0.01 mg/ml, with the voltage, deposition time and MWCNT concentration kept as 150V, 60 seconds and 0.05 mg/ml, respectively. At a relatively low concentration of 0.005 mg/ml, there were almost no aligned CNTs observed in the sample after washing and drying (Figure 3.3e). It can be concluded that although the MWCNTs can get aligned at a high deposition voltage, a holding layer is also crucial to keep them upright during sample drying, because the aligned CNT nanofrests have a strong tendency to be pulled down to the surface by the strong capillary forces present. It is found that the electrochemically deposited $\text{Mg}(\text{OH})_2$ without MWCNTs formed a non-uniform layer with pores (Appendix B, Figure B5) when 0.005 mg/ml Mg salt solution was used. Such morphology can explain its inability to hold the ACNT forest for the latter to survive the capillary pulling during drying. When the concentration of salt was increased to 0.025 mg/ml, aligned CNT forest (Figure 3.3f) was obtained, confirming that a strong holding layer had been formed at such a salt concentration. However, when the concentration of the Mg salt was further increased to 0.1 mg/ml, clusters of MWCNTs started to be seen on the surface (Figure 3.3g). It was also noticed that the MWCNTs in those clusters show more randomness in their orientation. A possible reason is that the relatively high ionic strength thinned the electrical double layers around the MWCNTs so that they can be easily collapsed in the electrical field.⁹⁵ As a result, aggregation could have started before the MWCNTs were fully aligned. It was therefore determined that 0.025 mg/ml is an appropriate concentration to form a uniform and sufficiently thick holding layer for an ACNT forest in the reported case. The increase in the weight yield with the salt concentration was not linear (Figure 3.3h), with a lower slope at the higher concentration. This can be interpreted as an indicator of slower deposition after a continuous nonconductive holding layer is formed.

3.4.2. Final Parameters Chosen for HVEPD

In summary, the final parameters chosen to obtain well-aligned, dense MWCNT forests by HVEPD are deposition voltage of 150V (or electrical field of 2.1×10^4 V/m), deposition time of 60 seconds, MWCNT concentration of 0.05 mg/ml and $\text{Mg}(\text{NO}_3)_2 \cdot 6\text{H}_2\text{O}$ salt concentration of 0.025 mg/ml. As a comparison, low voltage EPD (LVEPD) was performed at 30 V for 5 min with the same dispersion. Both processes gave the same weight yield (0.7 mg), which agrees well with the widely-accepted Hamaker's law¹⁰² for EPD yield:

$$w(t) = \int_{t_1}^{t_2} f \mu E A C_s dt \quad (3.5),$$

where $w(t)$ is the deposit yield, E is the electrical field strength, A is the electrode surface area, C_s is the particle mass concentration in suspension, f is the efficiency factor (to take into consideration that not all of the particles that migrate to the electrode will contribute to the deposited film), and μ is the electrophoretic mobility (depending on both particle properties and suspension properties). Figure 3.4 shows the FESEM pictures of the sample obtained with LVEPD and the sample obtained with HVEPD. It was clearly seen that the majority of MWCNTs deposited by LVEPD were horizontally oriented (to be called horizontal CNT film hereafter), while a fairly-dense, aligned nanoforest (to be called ACNT forest hereafter) has been obtained by the proposed HVEPD with the chosen parameters.

3.4.3. Other characterizations of alignment

3.4.3.1. Contact Angle Measurement:

It is well known that surfaces with aligned CNT forests can be coated with polytetrafluoroethylene (PTFE) to obtain a contact angle larger than 150° (superhydrophobic),⁸⁰ which is usually not observed for entangled CNT films. We thus tested the contact angles of our samples to verify alignment and their capability to form superhydrophobic surfaces. The horizontal CNT film with PTFE coating showed a

receding contact angle of $115 \pm 2.1^\circ$ (see insert in Figure 3.4a for a representative image) whereas the aligned CNT forest displayed superhydrophobicity with a receding contact angles of $160 \pm 2.8^\circ$ (see insert in Figure 3.4b for a representative image). These measurements have further verified that a well-aligned CNT forest was obtained by using the HVEPD method and indicated the potential application of HVEPD as a feasible method to obtain superhydrophobic coating without CVD deposition.

3.4.3.2. Electrical Contact Measurement:

The capability to maintain electrical contact with a parallel conductive plate while being separated from it is another indication of aligned CNTs forest on the sample. The measurement setup has been shown in Appendix B, Figure B6a. Figure 3.4e shows the curves of the measured resistance with the increasing distance. It was seen that the sample deposited with aligned CNT forest stayed in contact with the counter electrode until their distances were increased to 11 μm , while other samples lost contact at much closer distances. The result is consistent with the length of the MWCNT provided by the manufacturer ($7 \pm 5 \mu\text{m}$) and further indicates the alignment in the nanoforests obtained by HVEPD. This comparative study, together with other characterizations reported in this session, can provide quantitative ascertainment that the CNTs have been aligned as nanoforests. However, we currently haven't found a method accurate enough to quantify the extent of vertical alignment (e.g., exact density and alignment angle), which will be a focus of future research. The tests have also confirmed that a significant amount of the aligned CNTs deposited by HVEPD are electrically connected to the substrate, although the HVEPD method involves the formation of a nonconductive holding layer. The current-potential curve, shown in Appendix B, Figure B6, gives a resistance value of about 6 Ω for the aligned CNT forest. In contrast, a higher resistance of about 12 Ω was found for the horizontal CNT film (See Appendix B6 for details). We anticipate that most of this resistance is the contact resistance between CNTs and the substrate, which can be improved by employing conductive holding layer or annealing.

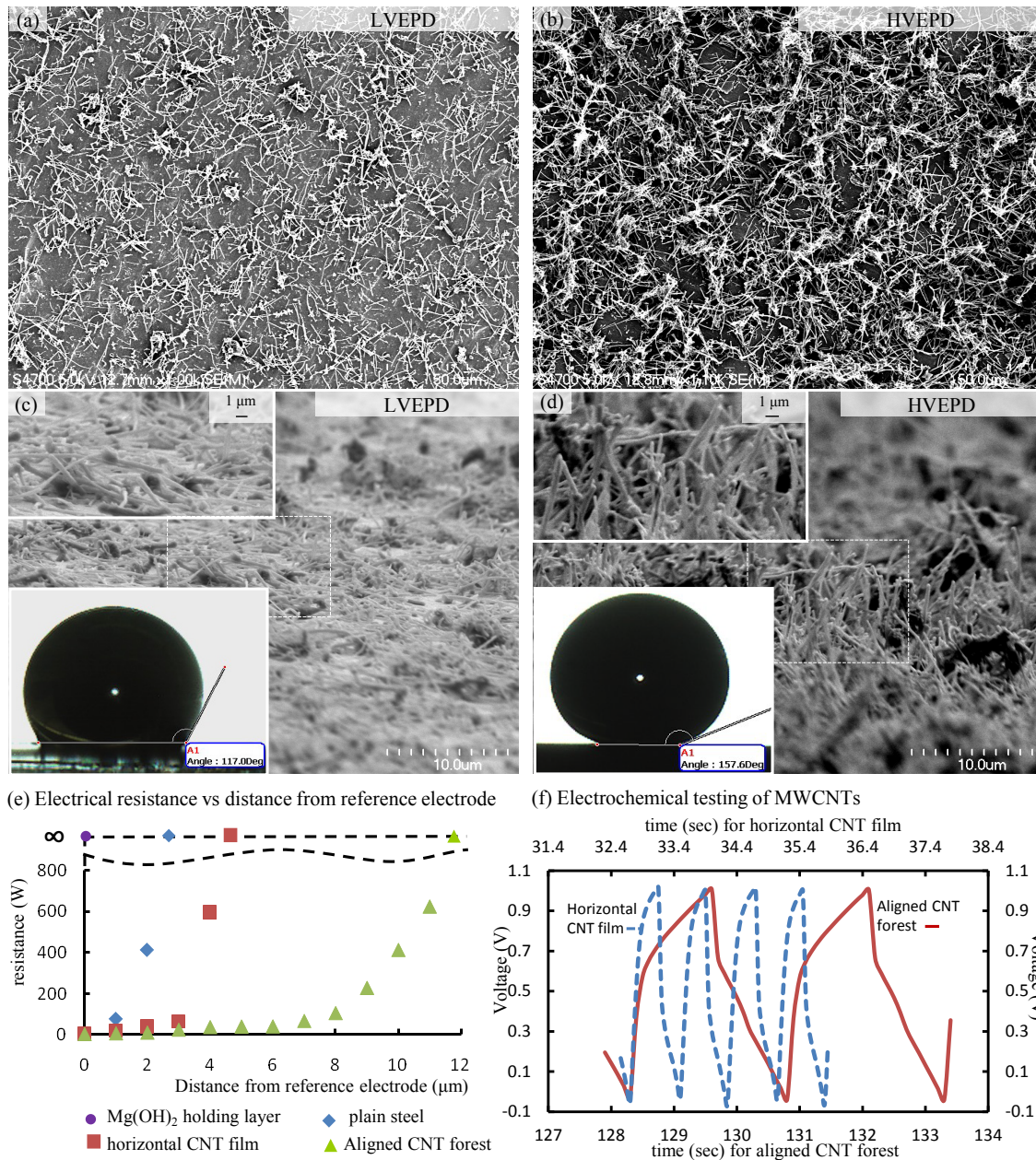


Figure 3.4. Further verification and characterization of alignment: Top-view (a, b) and side-view (c, d) FESEM images of a horizontal CNT film by low-voltage EPD (a, c) and an aligned CNT forest by HVEPD (b, d). The water contact angle measurement shown in the inserts of a, b indicate superhydrophobicity of the aligned CNT forest after PTFE-coating. (e) The electric contact to a parallel plate electrode with increasing gap measurement (f) Charge-discharge curves of a horizontal CNT film and an aligned CNT forest.

3.4.3.3. Electrochemical Testing:

Galvanostatic charge-discharge curves of the samples were measured to verify the alignment by comparing electrochemical capacitance of the samples. The areal specific capacitances of the deposited layer were calculated by the relation $C = I/A \cdot (dV/dt)$. 50 cycles were run to check for the stability of the curves. The final curves are presented in Figure 3.4d. With a voltage window of 0V to 1V and a current of 2 mA, the specific capacitance of the aligned CNT forest was measured to be 512 $\mu\text{F}/\text{cm}^2$, which was significantly larger than that of the horizontal CNT film (157 $\mu\text{F}/\text{cm}^2$). The difference can be attributed to the larger interfacial area of the aligned CNT forest exposed to the electrolyte⁷⁴ and smaller contact resistance of the active material with the substrate/current collector, further indicating the aligned morphology obtained by the HVEPD technique. Cyclic voltammograms were also obtained to confirm such a comparison, as shown in Appendix B, Figure B8.

3.4.4. Versatility of HVEPD Process.

The versatility of HVEPD process is demonstrated by depositing $\beta\text{-MnO}_2$ nanorods as alternative 1D nanoparticles and employing flexible and transparent substrates. As suggested earlier, the HVEPD technique can potentially be used for any nanomaterial as long the material can be charged suitably in the solvent. This has been successfully demonstrated by the deposition of aligned $\beta\text{-MnO}_2$ nanorods to form a nanoforest. A similar approach as in the case of the MWCNTs was used to align the $\beta\text{-MnO}_2$ nanorods and keep the aligned orientation using a holding layer. Control experiments were also carried out to determine the appropriate process parameters to obtain well-aligned forests of nanorods. A set of such parameters is found to be 150 V, 1 min, 0.02 mg/ml, and 0.01 mg/ml for the deposition voltage, time, $\beta\text{-MnO}_2$ nanorods concentration and $\text{Mg}(\text{NO}_3)_2 \cdot 6\text{H}_2\text{O}$ salt concentration respectively. LVEPD was also carried out under 30V for 5min with the same dispersion. FESEM images were taken for both the random film of $\beta\text{-MnO}_2$ nanorods obtained by LVEPD (Figure 3.5a) and the forest of aligned nanorods by HVEPD (Figure 3.5b). It is noticed that the straight $\beta\text{-MnO}_2$ nanorods have

been aligned with higher alignment angle and better uniformity, as compared with MWCNTs.

The electrochemical properties of the deposited nanorods were also tested by galvanostatic charge-discharge to further verify the alignment. The capacitance was measured and calculated with the same methods as they were done for the MWCNTs. Again, 50 cycles were run to stabilize the charge-discharge curves. The final curves for the aligned MnO₂ nanorod forest and the random MnO₂ nanorod film are presented in Figure 3.5c. The capacitance of the nanorod forest obtained by HVEPD was found to be 689 $\mu\text{F}/\text{cm}^2$, in contrast with 375 $\mu\text{F}/\text{cm}^2$ for the horizontal nanorod film obtained by LVEPD, further indicating the alignment of the MnO₂ nanorods. The CV curves of these samples were also measured to verify such difference, as presented in Appendix B, Figure B9.

Flexible, transparent, and stretchable electronics are deemed as important trends for many applications, ranging from paper displays, polymer solar cells to wearable devices.⁸⁸⁻⁹³ Considering the excellent properties and promising applications of aligned nanoforests, it is obvious that fabrication methods to integrate them on flexible and/or transparent conductive substrates are attractive. The proposed HVEPD method is a simple and versatile technology that can adopt such substrates with ease. To demonstrate the capability for HVEPD to adapt such substrates, aligned CNT forests were deposited on a flexible thin aluminum foil backed by ScotchTM tape (Figure 3.5e) and a piece of ITO-coated glass (Figure 3.5f). The tape-mounted aluminum foil shows great flexibility while the ITO glass still remains fairly transparent after the deposition. The deposition of aligned nanoforests by HVEPD imposes neither special requirement nor pre-treatment on these substrates other than a conductive surface. No alarming decrease of deposition yield was found in either case. The alignment quality did not show any deterioration as observed in the insets of Figures 3.5d and 3.5e.

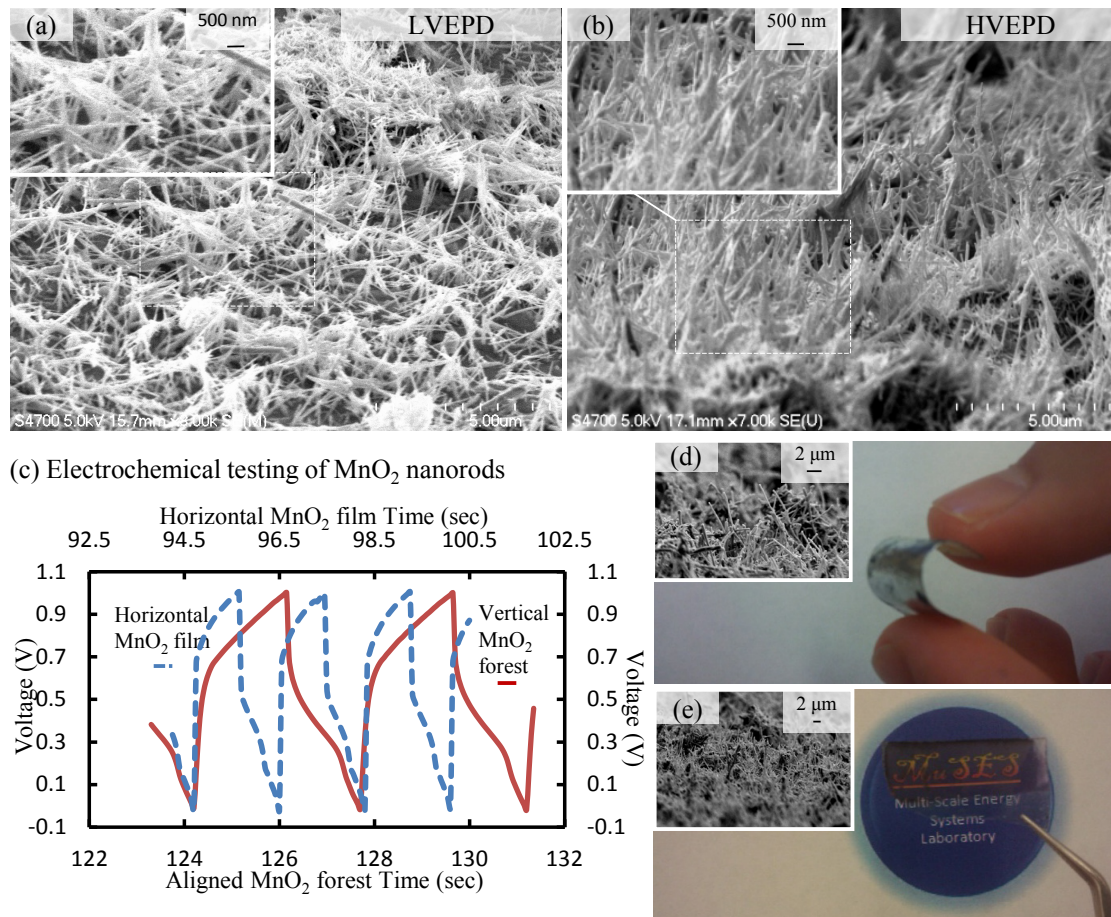


Figure 3.5. Versatility of the HVEPD technology: FESEM images of a random MnO₂-nanorod film obtained by LVEPD (a) and an aligned MnO₂-nanorod forest by HVEPD (b) are compared. Their charge-discharge curves are shown in (c). Aligned CNT forests were also deposited on flexible (d) and transparent substrates (e).

3.5. Conclusions

In conclusion, a new technique to obtain aligned forests of 1D nanoparticles under room temperature and mild conditions has been demonstrated by means of HVEPD. Deposition voltage, time, and concentrations of the 1D nanoparticles and Mg salt are identified as the key parameters to ensure a dense, well-separated, aligned nanoforest. Their impacts on the deposition morphology were revealed and explained. Theoretical estimation of the critical voltage for alignment agrees with the experimental results. Weight yield measurement turns out to be an effective tool to study the deposition and

alignment process. The alignment has been confirmed by FESEM observation, water contact angle measurement, electrical contact testing, and electrochemical characterization. The versatility of this room-temperature process has been demonstrated by depositing both MWCNTs and MnO₂ nanorods, as well as employing transparent and flexible substrates.

Chapter 4. High Voltage Electrophoretic Deposition of Aligned Nanoforests for Scalable Nanomanufacturing of Electrochemical Energy Storage Devices*

4.1. Introduction

Vertically-aligned one-dimensional (1D) nanomaterials (nanoforests) are desirable for electrochemical energy storage and conversion. Alignment can help to take full advantage of the excellent mechanical and electrical properties of 1D nanomaterials along their axis, while providing larger electrochemically active area and greater packing density.^{50, 73, 78} Vertically aligned carbon nanotubes have been shown to have superior electrochemical properties than their randomly oriented counterparts^{74-75, 103} and have been investigated extensively as electrode materials for batteries and supercapacitors.

However, it is still a great challenge to obtain a vertically-aligned nanoforest on large-area, flexible, conductive substrates. For example, there have been significant efforts to scale up the synthesis of aligned carbon nanotubes.^{77, 104-105} In spite of the limited success with catalytic vapor deposition methods,⁸⁶ the high process temperatures have seriously limited their substrate compatibility, cost effectiveness and scalability. On the other hand, the post-growth alignment methods^{45, 48, 94} are yet to achieve satisfactory alignment angle, density and scalability for electrochemical applications.

Electrophoretic deposition (EPD) is a simple, low-cost, room temperature technique with great promise for nanomanufacturing.⁵² The deposition works in two steps: the charged particles in the colloidal dispersion first move towards the oppositely-charged electrode and then get deposited due to surface interactions.^{44, 106} It is also known that a high voltage can be used during EPD to align carbon nanotubes.^{61, 71, 99} It was

* The material contained in this chapter was previously published in Journal of Key Engineering Materials. (Reprinted with permission from Sunand Santhanagopalan, A. B., Evan Lucas, Franco Marcano, Dennis Meng, Key Engineering Materials 2012, 507, 67-72. Copyright 2012, Trans Tech Publications.)

shown in our previous work that high voltage EPD (HVEPD) can be used to obtain well-aligned MWCNT forests on conductive substrates by the co-deposition of a $\text{Mg}(\text{OH})_2$ holding layer.¹⁰³ The ease of EPD and its capability to produce aligned structures shows great promise for the development of scalable processes to obtain large electrodes with aligned nanostructures.

In this work, we report a scalable fabrication setup to continuously print aligned MWCNT forests on long strips of flexible metal foils. It is also found that the use of a conductive holding layer would decrease the internal resistance of the supercapacitor device and help improve the electrochemical performance of electrodes with aligned MWCNT networks. Alignment of MWCNTs using a conductive holding layer is first investigated on small substrates to find the suitable parameters for alignment following which large-scale production of nanoforest electrodes is demonstrated by using the continuous HVEPD method. Electrochemical testing is performed to compare the performance of samples with conductive and non-conductive holding layers and the long strip using the scalable setup.

4.2. Working Mechanism

As Figure 4.1 shows, a setup was designed and fabricated to achieve continuous HVEPD of aligned MWCNT forests on long strips of flexible stainless steel (SS) sheets (Figure 4.1). Flexible SS sheets (2.54 cm wide X $\sim 13\ \mu\text{m}$ thick) were mounted on a roller and then fed through the continuous HVEPD setup. A DC motor was used to pull the long strips of these sheets at a speed of 2.54 cm/minute, so that every spot on the strip would get deposition for 1 minute, the optimal deposition time found in our previous work.¹⁰³ The non-conductive EPD vessel was filled with 100 ml of the EPD dispersion and two syringe pumps (Harvard Apparatus, MA) were used to keep the concentration and volume of the EPD bath constant. The counter electrode ($2.54 \times 2.54\ \text{cm}^2$) was fixed at the bottom of the EPD vessel. The working electrode was held in tension by two rollers above the EPD bath and two rollers (2.54 cm apart) within the EPD bath. DC voltage was applied across the fixed and moving electrodes for the continuous HVEPD process and a

Aligned MWCNT forests were obtained using a Ni salt concentration of 0.035 mg/ml with a MWCNT concentration of 0.05 mg/ml. The concentration of the stock dispersion required to be pumped in was calculated to be 0.0465 mg/ml for Ni salt and 0.119 mg/ml for MWCNTs. Alignment of CNTs at high voltages takes place due to the dipole moment created by polarization of the nanotubes under the influence of the electric field.⁶¹ The influence of fluid flow on the torque required for alignment was explored to check if the flow would impair alignment. We treated the flow between parallel plates as a plane Couette flow as shown in Figure 4.2. The Reynolds numbers for the top and the bottom plates were calculated to be 4.468 and 0.584 respectively using:

$$Re = \rho UL / \mu. \quad (4.2).$$

Here U is the free stream velocity given by: $U = V_f$ for the bottom plate; $U = V_p + V_f$ for the top plate. Amongst other terms, ρ is the density of the fluid (IPA), L is the length of the plate, μ is the dynamic viscosity of the fluid (IPA). Such small Reynolds numbers indicate creeping flows for which the boundary layer thickness is considered to be infinite. This indicates that the flow between the parallel plates can be considered as plane Couette flow with a fully developed velocity profile, wherein the shear stress and the drag force remain constant.¹⁰⁷ The fluid flow would thus exert only a constant force yet no additional torque on the MWCNTs in the dispersion.

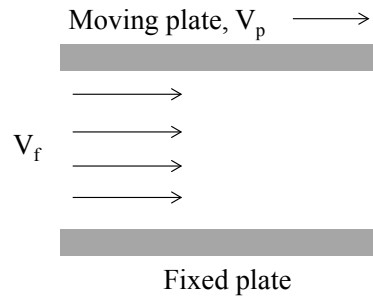


Figure 4.2. Flow configuration

4.3. Experimental Methods

The MWCNTs (MER Corporation, Arizona) in this study were used as purchased with a diameter of 140 ± 30 nm and a length of 7 ± 5 μm . We previously reported using the HVEPD process to deposit aligned MWCNTs and $\beta\text{-MnO}_2$ nanorods along with a non-conductive holding layer.¹⁰³ The non-conductive holding layer, employed to hold the MWCNTs in the aligned position, caused high internal resistance and thereby impaired the electrochemical performance. In this work, we co-deposited Ni to serve as the conductive holding layer to reduce the internal resistance and achieve improved electrochemical performance.

HVEPD in still dispersion was first conducted to find the suitable concentrations of Ni salt at which good MWCNT alignment could be achieved, while serving as control experiments for continuous HVEPD. Stable dispersions of MWCNTs and Nickel chloride hexahydrate ($\text{NiCl}_2 \cdot 6\text{H}_2\text{O}$) in isopropyl alcohol (IPA) were prepared by sonication for 45 minutes. Parallel stainless steel electrodes (McMaster, Illinois), with an exposed area of 2×2.54 cm^2 and a gap of 0.7 cm, were used for the control experiments. A DC voltage of 150 V was applied for 1 minute using a high voltage power source (Stanford Research Systems, California) for the HVEPD process. Optimal parameters at which well-aligned MWCNT forests can be obtained were then found by SEM observation and checking the electric bridging effect¹⁰³. The optimal concentrations for Ni and MWCNTs were found as 0.035 mg/ml and 0.05 mg/ml respectively and these parameters were then used to conduct HVEPD on gold coated Si wafers. The substrates were prepared in-house by sputtering 80-100 nm gold on Si wafers. The Si wafers were then cut and mounted on a vertical sample holder, to observe the cross-sectional view of the film deposited by HVEPD using a Hitachi S-4700 FESEM. HVEPD of MWCNT with non-conductive holding layer achieved in earlier work¹⁰³ was also conducted on such substrates to compare the cross-sectional views.

Continuous HVEPD was then conducted on flexible SS sheets (McMaster, Illinois) using the setup described in the working mechanism. The optimal HVEPD parameters

used to achieve alignment were maintained for continuous deposition over a long strip. The long strips were then cut out into smaller strips for FESEM visualization and electrochemical testing.

Electrochemical testing was conducted using a Swagelok-type cell where two aligned MWCNT samples were sandwiched along with a filter paper (Whatman, New Jersey) separator. The Swagelok-type cell was then immersed in 2M KCl electrolyte. A potentiostat (Princeton Applied Research, Tennessee) was used to conduct cyclic voltammetry and galvanometric charge-discharge cycles. Cyclic voltammetry was conducted within a window of -0.5 V and 0.5 V with a voltage scan rate of 50 mV/sec. The galvanometric scans were conducted within 0 V and 1 V at a current of 2 mA. 200 cycles were run for SS substrates ($2 \times 2.54 \text{ cm}^2$) coated with aligned MWCNT forests (both non-conductive and conductive holding layers) in still dispersion. The final data was collected after cycle stability was reached. A cut-out section from the long strip, with Ni holding layer, was then tested the same way to check for any deviation in performance.

4.4. Results and discussions

Samples with good alignment results during HVEPD in a still dispersion were characterized by FESEM visualization and electrochemical testing before continuous HVEPD was conducted.

4.4.1. FESEM visualization:

Figure 4.3 shows the cross-sectional views of aligned MWCNT forests with non-conductive ($\text{Mg}(\text{OH})_2$) and conductive (Ni) holding layers respectively. The alignment with the conductive holding layer was found to be similar to earlier alignment results¹⁰³ and well-aligned nanoforests with a conductive holding layer were seen in the FESEM images. The observed alignment was fairly uniform over the whole substrate. The cross-sectional views are at the center of the substrate to give a representative account of the alignment of the deposited MWCNT forests. Visualization at the center of the substrate was important to ensure that alignment was achieved across the entire substrate. The

insets in Figure 4.3 show magnified views of the aligned MWCNTs right where the Si wafer was cut.

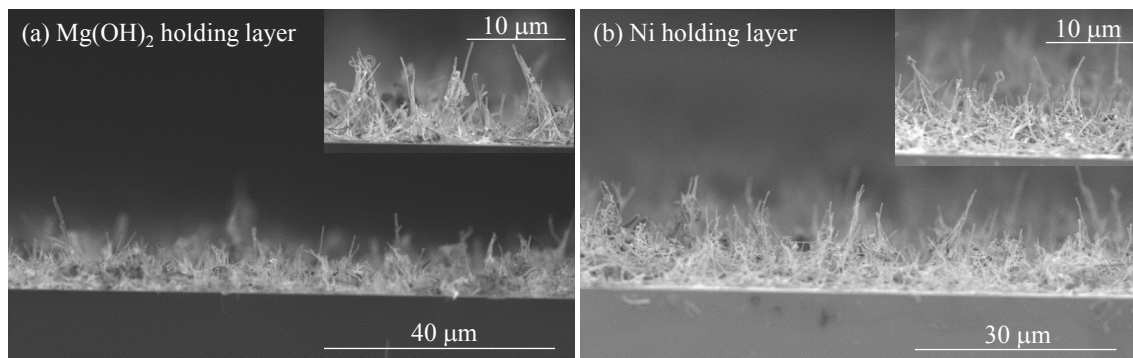


Figure 4.3. FESEM images of aligned MWCNT forests achieved by HVEPD (a) with non-conductive (Mg(OH)_2) holding layer, (b) with conductive (Ni) holding layer.

4.4.2. Electrochemical testing:

Cyclic voltammetry (CV) curves for the aligned MWCNT forests are shown in Figure 4.4a. The CV curve for the aligned CNT forests with a non-conductive holding layer has a greater slope in the middle of the curve than when a conductive holding layer is employed. Also, the total area under the curve increases in case of a conductive holding layer. A smaller slope in the middle of the curve qualitatively indicates that the aligned MWCNT forests with the conductive holding layer have lower internal resistance and the larger area shows its capability for higher capacitance. This was quantitatively measured using the galvanometric charge-discharge cycles shown in Figure 4.4b. The areal specific capacitance was calculated as:

$$\text{Sp. } C = I / A \text{ (dv/dt)}, \quad (4.3),$$

where I is the constant current at which the cycles are run; A is the area of the electrode; dv is the drop in voltage (1 V); dt is the time taken for the discharge cycle. We also measured the IR drop, which is the sudden drop in voltage for one time step at the beginning of the discharge cycle to gauge the internal resistance.

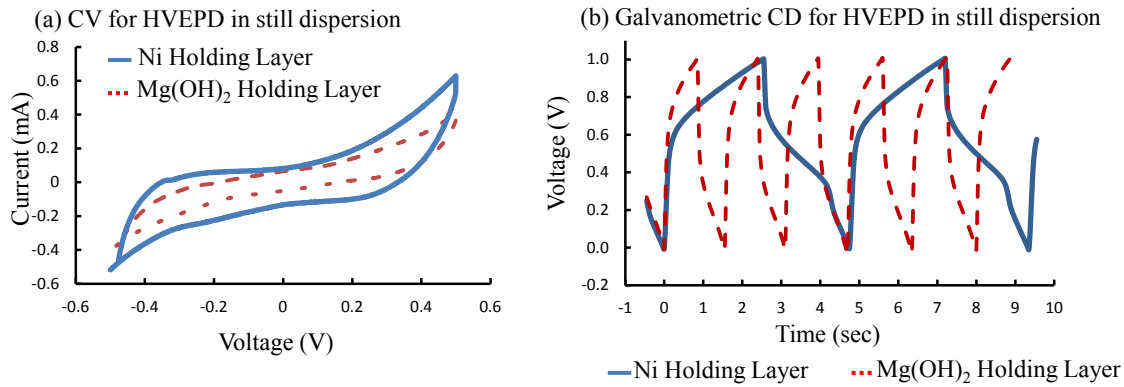


Figure 4.4. (a) Cyclic voltammograms and (b) galvanometric charge-discharge curves for small SS substrates (2 x 2.54 cm²) with aligned MWCNT forests.

The specific capacitance for the aligned MWCNT forests with the conductive holding layer was found to be around 846 $\mu\text{F}/\text{cm}^2$. This was significantly higher than the capacitance of the aligned MWCNT forests with the non-conductive holding layer, which was found to be 295 $\mu\text{F}/\text{cm}^2$, with an IR drop value of 0.479 V. On the other hand, the IR drop reduced to 0.249 V for the aligned MWCNT forests with the conductive holding layer indicating a lower internal resistance and a much higher capacitive performance.

4.4.3. FESEM visualization of continuous HVEPD sample on long strips:

Alignment was achieved on a long strip of about 12 inches using the setup described earlier. The long strip was cut into smaller strips for imaging in the FESEM. Figure 4.5 shows the long strip (with a ruler of 6 inch as reference) and the FESEM image of a section of the long strip. A tilted (8°) side view was observed to check for alignment. Well aligned MWCNT forests were found on different sections of the long strip indicating uniform deposition over a large length. In the initial stages of continuous HVEPD, the first inch does not receive a deposition of 1 minute and has sparse deposition as compared to the rest of the strip. As the strip moves along, from the second inch onwards, it receives a 1 minute deposition, resulting in uniform coating.

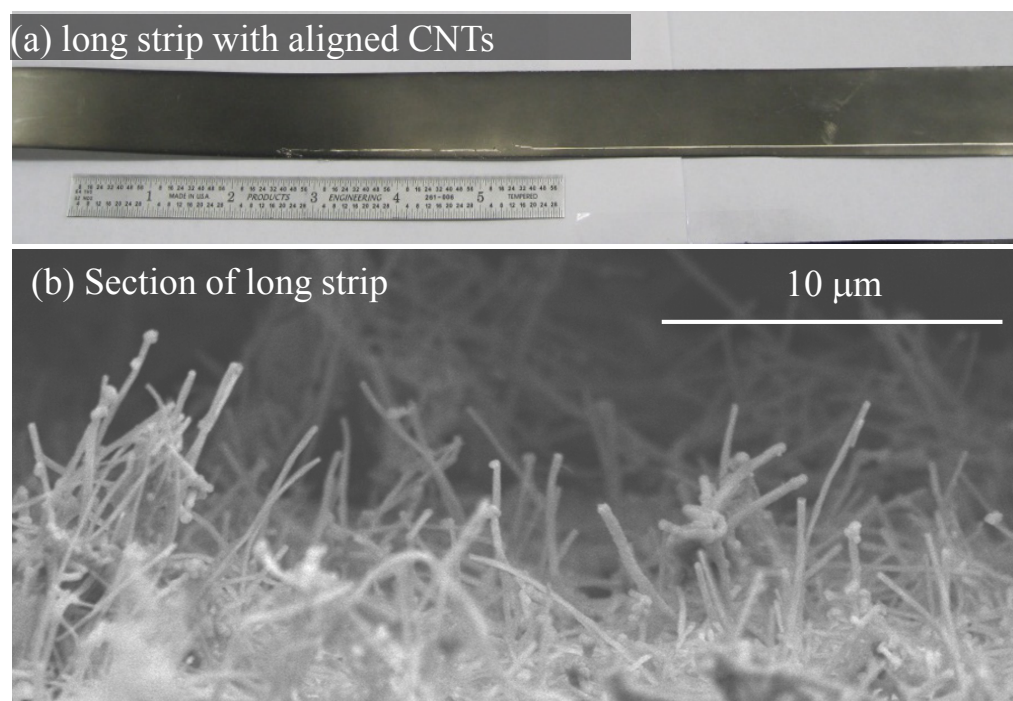


Figure 4.5. Aligned MWCNT forests on a long strip

4.4.4. Electrochemical testing of continuous HVEPD sample on long strips:

Cut-out sections of the long strip were also used to test the electrochemical performance of the aligned MWCNT forests. It was important to see that there was no loss of capacitance or increase of the internal resistance due to continuous deposition, as compared with the HVEPD with still dispersion. Figure 4.6 shows the cyclic voltammograms and the galvanometric charge-discharge curves for sections of the long strip. Calculated values for specific capacitance and IR drop were found to be $847 \mu\text{F}/\text{cm}^2$ and 0.252 V respectively, almost identical to that of the still HVEPD control samples ($846 \mu\text{F}/\text{cm}^2$ and 0.249 V respectively). The values were consistent over different sections of the strip, proving the uniformity of the continuous HVEPD process.

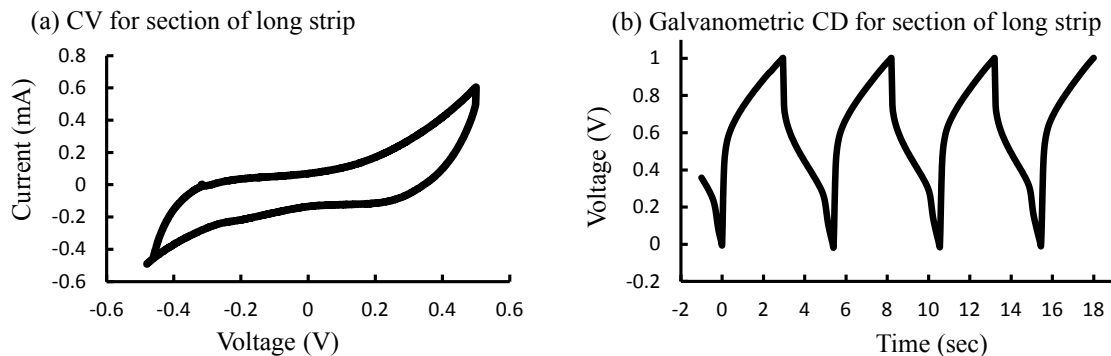


Figure 4.6. (a) Cyclic voltammograms and (b) galvanometric charge-discharge curves for a section of long strip with aligned MWCNT forests

4.5. Conclusions

Scalable fabrication of long electrodes with aligned MWCNTs was successfully demonstrated. The nanoforests of MWCNTs, have been formed on long strips of flexible stainless steel sheets using a single step deposition process, namely, continuous HVEPD. Improved electrochemical performance of such electrodes was shown with the use of a conductive holding layer. Continuous feeding of stock solution has proven to be effective in stabilizing the deposition and provide uniform deposition. It has also been found that the motion of the strip and feeding flow does not disturb the alignment during continuous deposition. The electrochemical performance of continuous HVEPD samples is found to be almost identical to the still HVEPD control samples. In conclusion, continuous HVEPD has been shown as a promising method for low-cost, scalable production of high-performance electrodes for electrochemical energy storage devices.

Chapter 5. Scalable High-Power Redox Capacitors with Aligned Nanoforests of Crystalline MnO₂ Nanorods by High Voltage Electrophoretic Deposition*

5.1. Introduction

Supercapacitors are considered as promising energy storage devices, especially surge power providers, in a broad range of applications, including energy harvesters, microelectromechanical systems (MEMS), portable electronics, electric vehicles, and high-performance, hybrid power sources by coupling with batteries.^{7-8, 108-109} They have gained increasing interest due to their high power density, quick charging, long cycling life and great reversibility.¹¹⁰⁻¹¹² Supercapacitors based on different electrode materials store/deliver energy with different working principles. Carbon materials are extensively used for electric double layer capacitors (EDLC) where charge is stored by non-faradaic surface interactions.^{38, 113-114} On the other hand, conductive polymers¹¹⁵⁻¹¹⁶ and various transition metal oxides¹¹⁷⁻¹²² are used for reduction-oxidation (redox) capacitors where faradaic reactions can be employed to improve charge/energy storage capability, while typically compromising the charge/discharge rate, power density and cyclability to a certain degree.¹²³

Amongst the transition metal oxides, manganese dioxide (MnO₂) is especially attractive due to its low cost, environmental friendliness, abundance in nature and relatively high specific capacitances. MnO₂ displays pseudo-capacitance, mainly due to reversible faradaic processes that involve transfer of electrons in Mn⁴⁺/Mn³⁺ redox system.¹²⁴⁻¹²⁵ Although ruthenium oxide (RuO₂) is considered as the metal oxide with the highest capacitive storage capabilities, the high cost, toxicity and low abundance associated with it poses serious limitation to its practical use. Manganese dioxide has thus

* The material contained in this chapter was previously published in ACS Nano. (Reprinted with permission from Santhanagopalan, S.; Balram, A.; Meng, D. D., ACS Nano 2013, 7 (3), 2114-2125. Copyright 2013, American Chemical Society.)

been seen as the green and economical alternative to RuO₂ as supercapacitor electrode material.^{124, 126-127}

Manganese dioxide exists in different crystallographic structures owing to the different ways the MnO₆ octahedra are inter-linked, that result in various tunnel sizes. These tunnels allow for foreign cations to be stored within them, while enabling the conversion of Mn⁴⁺ ions to Mn³⁺ ions for charge balance.¹²⁴ The amount of cations that can be stored depends on the size of these tunnels. Amongst the different MnO₂ structures, α -MnO₂ with 2 x 2 tunnels formed from double chains of MnO₆ has one of the largest tunnel sizes.^{124, 128-129} As a result, α -MnO₂ can store more foreign cations in reversible faradaic reactions, rendering it with the highest specific capacitance amongst all the known crystal phases of MnO₂.¹²⁸

The performance of a supercapacitor can be strongly affected by the crystallographic structure of active material, as well as other factors like morphology, exposed surface area, electrical contact with current collectors, amount of cations present *etc.* It is well known that one dimensional (1D), nanostructured morphology allows for large surface area, short diffusion paths that enable fast electron/ion transfer, better stress/strain accommodation and modified electrochemical properties.¹³ Ordered architectures with vertically-aligned forests of such 1D nanostructures provide additional advantages like greater packing density, ballistic electron transport along the vertical axis, better electrolyte access and better electrical contact that consequently lead to higher rate capabilities and greater cyclic stabilities.^{50, 73} Aligned forests of CNTs have inspired a few innovative configurations of electrodes and devices, such as interdigitated planar devices³⁶, Origami-folded electrodes¹³⁰, and forests of nanoflowers on vertically-aligned stems.⁴² For example, by integrating aligned CNT nanoforest into a microscale supercapacitor using a novel synthesis process, Jiang *et al.* achieved an impressive performance improvement by three orders of magnitude,³⁶ indicating the power of alignment and opening the door to new opportunities.

MnO₂ nanostructures have been synthesized by various methods such as coprecipitation, chemical reduction, sol-gel synthesis, thermal decomposition and electrochemical deposition.^{111, 131-133} Ordered/aligned MnO₂ nanostructures have also been obtained by sol-gel template synthesis,¹³⁴ template-based electrochemical deposition,¹²⁷ electrochemical anodization¹³⁵ and anodic electrochemical deposition¹²⁵ *etc.* However, it has been very challenging to obtain nanomaterial with both optimal crystallographic structure and highly ordered/aligned morphology at the same time. As a result, the performance can deteriorate quickly at high charge/discharge rate and during long cycling even if the nanorods can originally be well aligned, due to the lack of pure crystallographic structures, optimal 1D morphology, and low electrical contact resistance. Furthermore, the use of templates and high temperatures in the above-mentioned methods seriously limits the ability to obtain large flexible electrodes on current-collecting substrates for applications in large-scale supercapacitor devices.

On the other hand, hydrothermal synthesis has been used to produce 1D nanostructures of MnO₂ with superb process control by tuning the process temperature, time and other parameters.¹³⁶⁻¹³⁸ More importantly, due to the relatively higher process temperature and pressure, hydrothermal synthesis has been shown to result in highly crystalline structures with large tunnel gaps along with excellent control over desired morphology that are more difficult to achieve by other methods.^{129, 137, 139} Improved capacitive behavior of highly crystalline 1D MnO₂ nanostructures by hydrothermal synthesis has been repeatedly observed as compared with amorphous or other MnO₂ configurations with smaller tunnel gaps.^{128, 140-141} Moreover, the relatively high yields of hydrothermal synthesis made it a good choice for scale-up production.

However, hydrothermal synthesis has not been reported to directly produce ordered arrays on conductive substrates that can take the aforementioned advantages of aligned nanoforests. As a result, the crystalline MnO₂ nanostructures with excellent scalability have not been seen to benefit from the advantages of vertically alignment and the corresponding innovative device/electrode configuration shown with CNT nanoforests.^{36, 42, 87, 130} A versatile and facile technique for device fabrication using ordered, high-quality

MnO₂ nanostructures is yet to be realized. The performance, scalability and process compatibility (e.g., with flexible substrates and Si-microfabrication processes) of the nanostructured morphology for a supercapacitor device still need to be significantly improved. A promising approach is to combine hydrothermal synthesis with post synthesis technique to simultaneously achieve optimal crystallographic structures and electrode morphology, while enabling great compatibility with other process technologies (batch production, packaging etc.) to produce advantageous ordered structures over various conductive substrates.

In this work, we propose to first obtain highly-crystalline α -MnO₂ nanorods by low-cost, scalable hydrothermal synthesis method, and then align/deposit them by a post synthesis method named high voltage electrophoretic deposition (HVEPD),¹⁰³. Electrophoretic deposition (EPD) is a process in which DC voltage is used to move charged particles in a stable dispersion towards the oppositely-charged electrode. As a result, the particles are deposited on the electrode surface due to surface interactions.⁴⁴ The HVEPD process relies on three factors to achieve densely-aligned nanoforests under room temperature: 1) increasing the voltage to align the MnO₂ nanorods vertically to the electrode surface, 2) decreasing the concentration of 1D nanoparticles to avoid bundle formation during EPD and 3) simultaneously depositing a holding layer to keep the MnO₂ nanorods aligned after the electrical field is removed. HVEPD enables great flexibility on the choice of material (e.g. CNTs and various types of MnO₂) and substrates (e.g., flexible and transparent). It is also a template-free, room-temperature process with high compatibility to microfabrication. We have previously reported aligned nanoforests of CNT and β -MnO₂ nanorods using HVEPD and proved that the process is compatible with flexible and transparent electrodes.¹⁰³ The electrochemical performance though was hampered by factors such as the non-conductive holding layer (Mg(OH)₂), oxide layer formation on the substrates, suboptimal alignment quality/density and lower pseudocapacitance of β -MnO₂ nanorods. In this work, we have been able to show the full advantages of combining hydrothermal synthesis and HVEPD which turns out to enable supercapacitor electrodes with excellent retention of capacitance over high current

density and long cycling. Furthermore, the prospect of durable, high-power supercapacitors on roll-printed large flexible substrates has been demonstrated by verifying that such scale-up leads to no performance deterioration. The high performance in this work has been attributed to the optimal crystallographic structures of the hydrothermal α -MnO₂ nanorods, the alignment parameters optimized for the nanorods, the conductive holding layer and the pretreated substrate to remove any existing oxide layer. The work has provided a unique opportunity to look at MnO₂-based redox capacitors from the perspectives of not only material but also device configuration and electrode morphology.

5.2. Experimental methods

5.2.1. Chemicals:

All the chemicals used in the experiments were analytical grade and used as purchased without further purification. Deionized water was produced in-house and used for the hydrothermal synthesis. Manganese sulfate (MnSO₄·H₂O) and potassium permanganate (KMnO₄) used for nanorod synthesis were obtained from Sigma Aldrich.

5.2.2. Hydrothermal synthesis of α -MnO₂ nanorods:

The α -MnO₂ nanorods were produced in-house by adopting a hydrothermal process reported in literature.¹⁴² Typically, 0.21 g of KMnO₄ and 0.49 g of MnSO₄·H₂O were dissolved in 40 mL deionized water and magnetically stirred for about 20 min to form a homogeneous solution. Then, the solution was transferred into a Teflon-lined stainless steel autoclave and kept at 160 °C for 12 h. The product was collected by centrifugation, washed with DI water and then dried at 60 °C for 8 hrs.

5.2.3. Material Characterization:

The as-synthesized nanorods and the supercapacitor electrodes prepared by HVEPD were observed using the Hitachi S-4700 FESEM. Powder x-ray diffraction patterns of the α -MnO₂ nanorods were recorded using a Scintag XDS-2000 powder diffractometer with Cu_{k α} radiation ($\lambda = 1.5418$ Å). The readings were taken with an

operating voltage and current of 40 kV and 40 mA respectively and the 2θ range was set as $10 - 70^\circ$ in steps of 0.02° with a count time of 2s.

5.2.4. High voltage electrophoretic deposition:

Stable dispersions of as-synthesized α -MnO₂ nanorods (0.01 mg/ml) in isopropyl alcohol (IPA) were prepared by sonicating the mixture for 20 minutes using a probe sonicator (Sonics and Materials Inc., Connecticut). Precursor salts, Mg(NO₃)₂·6H₂O (0.005 mg/ml) and NiCl₂·6H₂O (0.0075 mg/ml) (Fisher Scientific, Pennsylvania) were then added to their respective α -MnO₂ nanorod dispersions and sonicated for an additional 15 minutes. The concentrations of the nanorods were determined from control experiments to maximize deposition density while avoiding bundle formation during HVEPD. The salt concentrations were chosen as the minimal value that the nanorods can receive sufficient positive charges and a uniform holding layer can be formed by the electroplating co-occurring with HVEPD. The dispersions were found stable for at least a couple of weeks. Small, rigid stainless steel (SS) electrodes (McMaster, Illinois) with an exposed area of $2.00 \times 2.54 \text{ cm}^2$ were used in the electrophoretic cell with an electrode gap of 10 mm controlled by a spacer. Care was taken to ensure that the electrodes were parallel to each other. A high voltage power source (Stanford Research Systems, California) was used to provide the high voltages needed for HVEPD. The weight of the deposit was measured using a micro balance (Adam Equipment Inc., Connecticut). About 10 samples were measured to obtain an accurate average value for the weight of the deposit. HVEPD for the α -MnO₂ nanorods with the Ni holding layer was also conducted on pretreated stainless steel substrates to further reduce contact resistance. A standard Wood's strike was used as pretreatment of the SS substrate to remove its oxide layer and coat a thin layer of nickel. Wood's strike was conducted on the SS electrodes with a nickel counter electrode. The two electrodes were placed in parallel and kept 10 mm away from each other in an electrochemical cell. A current density of around 200 A/m^2 is then applied in the Wood's strike solution with 240 g/L of NiCl₂·6H₂O and 125 mL/L of HCl.

5.2.5. Electrochemical characterization:

A two-electrode Swagelok cell was used to characterize the redox capacitor electrodes using an electrochemical workstation (Princeton Applied Research, Tennessee). The Swagelok cell was constructed by placing two HVEPD samples in parallel to each other with a filter paper (Whatman, New Jersey) as the separator and 0.1 M Na₂SO₄ as the electrolyte. The electrolyte was purged with nitrogen before testing. Cyclic voltammetry was conducted within a voltage window of -0.2 – 0.8 V at different scan rates to check the distortion in the shape of the curves at high cycling rates. Galvanostatic charge-discharge testing was conducted within a voltage window of 0 - 1 V at different current densities to estimate the capacitance and its retention at high cycling rates. 2000 cycles were run to check the capacitance retention over charge-discharge cycles. Electrochemical impedance spectroscopy was conducted with a 0V DC bias using a small AC excitation of 10 mV from 10 mHz to 100 kHz.

5.2.6. Continuous HVEPD:

The continuous HVEPD setup was used for the deposition of aligned α -MnO₂ nanorods on a long, flexible strip. A 2.54 cm wide, 50 μ m thick flexible SS strip (McMaster, Illinois) was mounted on the non-conductive rollers and fed at a speed of 5.08 cm/min using a DC motor (McMaster, Illinois). The feed speed of the strip was determined so that any particular point on it can get a deposition time of 30 second, the deposition time for a single layer of densely aligned nanoforest found with the small, rigid samples. Before HVEPD, a continuous Wood's strike was first conducted on the flexible SS sheet, and followed by washing and drying under room temperature. Continuous HVEPD was then conducted on the long strip of pre-treated SS sheet. The deposition chamber was first filled with 100 mL of HVEPD dispersion. A multichannel peristaltic pump (Thermo Scientific FH100M, Illinois) was used to continuously replenish the HVEPD dispersion to keep the concentration and volume constant. The pump was set to obtain an inlet and outlet pumping rate of 8 ml/min. The stock dispersion used to replenish the HVEPD bath had a α -MnO₂ nanorod concentration of 0.048 mg/mL and a Ni precursor salt concentration of 0.02 mg/mL. The current was recorded during

the continuous HVEPD using a digital multimeter (Universal Enterprises Inc., Orlando) to check for any variations and possible process errors. The deposited long strip was then dried at room temperature. Parts of the long strip with aligned nanoforest were cut and used for FESEM visualization and electrochemical testing.

5.3. Results and discussions

5.3.1. Hydrothermal synthesis of α -MnO₂ nanorods:

Crystalline α -MnO₂ nanorods were first synthesized using a facile hydrothermal synthesis technique.¹⁴² KMnO₄ was used to oxidize MnSO₄ under hydrothermal conditions and produce uniform nanorods. An optimal ratio of the reactants was adopted to obtain the desired morphology and crystallographic structure. It is believed that the formation of the α -MnO₂ nanorods is through the transformation of initially-formed δ -MnO₂ phase during hydrothermal process.¹⁴² The as-produced α -MnO₂ nanorods were characterized using the field emission scanning microscopy (FESEM) and by X-ray diffraction analysis (XRD) (Figure 5.1). The nanorods appeared fairly uniform with a length of 2-6 μ m and diameter of about 20-80 nm. XRD peaks were indexed by comparison to literature¹⁴²⁻¹⁴³ and JCPDS 44-141, which confirms the crystalline structure of the synthesized nanorods as α -MnO₂. The sharp peaks in the XRD analysis indicate high crystallinity of the synthesized material.

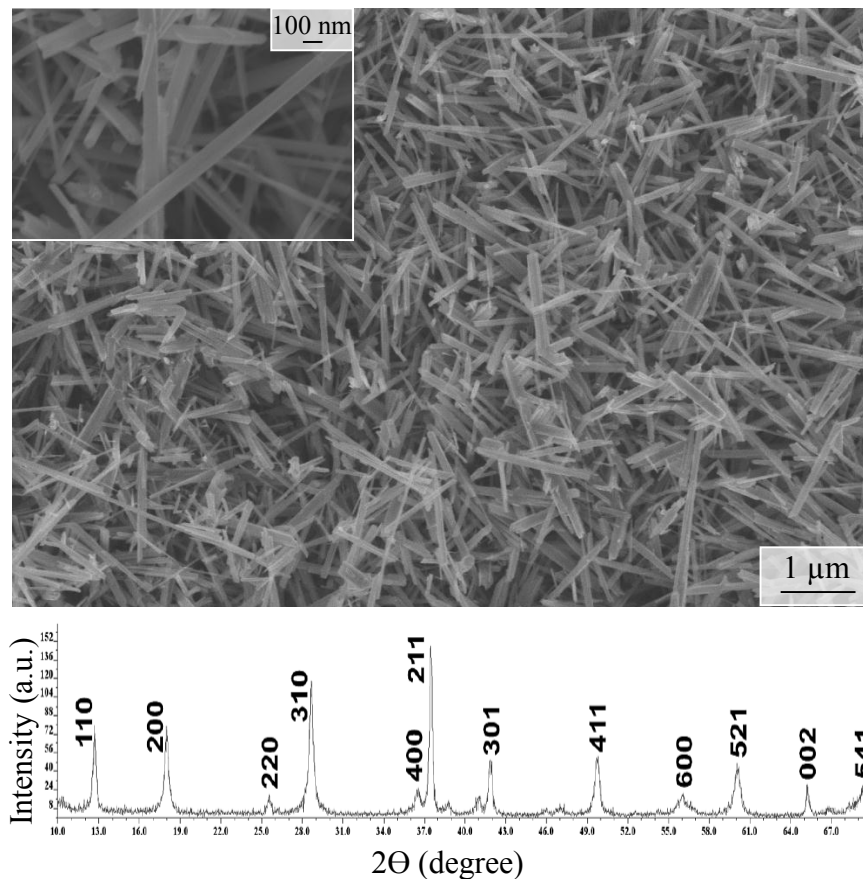


Figure 5.1. FESEM image and XRD analysis of α -MnO₂ nanorods synthesized by hydrothermal synthesis.

5.3.2. High voltage electrophoretic deposition:

HVEPD was used to obtain aligned forests of as-synthesized α -MnO₂ nanorods. The method relies on using a relatively high voltage (i.e., strong electric field) to align the nanorods along the electric field, maintaining a low concentration dispersion to avoid bundle formation during deposition and simultaneous deposition of a holding layer to maintain the aligned orientation. Figure 5.2 shows the working mechanism of the HVEPD process with the schematic of the continuous roll-printing HVEPD setup. α -MnO₂ nanorods were dispersed in isopropyl alcohol (IPA) with a precursor salt for the holding layer also being dissolved. A non-aqueous dispersion system was chosen to eliminate bubble formation during deposition caused by water electrolysis. With its

optimal concentration, the precursor salt fulfills two functions: ions in the solvent are adsorbed onto the surface of nanoparticles to stabilize them and facilitate their deposition,⁴⁴ while excess ions get reduced and deposit as the holding layer during HVEPD.¹⁰³ During deposition, the charged nanorods are moved through the dispersion by using a certain voltage, which, if high enough, would polarize the nanorods to overcome Brownian motion and align them along the electric field.^{61, 144} However, the polarized nanorods generally tend to attract oppositely charged ends and aggregate during deposition.⁷⁰ To limit such aggregation, relatively low concentration of the nanorods has been used to obtain densely-aligned nanoforests.¹⁰³ The time of deposition can also be controlled to avoid over deposition or crowding.

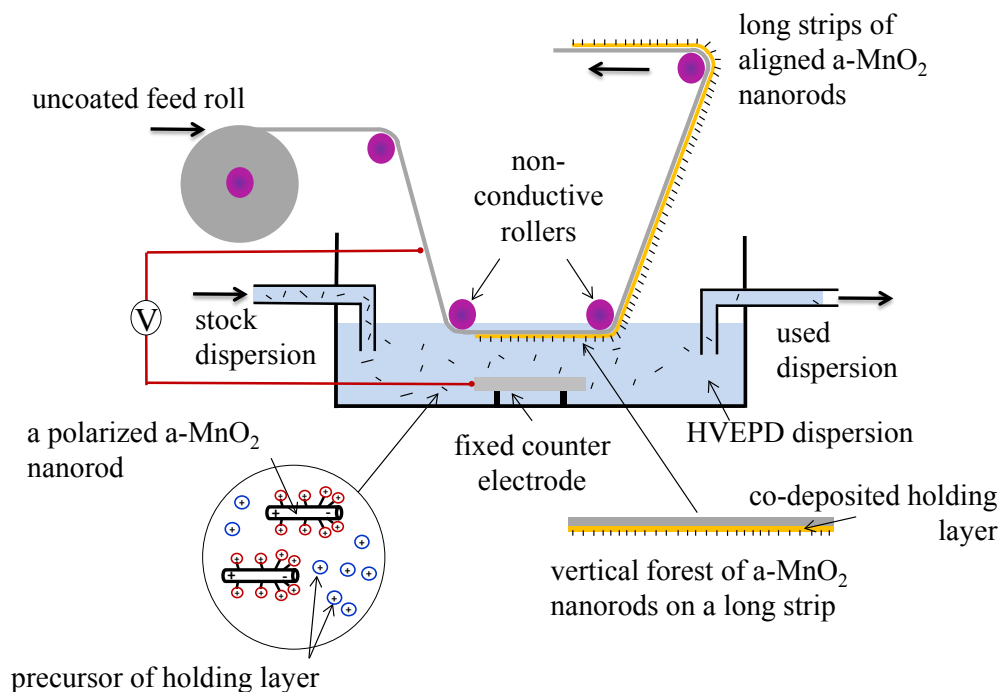


Figure 5.2. Schematic and working mechanism of continuous HVEPD setup.

Control experiments were carried out to find the optimal parameters needed to align the as-synthesized α -MnO₂ nanorods. Alignment was first achieved with a non-conductive Mg(OH)₂ holding layer by using a Mg precursor salt. Good alignment was obtained at a deposition voltage of 800 V and time of 30 seconds. The concentration of

α -MnO₂ nanorods was maintained at 0.01 mg/ml and that of the Mg precursor salt was kept at 0.005 mg/ml. In order to improve the electrical contact between the nanorods and the rigid stainless steel (SS) substrates, a conductive Ni holding layer has also been employed in this work. A Ni salt was used as the precursor with a concentration of 0.0075 mg/ml, while the nanorod concentration was kept at 0.01 mg/ml. It has been noticed that the amount of ions adsorbed on the nanorod surface, ionic mobility and the optimal amount of ions in the dispersion vary with the type of precursor salts. The salt concentrations have to be adjusted to provide enough charge on the nanorods and deposit a sufficiently thick holding layer. On the other hand, overdosed precursor salt may lead to unstable dispersion, deteriorated alignment and reduced specific capacitance due to excess Ni content. The deposition voltage and time for optimal alignment (determined by FESEM observation and electrochemical testing) were found to be 800 V and 30 seconds respectively, same as the values for HVEPD with Mg salt as the precursor. Figure 5.3 shows the tilted side views of the aligned nanoforests with the two different holding layers. Dense nanoforests of α -MnO₂ nanorods could be achieved using both the precursor salts. However, it is observed that the alignment and uniformity have been slightly improved in the samples with Ni holding layer. It can be attributed to the avoidance of electric field distortion by the patchy, non-conductive Mg(OH)₂ holding layer in the former case.

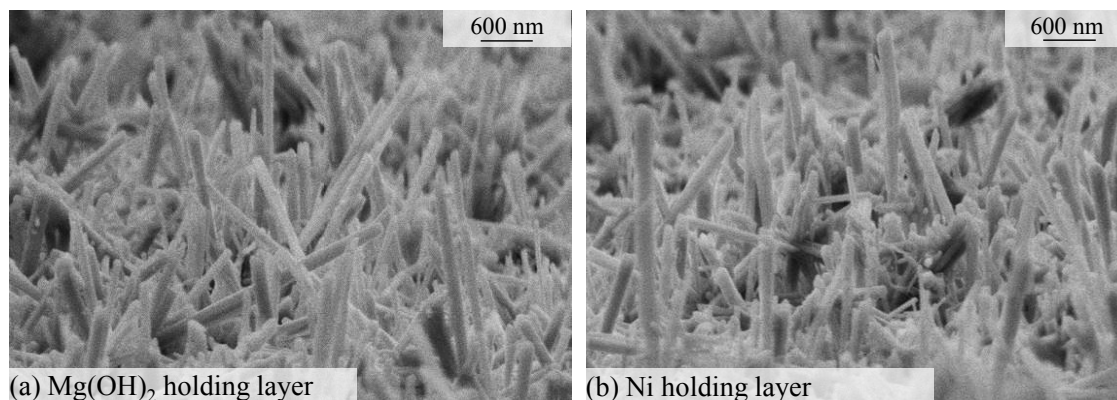


Figure 5.3. FESEM images of aligned nanoforests of α - MnO_2 nanorods with different holding layers.

To further improve the electrical contact, the SS substrates were pretreated to remove any existing oxide layer on the surface. A standard wood's strike¹⁴⁵ was used to remove the oxide layer and deposit a thin layer of Ni on the surface of the SS substrate. Wood's strike is commonly used in electroplating applications to improve mechanical adhesion.¹⁴⁵ In this case, the wood's strike was used to provide better electrical contact between the nanorods and the substrate while improving the adhesion. HVEPD was then conducted on the pretreated substrate to obtain aligned nanoforests with low contact resistance.

5.3.3. Electrochemical characterization:

The effect of improved electrical contact on the electrochemical performance was studied using a two-electrode Swagelok cell. Testing with a two-electrode setup represents the scenario of a practical, packaged cell.¹⁴⁶ Three types of samples were prepared, characterized and compared, as shown in the following table:

Table 5.1. The three types of samples being fabricated and characterized

Sample I	aligned α -MnO ₂ nanorods on pretreated SS substrate with Ni holding layer
Sample II	aligned α -MnO ₂ nanorods on untreated SS substrate with Ni holding layer
Sample III	aligned α -MnO ₂ nanorods on untreated SS substrates with Mg(OH) ₂ holding layer

Figure 5.4a shows the cyclic voltammetry (CV) curves for all three samples measured with a voltage scan rate of 20 mV/s. The CV curves indicated the superior performance of the aligned nanorods with conductive holding layer on the pretreated substrate. The curve for sample I is symmetrical and almost rectangular in shape, resembling that of a near ideal supercapacitor. The CV curve for the sample II has a greater slope with a smaller area under the curve indicating higher contact resistance and lower capacitance, which will be further confirmed in the galvanostatic charge-discharge and electrochemical impedance spectroscopy data to follow. Sample III shows further lack of symmetry and distortion from ideal rectangular shape, which can be attributed to the negative impact of the non-conductive holding layer and untreated substrate. The area under the CV curve for sample I is much greater than that of the other two samples thus qualitatively indicating higher capacitance. The high rate capabilities of Sample I were also verified by measuring the CV curves at different scan rates (Figure 5.4b). There is almost no distortion of the rectangular shape of the CV curves even at a high scan rate of 200 mV/s. The maintenance of the shape of the CV curves at different scan rates indicates good crystalline structure of the nanomaterial and effective electrolyte diffusion in the aligned structure. As a result, the stability of the sample during high rate cycling has opened up its great potential for high power applications to be demonstrated later in this work.

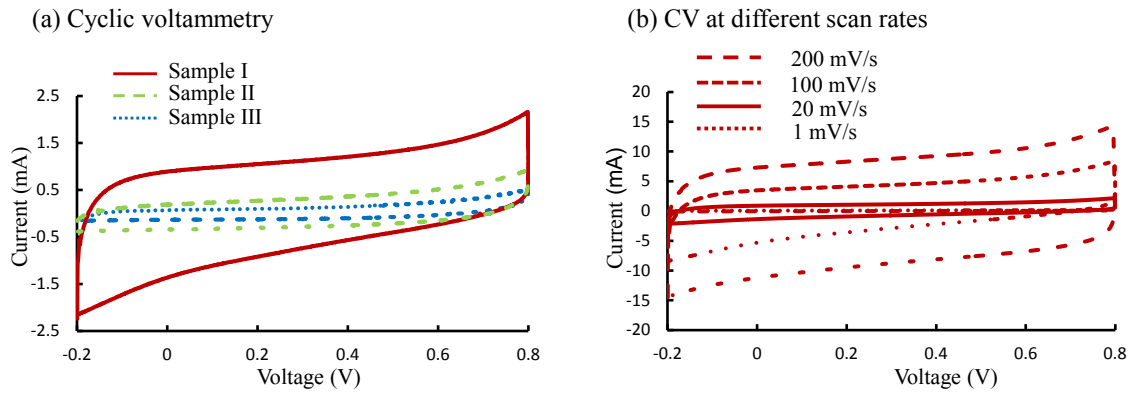


Figure 5.4. (a) Cyclic voltammetry curves at 20 mV/s for the three types of samples defined in Table 5.1 and (b) cyclic voltammetry curves at different scan rates for sample I showing high rate stability.

Galvanostatic charge-discharge was carried out to find the specific capacitance for the three samples. Figure 5.5a shows the typical charge-discharge curves measured at a constant current density of 0.25 mA/cm². The IR drop, as defined as the drop in voltage at the point of current switching, is indicative of the contact resistance of the sample. The capacitance values were calculated using the linear part of the discharge curve after the IR drop. The total areal specific capacitance of the complete two-electrode system was calculated using the relation given below:

$$C_A = C/A = (I \times dt) / (dv \times A) \quad (5.1),$$

where C is the total measured capacitance of the two-electrode system; I is the constant current used during discharge; dt is the discharge time from the near linear part of the discharge curve after the IR drop; dv is the voltage difference during time dt and A is the area of a single electrode.

As compared with Samples II and III, the use of a conductive holding layer and pretreated substrate in Sample I has led to greatly reduced IR drop which indicates a lower contact resistance. The impact of improved contact is seen by a roughly twofold increase in the capacitance values.

Table 5.2. IR drop and capacitance values for the three types of samples defined in Table 5.1

	IR drop (V)	Areal Sp. Cap. ($\mu\text{F}/\text{cm}^2$)
Sample I	0.03	8501
Sample II	0.11	4140
Sample III	0.40	3023

The high rate capability of these samples was checked by characterizing at different current densities. Figure 5.5b shows the variation of C_A (the areal specific capacitance) in response to ~ 40 times increase in the current density, from $0.25 \text{ mA}/\text{cm}^2$ up to $10 \text{ mA}/\text{cm}^2$. The highest retention in C_A was seen for sample I which retained over 93% of its original value. In comparison samples II and III were able to retain around 88% and 78% of their original C_A values. High rate capability of the reported samples, especially sample I, is attributed to the crystallographic structure of the nanomaterials used which allows for faster intercalation/deintercalation of ions. It is known that the material utilization in a pseudo-capacitor decrease with faster charge/discharge as the speed of intercalation/deintercalation may not be able to keep up with the speed of the current. Thus, at high current densities the charge storage phenomena becomes more of a surface phenomenon than redox reactions.¹³⁷ A well-aligned crystalline nanoforest with good electrical contact allows for higher rates of intercalation/deintercalation, better electrolyte access to the material and faster ion/electron transport through the current collector. It has also been reported that the rate capabilities of MnO_2 improves when doped by certain materials¹⁴⁷⁻¹⁴⁸ or when combined with conductive materials in the deposit.¹⁴⁹ In case of samples I and II, Ni ions get adsorbed and deposited over the nanorod surface which may also have contributed to the improvement of the high rate stability of the electrode.

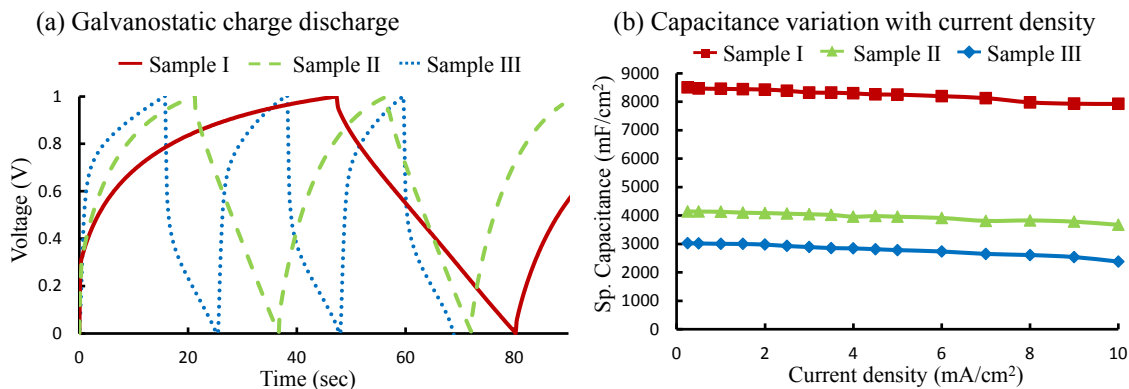


Figure 5.5. (a) Galvanostatic charge discharge curves at 0.25 mA/cm² current for the three types of samples defined in Table 5.1 and (b) Variation of device capacitance with increasing current density for sample I showing high rate stability.

The serial contact resistance of the three samples was characterized using electrochemical impedance spectroscopy (EIS). Figure 5.6 shows the Nyquist plots which have further confirmed the lowest contact resistance of sample I. The first intercept of the semicircle formed in the high frequency range with the x-axis indicates the solution resistance and is the same for all three samples. The sample with the smallest semicircle has the lowest contact resistance which is seen in case of sample I. The EIS is consistent with the IR drop values of the charge-discharge curves. It can thus be concluded with qualitatively confirmation that sample I has the lowest contact resistance.

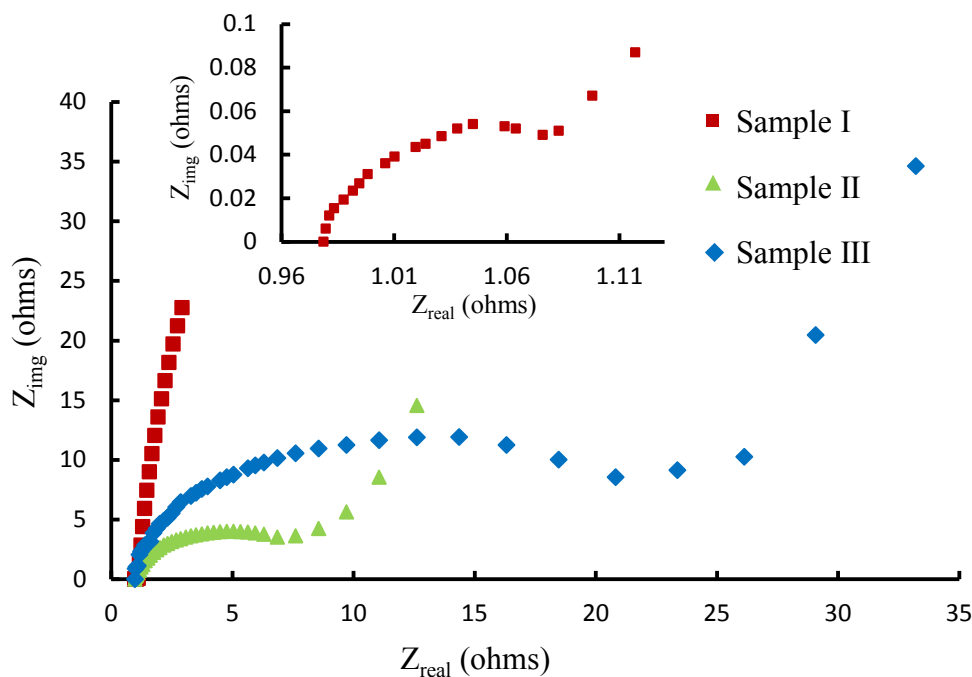


Figure 5.6. Electrochemical impedance spectroscopy at 0V DC bias with small 10 mV AC excitation from 10 mHz to 100 kHz for the three types of samples defined in Table 5.1.

Another important factor in gauging the performance of a supercapacitor electrode is its cycle life. Although EDLCs are known for their excellent durability, substantial loss of capacitance during long cycling (number of cycles) is very common with redox capacitors. The main degradation mechanisms considered for such capacitance fading are the loss of material during cycling and deteriorating contact between with the current collector.^{128, 150} Physiochemical feature evolution of the material during cycling may also cause significant loss of capacitance.^{125, 150} In the reported approach, nanocrystalline structures allow for better structural accommodation with more free space allowance for stress relief during ion intercalation/deintercalation.

The tendency for lattice structure distortion or morphology change during long-term cycling would thus be less in highly crystalline nanomaterials.¹²⁵ At the same time, well-aligned nanoforests and good electrical contact allow for better electrolyte access, little deterioration of contact due to better stress accommodation on the tiny end of

nanorods and less loss of material. As a result, the loss of capacitance over cycling has been dramatically reduced as compared to previously reported for similar nano-MnO₂ systems, which is typically 70% - 85% over 1000 cycles.¹⁵¹ For example, 69.0% retention over 1000 cycles has been reported for nano-MnO₂ system, which was improved to 84.1% by incorporating graphene oxide.¹⁵² Figure 5.7 shows the capacitance fading over 2000 cycles for the three samples. Samples II and III are able to retain about 87% and 81% of their original capacitance. Sample I on the other hand shows excellent capacitance retention of over 92%. The results have confirmed that the cycle stability of a redox capacitor can be dramatically improved by synergistically combine highly-crystallinity of hydrothermal nanorods with alignment and reduction of contact resistance. At the same time, the results also indicate good adhesion between the nanoforests and the substrate.

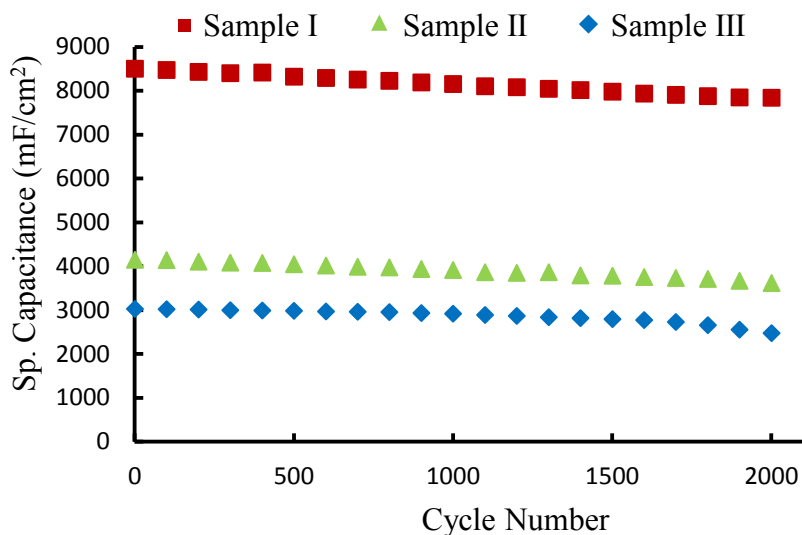


Figure 5.7. Drop of device capacitance over 2000 cycles for the three types of samples defined in Table 5.1.

High rate capability of the aligned α -MnO₂ nanoforests achieved with Sample I implies its great potential for high power applications. The power and energy densities for the three samples were calculated according to the following relations:

$$P_D = IV/2m \quad (5.2);$$

$$E_D = CV^2/2(2m) \quad (5.3).$$

Here I is the constant current at which galvanostatic charge-discharge cycles were run; V is the voltage drop in the near-linear portion of the discharge curve after the IR drop (i.e., attainable cell voltage); m is the mass of active material on one electrode and C is the total capacitance measured from the two-electrode system. The power and energy densities are correlated with each other in the Ragone plots as Figure 5.8 shows, where each data point is calculated from the capacitance and voltage values from a particular discharge current. It is important to note that as the cycling rate (current during cycling) changes, the IR drop tends to change accordingly, leading to a different attainable cell voltage V for the calculation of attainable power density and the corresponding energy density at a particular discharge current. The Ragone plots of all three types of samples are shown in Figure 5.8. Sample I shows an impressive trait to offer high power density without significantly sacrificing its energy density. Particularly, when the power density was increased by ~3500 times from 97 W/Kg to 340 kW/Kg, the energy density only dropped by ~27% from 6.5 Wh/kg to 4.7 Wh/kg. As a result, well-balanced performance on power and energy can be achieved.

For example, to take the high power density before a significant drop in energy density occurs, sample I can achieve a power density of 340 kW/kg with an energy density of 4.7 Wh/kg. In comparison Sample II and III achieved power density of around 104 and 61 kW/kg respectively before severe drop of energy density happens. Such high performance of sample I is a direct result of its capability to retain high attainable cell voltage. For reference, the Ragone plot is also marked with a few examples of the highest performance achieved with MnO₂ nanostructures and their composites in the most recent literature.^{151, 153-155} It is noticed that the 340 kW/kg attainable power density obtained in

this work is about 3 times of that reported in¹⁵¹ and more than 1 order of magnitude higher than the typical values with MnO₂-based systems.¹⁵³⁻¹⁵⁵ The power density achieved in this work is also significantly higher than that of a typical CNT-based EDLC.¹⁵⁶ (For comparison purpose, only room-temperature data of¹⁵⁶ was replotted.) The excellent high-power performance can be again attributed to the combination of highly crystalline redox material, 1D morphology, well aligned dense nanoforests and good electrical contact, especially in sample I.

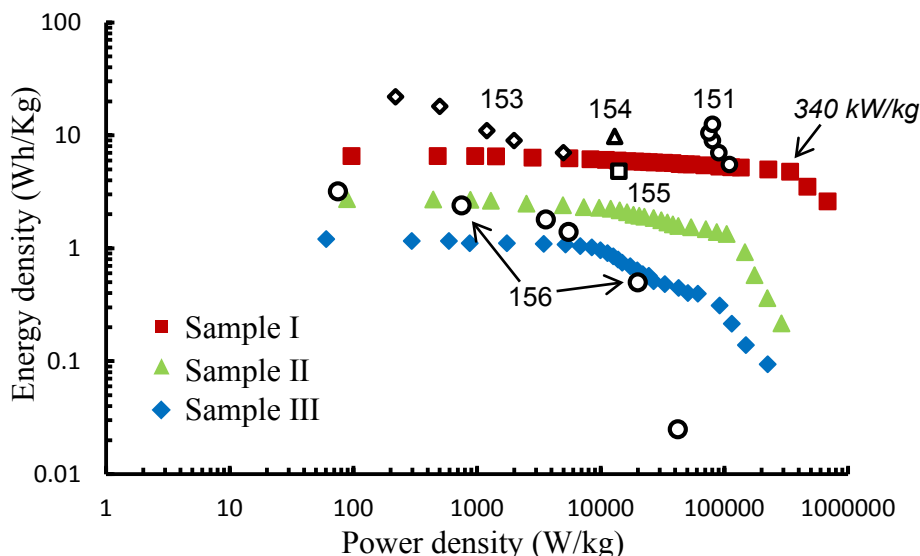


Figure 5.8. Ragone plot for the three types of samples defined in Table 5.1, as compared with a few examples of the highest performance achieved with MnO₂ nanostructures and their composites in the most recent literature. The 340 kW/kg attainable power density obtained in this work is about 3 times of that reported in¹⁵¹ and more than 1 order of magnitude higher than the typical values with MnO₂-based systems.¹⁵³⁻¹⁵⁵ The power density achieved is also significantly higher than that of a typical CNT-based EDLC (room temperature).¹⁵⁶

It should be noted that higher power density can be obtained with hydrous ruthenium oxide (e.g., 1100 kW/Kg at 76.4 Wh/kg).¹⁵⁷ However, the toxicity and high cost of the latter may seriously limit its practical applications. On the other hand, the HVEPD technique gives great flexibility on material and substrate thus enabling the fabrication aligned forests of other high capacitance 1D nanomaterials, including ruthenium oxide nanorods or nanotubes, on highly conductive substrates.

5.3.4. Continuous HVEPD:

In many practical applications, such as electrical vehicles, the size of capacitors needs to be significantly larger than typical lab-scale devices, to provide enough total power and energy.¹⁵⁸⁻¹⁵⁹ The HVEPD approach demonstrated in this work allows for scaling up the electrodes to much larger substrates, due to its mild deposition condition and robust process. To demonstrate such scalability, a continuous HVEPD setup, as illustrated in Figure 5.2, was built to achieve aligned nanoforests on long strips of flexible SS sheets. The flexible SS sheet was mounted on non-conductive rollers and run through the HVEPD dispersion using a DC motor. To achieve a well-aligned nanoforest all through the long substrate, it was important to control three key factors, namely feed speed of substrate, constant concentration of the dispersion and moderate dispersion agitation to ensure uniformity of the dispersion while avoiding disturbance on alignment of the nanorods. The feed speed of flexible SS substrate, together with its total length that is immersed in the dispersion, determines the time of deposition, which should match the optimal deposition time found on the rigid small substrate (30 second in this case). As deposition occurs on the long moving strip, the α -MnO₂ nanorods and Ni²⁺ ions in the HVEPD dispersion get depleted. A multi-channel pump was used to continuously replenish the dispersion while keeping the volume constant. A stock dispersion with a higher concentration was used to replenish the HVEPD dispersion. The concentration of α -MnO₂ nanorods and Ni precursor salt in the stock dispersion was calculated using a simple mass balance:

$$\text{Mass in deposit} + \text{Mass being pumped out} = \text{Mass required to be pumped in} \quad (5.4).$$

During replenishment, the incoming/outgoing fluid flow may agitate the dispersion and thus affect the disposition. Fortunately, under laminar conditions the fluid flow would not cause a torque on the nanorods but only a constant drag force.¹⁰⁷ The alignment will thus not be affected. However, if the nanorods experience significant random motion due to turbulent disturbance, the electric field required to align them would have to be increased to overcome that motion. To avoid such effect, the speed at

which the HVEPD dispersion is replenished was controlled to avoid turbulent disturbance of the HVEPD dispersion. This speed was maintained constant by running the pump at a rate of 8 ml/min. Considering the flow between parallel plates as a plane Couette flow, the maximum Reynold's number (R_e) are calculated to be ~ 4 , far from the turbulent regime $R_e > 4000$. In our previous work,¹⁶⁰ aligned nanoforests of CNTs were achieved on long strips of flexible SS sheets by controlling these key factors at similar range. The quality of nanoforests had been confirmed to be near identical on the large flexible substrate by continuous HVEPD and the small rigid substrate, providing further evidence that no excess torque would act on the nanomaterials. It is thus expected that the alignment and deposition in this work will also not be significantly disturbed by the flow of dispersion, which will be confirmed in the following paragraph.

Figure 5.9a shows part of the long strip placed against a 6-inch ruler. The high-quality deposition over the whole strip has been visually confirmed as a uniform mirror-like finish. The FESEM image in Figure 5.9b shows the alignment of the deposited α -MnO₂ nanorods on a piece cut from the long strip sample. There is no visible deterioration of alignment in the sample obtained by the continuous HVEPD process. Figure 5.9c shows the galvanostatic charge-discharge curves for parts of the long strip with similar area as a small rigid Sample I. It has been tested in a two-electrode setup and evaluated against the galvanostatic charge-discharge curves of Sample I. The specific capacitance and IR drop values found for the long strip were 8496.8 $\mu\text{F}/\text{cm}^2$ and 0.036 V respectively, as compared with 8501.3 $\mu\text{F}/\text{cm}^2$ and 0.038 V measured in Sample I. No substantial deterioration in the electrochemical performance has been observed in the scaled up electrodes. It is thus verified that the continuous HVEPD has the potential to print large-scale electrodes with aligned forests of α -MnO₂ nanorods for various applications, which had been difficult with electrode preparation methods based on templated deposition and many other existing methods.

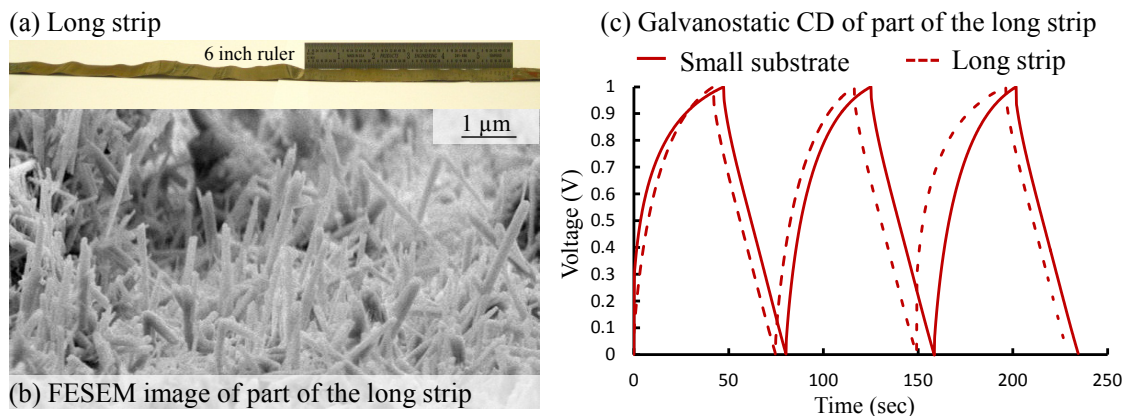


Figure 5.9. (a) Aligned nanoforests of α -MnO₂ nanorods deposited on a long flexible strip (b) FESEM image of part of the long strip (c) Galvanostatic charge discharge curves of part of the long strip compared to the small rigid substrate

In this work, the flexible SS sheets were also first pretreated with a continuous wood's strike. Subsequently, aligned forests of α -MnO₂ nanorods were deposited uniformly on a SS strip of a foot long using the continuous HVEPD setup. The deposition current during continuous HVEPD is monitored and used as an indicator of uniform deposition over the long strip. Figure 5.10 shows the deposition current measured over 3 minutes (the time to deposit on a long strip of about 6 inches) using a digital multimeter connected in series with the continuous HVEPD setup. The current stays pretty constant during the entire deposition process, indicating that the concentration of the HVEPD dispersion is maintained constant. A significant variation in the deposition current would indicate a distortion of deposition, which may be caused by errors such as loss of wire connections, stuck strip, empty tank of stock solution etc. With this simple in-process monitoring mechanism, such kind of errors can be immediately recognized and corrected.

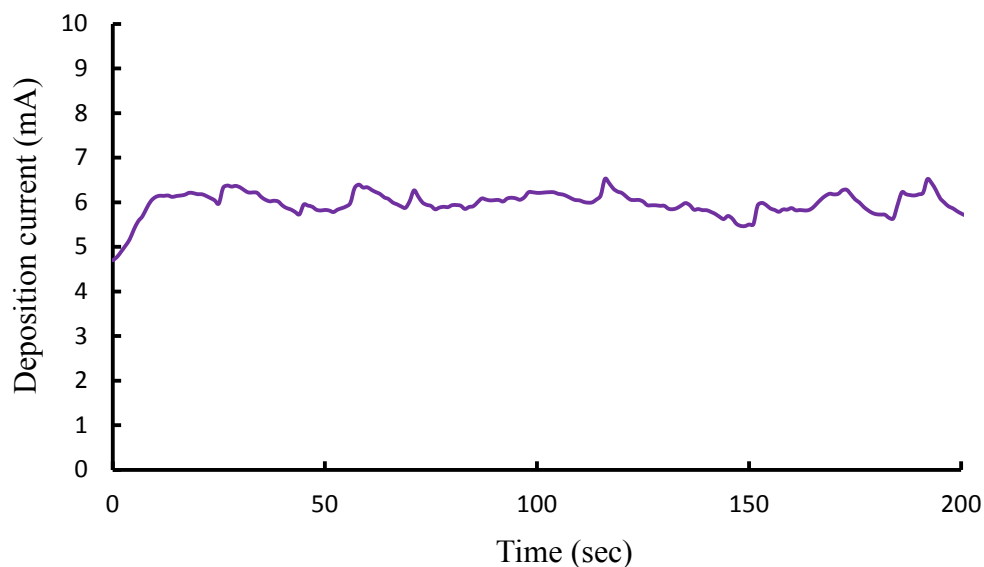


Figure 5.10. Deposition current during continuous HVEPD

5.4. Conclusions

Aligned forests of highly crystalline α -MnO₂ nanorods with excellent electrical contact to the current-collecting substrates have been fabricated by a novel HVEPD process. The effect of improving electrical contact, with a conductive holding layer and pretreated substrate, on the electrochemical performance has been investigated using cyclic voltammetry, galvanostatic charge-discharge and electrochemical impedance spectroscopy. Highly-crystalline α -MnO₂ nanorods, well-aligned nanoforests, good electrical contact and strong adhesion have been simultaneously achieved, yielding a high single electrode capacitance of 200 F/g. Excellent capacitance retention of 92% over 2000 cycles has been observed with the fabricated electrodes.

The high rate capability of the electrode was also confirmed by retaining 93 % of its original specific capacitance in response to ~ 40 times increase in the current density, up to 10 mA/cm². The high rate capability has led to a very high power density of 340 kW/kg at a decent energy density of 4.7 Wh/Kg. The high power density achieved in this work thus provides clear evidence against the common perception that redox capacitors

have to sacrifice power density to achieve higher energy density than EDLCs. HVEPD was also shown as a versatile, simple method to achieve such high performance electrodes on a large scale by continuous printing on long strips of flexible electrodes. A simple in-process monitoring mechanism, based on current measurement, can be employed to continuously detect process errors and ensure the process reliability. Large-scale electrodes produced by continuous HVEPD have been shown to have consistent electrochemical performance as the small rigid samples. The excellent scalability has made the reported approach very promising in practical applications of various cell sizes.

Chapter 6. Further Improvements of Electrochemical Performance and Alignment Quality

6.1. Hybrid deposition for improved electrochemical performance

Further improvement of electrochemical performance was sought and investigated. Hybrid co-deposition of MWCNTs with branches of crystalline α -MnO₂ nanorods were prepared by using HVEPD.⁵⁹ The effects of high conductivity and pseudo-capacitance were thus combined to achieve supercapacitor electrodes with very high power and energy densities. The effect of improving the electrical contact of pseudo-capacitor was also seen in earlier work discussed in chapters 4 and 5. A better conductive network could be provided with highly conductive MWCNTs acting as the support structure for the highly crystalline α -MnO₂ nanorods.^{149, 152} Energy is then stored actively by intercalation/deintercalation of ions in the redox material MnO₂ as well as via electric double layer formation around the high surface area MWCNTs.^{42, 153} Along with the reduced contact resistance due to conductive holding layer, the MWCNTs help to increase the electron transfer rate resulting in stable high rate cycling. High cycle stability is also achieved because of good electrical contact.

Control experiments were conducted to achieve a structured hybrid configuration. High areal capacitances of 20 mF/cm² were found at the optimal HVEPD parameters. With the combination of highly crystalline MnO₂ nanorods, conductive MWCNTs, low contact resistance and a structured branched film it was possible to achieve an exceptionally high power density of around 850 kW/kg with a moderate energy density of about 11 Wh/kg. Such structures have also been shown to retain almost 97% of their original capacitance over 2000 cycles. The high power/energy densities were enabled by the excellent capacitance retention of 96% over high cycling rates from 0.25 mA/cm² to 10 mA/cm². Figure 6.1 shows the Ragone plot for the hybrid deposit on small rigid substrates. Large electrode with such hybrid deposits were fabricated using the roll printing technique discussed earlier, giving similar performance as Figure 6.1 shows.

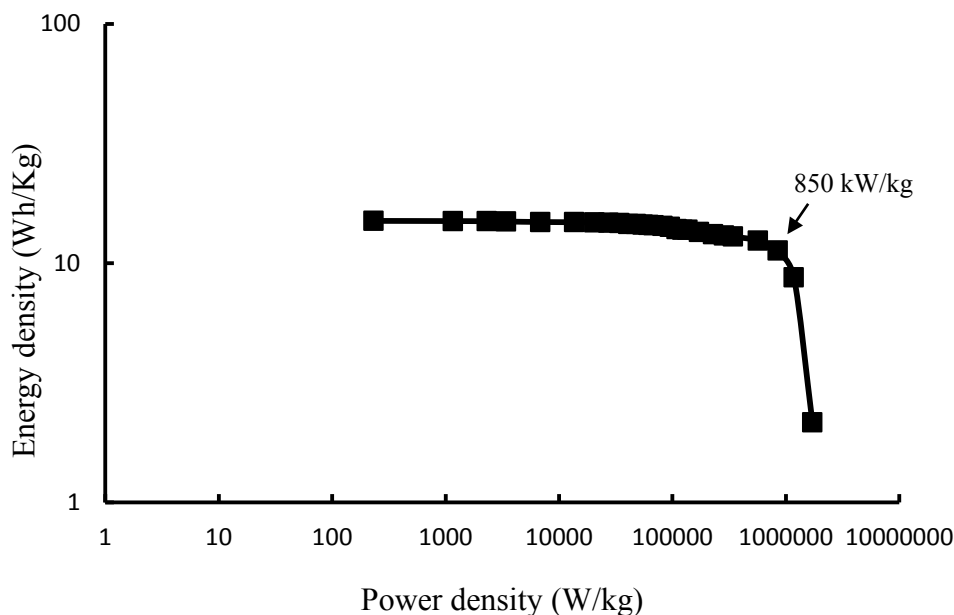


Figure 6.1. Ragone plot of structured hybrid deposits obtained by HVEPD

6.2. AC/DC pulsed deposition for improved alignment quality

Although HVEPD allows for many particles in the dispersion to be vertically aligned, it also results in significant amount of randomly oriented and poorly aligned nanoparticles. A critical issue in HVEPD is to align 1D nanoparticles vertically to the substrate while employing the same electric field to deposit them onto the substrate. However, simultaneous alignment and deposition may not necessary be the best approach for optimal alignment quality.

The high voltage applied for HVEPD not only creates a torque enough to align the nanoparticles but also increases the velocity with which they reach the surface of the electrode.^{44, 61} Under higher velocity, some nanoparticles tend to reach the surface of the electrode before getting a chance to completely align along the electric field direction. This may especially be true for particles that are close to the electrode surface because they may get deposited even before being aligned. In a DC field, the voltage always plays the dual role of simultaneously aligning and accelerating the nanoparticles. Thus the aligned forests achieved by HVEPD are bound to have some nanoparticles with random

orientation, especially at the beginning of the process, as seen in Figure B4a in Appendix B as compared with Figure 3.2b.

This provides scope for further improvement in the quality of the alignment. Higher packing density, larger surface area and more material active sites for electrolyte access can be achieved if the deposition of randomly oriented nanoparticles can be decreased substantially. Such an improvement may be achieved by decoupling the alignment and deposition functionalities of the HVEPD process.

An AC/DC pulsed deposition has been used to investigate the possibility of such an improvement. High quality aligned forests of MWCNTs have been obtained using this method. The MWCNTs were first aligned using an AC voltage at a high frequency. This was immediately followed by the application of a DC voltage for deposition of the aligned MWCNTs.

The application of the AC field involves two major considerations. Firstly, the voltage used should be able to apply a torque enough for alignment of the MWCNTs along the electric field direction. At the same time, a high enough frequency must be used so as to avoid the deposition of the MWCNTs. The MWCNTs can then oscillate between the electrodes to allow more time for improving alignment. At the same time, the concentration of nanomaterials and total time of AC alignment process still need to be controlled so as to avoid bundle formation due to attraction between polarized ends of the MWCNTs. The AC field is then immediately followed by the application of a DC voltage for deposition. A high DC voltage is maintained so as to not lose the alignment due to Brownian motion during the deposition process. This cycle is then repeated several times as continuous deposition cycles to sequentially align and deposit the MWCNTs while avoiding aggregation.

Based on these working principles, the optimal parameters for the AC/DC pulsed deposition technique were found to obtain high quality aligned MWCNT forests. The quality of alignment was characterized by scanning electron microscopy visualization and electrochemical testing. With improvement in alignment quality, the aligned forest

consequently displayed improved electrochemical characteristics. Almost twice the capacitance ($\sim 974 \mu\text{F}/\text{cm}^2$) could be achieved with this approach as compared with the results found by HVEPD in chapter 3 ($\sim 512 \mu\text{F}/\text{cm}^2$). Figure 6.2 shows the variation of capacitance and IR drop with varying number of deposition cycles of AC/DC pulsed EPD. Table 6.1 below gives the values of capacitance obtained at different number of deposition cycles. Less number of deposition cycles result in a sparse deposition and thus lower electrochemical performance. Too much increase in deposition seems to cause excess crowding. This increases the contact resistance and reduces the energy storage capacity of the deposit. Optimal packing is reached when 20 deposition cycles are run resulting in a dense network of well aligned MWCNTs. It is observed that the maximum specific capacitance falls in the region of low contact resistance, although not perfectly coincide with the minimal value of the later.

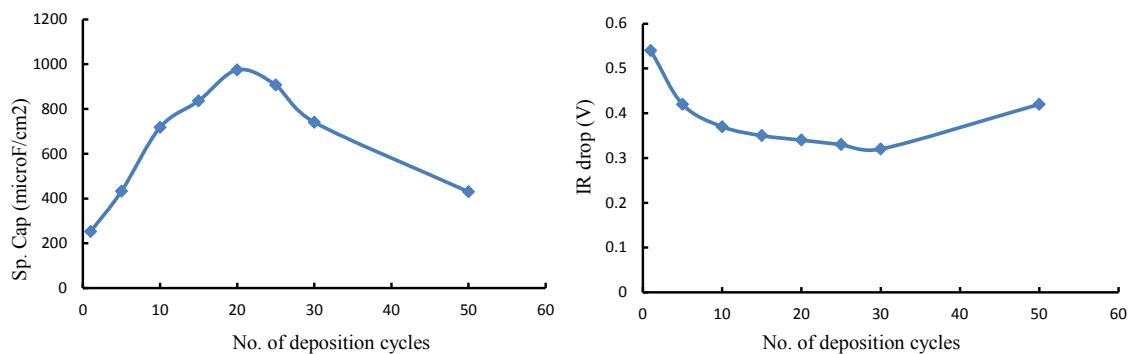


Figure 6.2. Variation of capacitance and IR drop with number of AC/DC pulsed deposition cycles.

Table 6.1. Capacitance and IR drop values for samples obtained by different number of AC/DC pulsed deposition cycles.

Number of AC/DC cycles	IR drop (V)	Areal Sp cap $\mu\text{F}/\text{cm}^2$
1	0.54	252.56
5	0.42	432.82
10	0.37	717.74
15	0.35	836.15
20	0.34	974.36
25	0.33	906.73
30	0.32	740.87
50	0.42	430.08

Chapter 7. Conclusions

In this work, high voltage electrophoretic deposition (HVEPD) is presented as a novel, versatile and generic approach to obtain vertically aligned forests of one-dimensional nanomaterials. Improvements on material chemistry and reduction of contact resistance have enabled the fabrication of high performance electrodes for energy storage applications. Scalable fabrication of such high performance supercapacitor electrodes was successfully achieved to pave the way for practical device construction. Potential of further advancement has been revealed by employing hybrid material systems and enhancing nanoforest quality with pulsed AC/DC deposition.

- (a) HVEPD was used to obtain vertically aligned forests of MWCNTs and β -MnO₂ nanorods on conductive, flexible and transparent electrodes. The working mechanism of HVEPD was thoroughly investigated to confirm that the process was enabled by three key parameters: high deposition voltage for alignment, low dispersion concentration to avoid aggregation and simultaneous formation of a holding layer by electrodeposition for reinforcement of nanoforests. The electrochemical performance of the aligned structures obtained by HVEPD (CNTs – 512 $\mu\text{F}/\text{cm}^2$; β -MnO₂ – 689 $\mu\text{F}/\text{cm}^2$) was shown to be better than that of their randomly oriented counterparts (CNTs – 157 $\mu\text{F}/\text{cm}^2$; β -MnO₂ – 375 $\mu\text{F}/\text{cm}^2$).
- (b) Reduction of contact resistance between the aligned MWCNT forests and the substrate was achieved by using of a conductive holding layer during HVEPD. Capacitance was improved to obtain 846 $\mu\text{F}/\text{cm}^2$ with a Nickel holding layer. The reduced contact resistance was proved to facilitate faster charge/discharge rate and enhance the electrochemical performance. Capacitance was improved
- (c) Scalable nanofabrication was demonstrated by a continuous roll-printing HVEPD process to obtain large-scale (1-foot long) flexible electrodes with aligned MWCNT forests. A setup was designed and employed to achieve such scalability without impeding the alignment process or diminish the electrochemical performance.

- (d) High power redox capacitors were fabricated by HVEPD of highly crystalline α -MnO₂ nanorods. A record high power density of ~ 340 kW/kg was obtained using the HVEPD technique. The synergetic combination of hydrothermally synthesized, highly crystalline α -MnO₂ nanorods, vertically aligned forests and reduced contact resistance enabled high rate and cycling stability thus achieved high power densities without sacrificing the capability for energy storage. The continuous roll printing process was used to fabricate large-scale (1-foot long) flexible electrodes with no deterioration of electrochemical performance indicating the capability for the fabrication of practical, large devices.
- (e) Further improvement of the electrochemical performance was achieved using hybrid material chemistry. Structured deposits of aligned MWCNTs with branches of highly crystalline α -MnO₂ nanorods were obtained by HVEPD. The effects of high conductivity, pseudo-capacitance and low contact resistance were combined to achieve supercapacitor electrodes with exceptional high power density at a moderate energy density. Scale-up fabrication was again employed to produce long strips of flexible electrodes.
- (f) AC/DC pulsed deposition was used to improve the alignment quality of aligned MWCNT forests. Decoupling of alignment and deposition was achieved by sequentially applying an AC field for alignment followed by a DC field for deposition. Improvement of alignment quality was shown to improve electrochemical performance indicating the importance of high quality aligned structures.

Chapter 8. Recommendations for Future Work

The objectives of this work have been primarily focused on the development of an efficient scalable nanofabrication technique for electrochemical energy storage applications. However, the potential of the developed HVEPD method ranges far beyond this scope and can be further explored for many other applications. A few of such prospective applications are discussed in this chapter.

8.1. Field Emission

Carbon nanotubes (CNTs) have been intensively studied for field emission systems applications.^{11, 43} With the decrease in the size of the electron emitters it is possible to obtain displays with higher resolution, smaller form factor and improved energy efficiency. A high-quality array of aligned CNT emitters can ensure very small turn-on voltages and high current outputs as compared to traditional field emitters.¹¹ Significant work has been carried out to fabricate carbon nanotube cathodes for high-performance field emission devices.^{43, 47, 60, 161-164} Flexible and transparent substrates deposited with carbon nanotube film for such application are also being developed.¹⁶⁵ Such application provides a good example of flexible and transparent electronics, which are regarded as an important research and development trend. Facile, scalable fabrication approach to integrate nanomaterials into such applications could immensely benefit the development of displays and many other critical components of flexible electronics.

The capability of obtaining aligned nanoforests on transparent substrates has already been demonstrated earlier in this work. Vertically aligned carbon nanotubes expose their tips for electron emission which makes them excellent candidates for such applications.¹⁶¹ HVEPD can be used as a simple fabrication method for producing large scale transparent field emitters. The effect of low contact resistance could be an added benefit for this purpose. Controlling the density of nanomaterials in the aligned forests and depositing within desired patterns may be some of the factors explored in such a research. Given the generic nature of HVEPD and continuing advances in material

chemistry, other suitable nanomaterials may also be aligned to obtain superior performance.

8.2. Dopamine detection for neural applications

Detection of dopamine (DA), an important neurotransmitter in the human brain, is an interesting and challenging research endeavor. Electrochemical techniques are being investigated for dopamine detection owing to its high sensitivity to electrochemical activity.¹⁶⁶⁻¹⁶⁷ One of the major issues with its detection is the capability to differentiate DA from ascorbic acid (AA). Ascorbic acid exists in high concentrations in the vicinity of dopamine and displays electrochemical activity in a similar range.¹⁶⁷

Several studies have shown the use of CNTs in various neural applications,¹⁶⁸⁻¹⁷⁰ including effective dopamine detection.¹⁶⁶ EPD-based neural probes are explored in this study to provide fabrication compatibility with other components in the system. Figure 8.1 shows the cyclic voltammetry curve with different peaks for ascorbic acid and dopamine in an artificial cerebrospinal fluid (aCSF) environment. HVEPD provides an opportunity for easy deposition of high surface area CNT forests on various types of substrates. This flexibility may be used to design and fabricate in-vitro and in-vivo dopamine sensors.

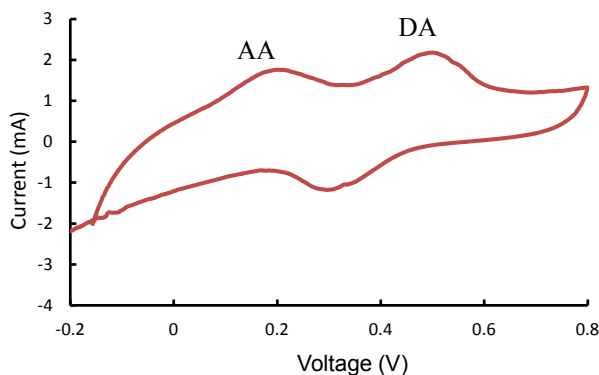


Figure 8.1. CV curve of CNT film in aCSF with dopamine + ascorbic acid electrolyte

8.3. Three-dimensional (3D) structures

In this work, HVEPD has mainly been used to fabricate thin film supercapacitor electrodes. Such electrodes provide the advantages of having low mass content and thereby provide high gravimetric power/energy densities. Certain applications may however require higher areal power/energy densities on a device with a limited footprint, where 3D architectures can be employed to increase the available amount of active material on top of a given area.^{171-172 173}

High aspect ratio 3D structures can pack a lot of active materials in a confined area. A major challenge in achieving 3D architectures is process complexity.¹⁷¹ EPD can be used as the fabrication method to obtain packed randomly oriented deposits for any kind of nanomaterials. To achieve high aspect ratio 3D structures, EPD into microscale patterns will have to be investigated. This may pose some issues due to the concentration of electric field around such small patterns. Randomly oriented nanoparticles as a packed structure may also tend to reduce packing density and increase contact resistance.¹⁷¹ This consequently limits the achievable power/energy densities. An aligned morphology may help solve these issues. HVEPD can be explored to achieve aligned networks of 1D nanomaterials standing on top of subsequent layers. Multiple depositions of aligned forests may be investigated to obtain a 3D network of aligned nanoforests. The porous nature of such a deposit may help enhance electrolyte access and thereby improve electrochemical performance. HVEPD presents the opportunity to seek innovative fabrication structures for obtaining 3D structures with high performance.

References

1. Liu, J.; Cao, G.; Yang, Z.; Wang, D.; Dubois, D.; Zhou, X.; Graff, G. L.; Pederson, L. R.; Zhang, J.-G. Oriented Nanostructures for Energy Conversion and Storage. *ChemSusChem* **2008**, *1* (8-9), 676-697.
2. Dahcredyns <http://www.hybridcarblogger.com/2008/03/supercapacitors-hybrid-vehicle-turbo.html>.
3. Hamilton, T. <http://www.technologyreview.com/news/415773/next-stop-ultracapacitor-buses/>.
4. Sinautec <http://www.youtube.com/watch?v=LYL6NyU1g3k>.
5. Solarey, I. <http://www.amazon.com/Ecolight-Rechargeable-Flashlight-Supercapacitor-4-minute/dp/B002EASSZS>.
6. Chang, S.-w.; Oh, J.; Boles, S. T.; Thompson, C. V. Fabrication of silicon nanopillar-based nanocapacitor arrays. *Applied Physics Letters* **2010**, *96* (15), 153108-153108-3.
7. Kuperman, A.; Aharon, I. Battery-ultracapacitor hybrids for pulsed current loads: A review. *Renewable and Sustainable Energy Reviews* **2011**, *15* (2), 981-992.
8. Camara, M. B.; Gualous, H.; Gustin, F.; Berthon, A. Design and New Control of DC/DC Converters to Share Energy Between Supercapacitors and Batteries in Hybrid Vehicles. *Vehicular Technology, IEEE Transactions on* **2008**, *57* (5), 2721-2735.
9. Ltd., W. C. <http://www.mpoweruk.com/performance.htm>.
10. G. Q. Lu, X. S. Z., *Nanoporous materials Science and engineering*. Imperial College press: London, 2004; Vol. 4.
11. Liming, D.; Ajeeta, P.; Xiaoyi, G.; Zhixin, G.; Luqi, L.; Yong, L.; Daoben, Z. Aligned Nanotubes. *ChemPhysChem* **2003**, *4* (11), 1150-1169.
12. A.N.Goldstein, *Handbook of Nanophase Materials*. Marcel Dekker Inc.: New York, 1997.
13. Arico, A. S.; Bruce, P.; Scrosati, B.; Tarascon, J.-M.; van Schalkwijk, W. Nanostructured materials for advanced energy conversion and storage devices. *Nat Mater* **2005**, *4* (5), 366-377.
14. Nazar, L. F.; Goward, G.; Leroux, F.; Duncan, M.; Huang, H.; Kerr, T.; Gaubicher, J. Nanostructured materials for energy storage. *International Journal of Inorganic Materials* **2001**, *3* (3), 191-200.

15. Winter, M.; Besenhard, J. O. Electrochemical lithiation of tin and tin-based intermetallics and composites. *Electrochimica Acta* **1999**, *45* (1-2), 31-50.
16. Idota, Y.; Kubota, T.; Matsufuji, A.; Maekawa, Y.; Miyasaka, T. Tin-Based Amorphous Oxide: A High-Capacity Lithium-Ion-Storage Material. *Science* **1997**, *276* (5317), 1395-1397.
17. Mao, O.; Dunlap, R. A.; Dahn, J. R. Mechanically Alloyed Sn-Fe(-C) Powders as Anode Materials for Li-Ion Batteries: I. The Sn₂Fe-C System. *Journal of The Electrochemical Society* **1999**, *146* (2), 405-413.
18. Beaulieu, L. Y.; Dahn, J. R. The Reaction of Lithium with Sn-Mn-C Intermetallics Prepared by Mechanical Alloying. *Journal of The Electrochemical Society* **2000**, *147* (9), 3237-3241.
19. Graetz, J.; Ahn, C. C.; Yazami, R.; Fultz, B. Highly Reversible Lithium Storage in Nanostructured Silicon. *Electrochemical and Solid-State Letters* **2003**, *6* (9), A194-A197.
20. Yang, J.; Wang, B. F.; Wang, K.; Liu, Y.; Xie, J. Y.; Wen, Z. S. Si/C Composites for High Capacity Lithium Storage Materials. *Electrochemical and Solid-State Letters* **2003**, *6* (8), A154-A156.
21. Armstrong, A. R.; Armstrong, G.; Canales, J.; García, R.; Bruce, P. G. Lithium-Ion Intercalation into TiO₂-B Nanowires. *Advanced Materials* **2005**, *17* (7), 862-865.
22. Chan, C. K.; Peng, H.; Liu, G.; McIlwrath, K.; Zhang, X. F.; Huggins, R. A.; Cui, Y. High-performance lithium battery anodes using silicon nanowires. *Nat Nano* **2008**, *3* (1), 31-35.
23. Green, M.; Fielder, E.; Scrosati, B.; Wachtler, M.; Moreno, J. S. Structured Silicon Anodes for Lithium Battery Applications. *Electrochemical and Solid-State Letters* **2003**, *6* (5), A75-A79.
24. Li, W.; Wang, X.; Chen, Z.; Waje, M.; Yan Carbon Nanotube Film by Filtration as Cathode Catalyst Support for Proton-Exchange Membrane Fuel Cell. *Langmuir* **2005**, *21* (21), 9386-9389.
25. Srinivasan, S.; Mosdale, R.; Stevens, P.; Yang, C. FUEL CELLS: Reaching the Era of Clean and Efficient Power Generation in the Twenty-First Century. *Annual Review of Energy and the Environment* **1999**, *24* (1), 281-328.
26. Freund, A.; Lang, J.; Lehmann, T.; Starz, K. A. Improved Pt alloy catalysts for fuel cells. *Catalysis Today* **1996**, *27* (1-2), 279-283.

27. Mukerjee, S.; Srinivasan, S.; Soriaga, M. P.; McBreen, J. Role of Structural and Electronic Properties of Pt and Pt Alloys on Electrocatalysis of Oxygen Reduction. *Journal of The Electrochemical Society* **1995**, *142* (5), 1409-1422.
28. Gong, K.; Du, F.; Xia, Z.; Durstock, M.; Dai, L. Nitrogen-Doped Carbon Nanotube Arrays with High Electrocatalytic Activity for Oxygen Reduction. *Science* **2009**, *323* (5915), 760-764.
29. Tang, Y.; Allen, B. L.; Kauffman, D. R.; Star, A. Electrocatalytic Activity of Nitrogen-Doped Carbon Nanotube Cups. *Journal of the American Chemical Society* **2009**, *131* (37), 13200-13201.
30. Lyth, S. M.; Nabae, Y.; Moriya, S.; Kuroki, S.; Kakimoto, M.-a.; Ozaki, J.-i.; Miyata, S. Carbon Nitride as a Nonprecious Catalyst for Electrochemical Oxygen Reduction. *The Journal of Physical Chemistry C* **2009**, *113* (47), 20148-20151.
31. Li, X.; Wang, H.; Robinson, J. T.; Sanchez, H.; Diankov, G.; Dai, H. Simultaneous Nitrogen Doping and Reduction of Graphene Oxide. *Journal of the American Chemical Society* **2009**, *131* (43), 15939-15944.
32. Hwang, Y. J.; Boukai, A.; Yang, P. High Density n-Si/n-TiO₂ Core/Shell Nanowire Arrays with Enhanced Photoactivity. *Nano Letters* **2008**, *9* (1), 410-415.
33. Peng, K.; Xu, Y.; Wu, Y.; Yan, Y.; Lee, S.-T.; Zhu, J. Aligned Single-Crystalline Si Nanowire Arrays for Photovoltaic Applications. *Small* **2005**, *1* (11), 1062-1067.
34. Sharma, P.; Bhatti, T. S. A review on electrochemical double-layer capacitors. *Energy Conversion and Management* **2010**, *51* (12), 2901-2912.
35. Conte, M. Supercapacitors Technical Requirements for New Applications. *Fuel Cells* **2010**, *10* (5), 806-818.
36. Jiang, Y. Q.; Zhou, Q.; Lin, L. In *Planar MEMS Supercapacitor using Carbon Nanotube Forests*, Micro Electro Mechanical Systems, 2009. MEMS 2009. IEEE 22nd International Conference on, 2009; pp 587-590.
37. Liu, C.-y.; Bard, A. J.; Wudl, F.; Weitz, I.; Heath, J. R. Electrochemical Characterization of Films of Single-Walled Carbon Nanotubes and Their Possible Application in Supercapacitors. *Electrochemical and Solid-State Letters* **1999**, *2* (11), 577-578.
38. Chunsheng, D.; et al. High power density supercapacitors using locally aligned carbon nanotube electrodes. *Nanotechnology* **2005**, *16* (4), 350.

39. Kuzuoka, Y.; Wen, C.-j.; Otomo, J.; Ogura, M.; Kobayashi, T.; Yamada, K.; Takahashi, H. Characteristics of MnOx electrochemical capacitors with solid electrolyte (CsHSO4) operated at elevated temperatures. *Solid State Ionics* **2004**, *175* (1-4), 507-510.
40. Lee, C. Y.; Tsai, H. M.; Chuang, H. J.; Li, S. Y.; Lin, P.; Tseng, T. Y. Characteristics and Electrochemical Performance of Supercapacitors with Manganese Oxide-Carbon Nanotube Nanocomposite Electrodes. *Journal of The Electrochemical Society* **2005**, *152* (4), A716-A720.
41. Wang, Y.; Zhitomirsky, I. Electrophoretic Deposition of Manganese Dioxide/Multiwalled Carbon Nanotube Composites for Electrochemical Supercapacitors. *Langmuir* **2009**, *25* (17), 9684-9689.
42. Zhang, H.; Cao, G.; Wang, Z.; Yang, Y.; Shi, Z.; Gu, Z. Growth of Manganese Oxide Nanoflowers on Vertically-Aligned Carbon Nanotube Arrays for High-Rate Electrochemical Capacitive Energy Storage. *Nano Letters* **2008**, *8* (9), 2664-2668.
43. Melechko, A. V.; Merkulov, V. I.; McKnight, T. E.; Guillorn, M. A.; Klein, K. L.; Lowndes, D. H.; Simpson, M. L. Vertically aligned carbon nanofibers and related structures: Controlled synthesis and directed assembly. *Journal of Applied Physics* **2005**, *97* (4), 041301-39.
44. Boccaccini, A. R.; Cho, J.; Roether, J. A.; Thomas, B. J. C.; Jane Minay, E.; Shaffer, M. S. P. Electrophoretic deposition of carbon nanotubes. *Carbon* **2006**, *44* (15), 3149-3160.
45. Liu, Z.; Shen, Z.; Zhu, T.; Hou, S.; Ying, L.; Shi, Z.; Gu, Z. Organizing Single-Walled Carbon Nanotubes on Gold Using a Wet Chemical Self-Assembling Technique. *Langmuir* **2000**, *16* (8), 3569-3573.
46. Youn, S. C.; Jung, D.-H.; Ko, Y. K.; Jin, Y. W.; Kim, J. M.; Jung, H.-T. Vertical Alignment of Carbon Nanotubes Using the Magneto-Evaporation Method. *Journal of the American Chemical Society* **2008**, *131* (2), 742-748.
47. Jin, Y. W.; Jung, J. E.; Park, Y. J.; Choi, J. H.; Jung, D. S.; Lee, H. W.; Park, S. H.; Lee, N. S.; Kim, J. M.; Ko, T. Y.; Lee, S. J.; Hwang, S. Y.; You, J. H.; Yoo, J.-B.; Park, C.-Y. Triode-type field emission array using carbon nanotubes and a conducting polymer composite prepared by electrochemical polymerization. *Journal of Applied Physics* **2002**, *92* (2), 1065-1068.
48. Liu, Y.-T.; Xie, X.-M.; Gao, Y.-F.; Feng, Q.-P.; Guo, L.-R.; Wang, X.-H.; Ye, X.-Y. Polymer-assisted assembly of carbon nanotubes via a template-based method. *Carbon* **2006**, *44* (3), 599-602.
49. Hirscher, M. Nanoscale materials for energy storage. *Materials Science and Engineering B* **2004**, *108* (1-2), 1-1.

50. Dai, L.; Patil, A.; Gong, X.; Guo, Z.; Liu, L.; Liu, Y.; Zhu, D. Aligned Nanotubes. *ChemPhysChem* **2003**, *4* (11), 1150-1169.
51. Reddy, A. L. M.; Shaijumon, M. M.; Gowda, S. R.; Ajayan, P. M. Coaxial MnO₂/Carbon Nanotube Array Electrodes for High-Performance Lithium Batteries. *Nano Letters* **2009**, *9* (3), 1002-1006.
52. Besra, L.; Liu, M. A review on fundamentals and applications of electrophoretic deposition (EPD). *Progress in Materials Science* **2007**, *52* (1), 1-61.
53. Van der Biest, O. O.; Vandeperre, L. J. ELECTROPHORETIC DEPOSITION OF MATERIALS. *Annual Review of Materials Science* **1999**, *29* (1), 327-352.
54. Besra, L.; Liu, M. A review on fundamentals and applications of electrophoretic deposition (EPD). *Prog. Mater. Sci.* **2007**, *52* (1), 1-61.
55. Zhang, X.; Yang, W. Electrophoretic Deposition of a Thick Film of Layered Manganese Oxide. *Chemistry Letters* **2007**, *36* (10), 1228-1229.
56. Li, J.; Zhitomirsky, I. Electrophoretic deposition of manganese oxide nanofibers. *Materials Chemistry and Physics* **2008**, *112* (2), 525-530.
57. Thomas, B. J. C.; Boccaccini, A. R.; Shaffer, M. S. P. Multi-Walled Carbon Nanotube Coatings Using Electrophoretic Deposition (EPD). *Journal of the American Ceramic Society* **2005**, *88* (4), 980-982.
58. Grandfield, K.; Sun, F.; FitzPatrick, M.; Cheong, M.; Zhitomirsky, I. Electrophoretic deposition of polymer-carbon nanotube-hydroxyapatite composites. *Surface and Coatings Technology* **2009**, *203* (10-11), 1481-1487.
59. Li, J.; Zhitomirsky, I. Electrophoretic deposition of manganese dioxide-carbon nanotube composites. *Journal of Materials Processing Technology* **2009**, *209* (7), 3452-3459.
60. Choi, W. B.; Jin, Y. W.; Kim, H. Y.; Lee, S. J.; Yun, M. J.; Kang, J. H.; Choi, Y. S.; Park, N. S.; Lee, N. S.; Kim, J. M. Electrophoresis deposition of carbon nanotubes for triode-type field emission display. *Applied Physics Letters* **2001**, *78* (11), 1547-1549.
61. Cho, J.; Konopka, K.; Rozniatowski, K.; García-Lecina, E.; Shaffer, M. S. P.; Boccaccini, A. R. Characterisation of carbon nanotube films deposited by electrophoretic deposition. *Carbon* **2009**, *47* (1), 58-67.
62. Nakayama, Y.; Akita, S. Field-emission device with carbon nanotubes for a flat panel display. *Synth. Met.* **2001**, *117* (1-3), 207-210.

63. Coll, B. F.; Dean, K. A.; O'Rourke, S. M.; Stainer, M.; Subrahmanyam, R.; Talin, A. A. FED cathode structure using electrophoretic deposition and method of fabrication. U.S. Patent 6902658, 2005.
64. Quale, S. L.; Talbot, J. B. Electrophoretic Deposition of Substrate-Normal-Oriented Single-Walled Carbon Nanotube Structures. *J. Electrochem. Soc.* **2007**, *154* (8), K25-K28.
65. Jin, Y. W.; Jung, J. E.; Park, Y. J.; Choi, J. H.; Jung, D. S.; Lee, H. W.; Park, S. H.; Lee, N. S.; Kim, J. M.; Ko, T. Y.; Lee, S. J.; Hwang, S. Y.; You, J. H.; Yoo, J.-B.; Park, C.-Y. Triode-type field emission array using carbon nanotubes and a conducting polymer composite prepared by electrochemical polymerization. *J. Appl. Phys.* **2002**, *92* (2), 1065-1068.
66. Kim, S.-K.; Lee, H.; Tanaka, H.; Weiss, P. S. Vertical Alignment of Single-Walled Carbon Nanotube Films Formed by Electrophoretic Deposition. *Langmuir* **2008**, *24* (22), 12936-12942.
67. Grandfield, K.; Sun, F.; FitzPatrick, M.; Cheong, M.; Zhitomirsky, I. Electrophoretic deposition of polymer-carbon nanotube-hydroxyapatite composites. *Surf. Coat. Technol.* **2009**, *203* (10-11), 1481-1487.
68. Xiao, J.; Dunham, S.; Liu, P.; Zhang, Y.; Kocabas, C.; Moh, L.; Huang, Y.; Hwang, K.-C.; Lu, C.; Huang, W.; Rogers, J. A. Alignment Controlled Growth of Single-Walled Carbon Nanotubes on Quartz Substrates. *Nano Letters* **2009**, *9* (12), 4311-4319.
69. Chicat, F.; Cho, J.; Schaab, S.; Brusatin, G.; Colombo, P.; Roether, J. A.; Boccaccini, A. R. Carbon nanotube deposits and CNT/SiO₂ composite coatings by electrophoretic deposition. *Adv. Appl. Ceram.* **2007**, *106*, 186-195.
70. Kamat, P. V.; Thomas, K. G.; Barazzouk, S.; Girishkumar, G.; Vinodgopal, K.; Meisel, D. Self-Assembled Linear Bundles of Single Wall Carbon Nanotubes and Their Alignment and Deposition as a Film in a dc Field. *Journal of the American Chemical Society* **2004**, *126* (34), 10757-10762.
71. Han, S. P.; Yang, S.-M. Orientation Distribution and Electrophoretic Motions of Rod-like Particles in a Capillary. *J. Colloid Interface Sci.* **1996**, *177* (1), 132-142.
72. Fleming, G. R.; Ratner, M. A. Grand challenges in basic energy sciences. *Phys. Today* **2008**, *61* (7), 28-33.
73. Liu, J.; Cao, G.; Yang, Z.; Wang, D.; Dubois, D.; Graff, X. Z. G. L.; Pederson, L. R.; Zhang, J.-G. Oriented Nanostructures for Energy Conversion and Storage. *ChemSusChem* **2008**, *1* (8-9), 676-697.

74. Zhang, H.; Cao, G.; Yang, Y.; Gu, Z. Comparison Between Electrochemical Properties of Aligned Carbon Nanotube Array and Entangled Carbon Nanotube Electrodes. *J. Electrochem. Soc.* **2008**, *155* (2), K19-K22.
75. Futaba, D. N.; Hata, K.; Yamada, T.; Hiraoka, T.; Hayamizu, Y.; Kakudate, Y.; Tanaike, O.; Hatori, H.; Yumura, M.; Iijima, S. Shape-engineerable and highly densely packed single-walled carbon nanotubes and their application as super-capacitor electrodes. *Nat. Mater.* **2006**, *5* (12), 987-994.
76. Iijima, S. Helical microtubules of graphitic carbon. *Nature* **1991**, *354* (6348), 56-58.
77. Li, W. Z.; Xie, S. S.; Qian, L. X.; Chang, B. H.; Zou, B. S.; Zhou, W. Y.; Zhao, R. A.; Wang, G. Large-Scale Synthesis of Aligned Carbon Nanotubes. *Science* **1996**, *274* (5293), 1701-1703.
78. Melechko, A. V.; Merkulov, V. I.; McKnight, T. E.; Guillorn, M. A.; Klein, K. L.; Lowndes, D. H.; Simpson, M. L. Vertically aligned carbon nanofibers and related structures: Controlled synthesis and directed assembly. *J. Appl. Phys.* **2005**, *97* (4), 041301-39.
79. Fan, S. Self-oriented regular arrays of carbon nanotubes and their field emission properties. *Science* **1999**, *283*, 512-514.
80. Lau, K. K. S.; Bico, J.; Teo, K. B. K.; Chhowalla, M.; Amaratunga, G. A. J.; Milne, W. I.; McKinley, G. H.; Gleason, K. K. Superhydrophobic Carbon Nanotube Forests. *Nano Lett.* **2003**, *3* (12), 1701-1705.
81. Sun, T.; Wang, G.; Liu, H.; Feng, L.; Jiang, L.; Zhu, D. Control over the Wettability of an Aligned Carbon Nanotube Film. *J. Am. Chem. Soc.* **2003**, *125* (49), 14996-14997.
82. Niu, C.; Sichel, E. K.; Hoch, R.; Moy, D.; Tennent, H. High power electrochemical capacitors based on carbon nanotube electrodes. *Appl. Phys. Lett.* **1997**, *70* (11), 1480-1482.
83. Qu, L.; Dai, L.; Stone, M.; Xia, Z.; Wang, Z. L. Carbon Nanotube Arrays with Strong Shear Binding-On and Easy Normal Lifting-Off. *Science* **2008**, *322* (5899), 238-242.
84. Wang, Z. L. Zinc oxide nanostructures: growth, properties and applications. *J. Phys.: Condens. Matter* **2004**, *16*, R829-R858.
85. Hochbaum, A. I.; Yang, P. Semiconductor Nanowires for Energy Conversion. *Chem. Rev.* **2009**, *110* (1), 527-546.
86. Nessim, G. D.; Seita, M.; O'Brien, K. P.; Hart, A. J.; Bonaparte, R. K.; Mitchell, R. R.; Thompson, C. V. Low Temperature Synthesis of Vertically Aligned Carbon

Nanotubes with Electrical Contact to Metallic Substrates Enabled by Thermal Decomposition of the Carbon Feedstock. *Nano Lett.* **2009**, *9* (10), 3398-3405.

87. Talapatra, S.; Kar, S.; Pal, S. K.; Vajtai, R.; Ci, L.; Victor, P.; Shaijumon, M. M.; Kaur, S.; Nalamasu, O.; Ajayan, P. M. Direct growth of aligned carbon nanotubes on bulk metals. *Nat. Nanotechnol.* **2006**, *1* (2), 112-116.

88. Jung, Y. J.; Kar, S.; Talapatra, S.; Soldano, C.; Viswanathan, G.; Li, X.; Yao, Z.; Ou, F. S.; Avadhanula, A.; Vajtai, R.; Curran, S.; Nalamasu, O.; Ajayan, P. M. Aligned Carbon Nanotube-Polymer Hybrid Architectures for Diverse Flexible Electronic Applications. *Nano Lett.* **2006**, *6* (3), 413-418.

89. Cao, Q.; Kim, H.-s.; Pimparkar, N.; Kulkarni, J. P.; Wang, C.; Shim, M.; Roy, K.; Alam, M. A.; Rogers, J. A. Medium-scale carbon nanotube thin-film integrated circuits on flexible plastic substrates. *Nature* **2008**, *454* (7203), 495-500.

90. Nomura, K.; Ohta, H.; Takagi, A.; Kamiya, T.; Hirano, M.; Hosono, H. Room-temperature fabrication of transparent flexible thin-film transistors using amorphous oxide semiconductors. *Nature* **2004**, *432* (7016), 488-492.

91. Ishikawa, F. N.; Chang, H.-k.; Ryu, K.; Chen, P.-c.; Badmaev, A.; Gomez De Arco, L.; Shen, G.; Zhou, C. Transparent Electronics Based on Transfer Printed Aligned Carbon Nanotubes on Rigid and Flexible Substrates. *ACS Nano* **2008**, *3* (1), 73-79.

92. Rogers, J. A.; Someya, T.; Huang, Y. Materials and Mechanics for Stretchable Electronics. *Science* **2010**, *327* (5973), 1603-1607.

93. Hu, L.; Pasta, M.; Mantia, F. L.; Cui, L.; Jeong, S.; Deshazer, H. D.; Choi, J. W.; Han, S. M.; Cui, Y. Stretchable, Porous, and Conductive Energy Textiles. *Nano Lett.* **2010**, *10* (2), 708-714.

94. Youn, S. C.; Jung, D.-H.; Ko, Y. K.; Jin, Y. W.; Kim, J. M.; Jung, H.-T. Vertical Alignment of Carbon Nanotubes Using the Magneto-Evaporation Method. *J. Am. Chem. Soc.* **2008**, *131* (2), 742-748.

95. Corni, I.; Ryan, M. P.; Boccaccini, A. R. Electrophoretic deposition: From traditional ceramics to nanotechnology. *J. Eur. Ceram. Soc.* **2008**, *28* (7), 1353-1367.

96. Van der Biest, O. O.; Vandeperre, L. J. ELECTROPHORETIC DEPOSITION OF MATERIALS. *Annu. Rev. Mater. Sci.* **1999**, *29* (1), 327-352.

97. Wang, Y.; Zhitomirsky, I. Electrophoretic Deposition of Manganese Dioxide-Multiwalled Carbon Nanotube Composites for Electrochemical Supercapacitors. *Langmuir* **2009**, *25* (17), 9684-9689.

98. Thess, A.; Roland, L.; Nikolaev, P.; Dai, H.; Petit, P.; Robert, J.; Xu, C.; Lee, Y. H.; Seong Gon, K.; Rinzler, A. G.; Colbert, D. T.; Scuseria, G. E.; Tomanek, D.; Fischer, J. E.; Smalley, R. E. Crystalline Ropes of Metallic Carbon Nanotubes. *Science* **1996**, 273 (5274), 483-487.
99. Kamat, P. V.; Thomas, K. G.; Barazzouk, S.; Girishkumar, G.; Vinodgopal, K.; Meisel, D. Self-Assembled Linear Bundles of Single Wall Carbon Nanotubes and Their Alignment and Deposition as a Film in a dc Field. *J. Am. Chem. Soc.* **2004**, 126 (34), 10757-10762.
100. Zou, G.; Liu, R.; Chen, W. Highly textural lamellar mesostructured magnesium hydroxide via a cathodic electrodeposition process. *Mater. Lett.* **2007**, 61 (10), 1990-1993.
101. Santhanagopalan, S.; Teng, F.; Meng, D. D. In *IC-Compatible Deposition of Vertically-Aligned CNT Forests for Micro-Supercapacitors*, Proceedings of the 9th Power MEMS International Workshop, Washington DC, USA, December 1-4; Washington DC, USA, 2009; pp 593-596.
102. Hamaker, H. C. Formation of deposit by electrophoresis. *Trans. Faraday Soc.* **1940**, 36, 279-287.
103. Santhanagopalan, S.; Teng, F.; Meng, D. D. High-Voltage Electrophoretic Deposition for Vertically Aligned Forests of One-Dimensional Nanoparticles. *Langmuir* **2010**, 27 (2), 561-569.
104. Ren, Z. F.; Huang, Z. P.; Xu, J. W.; Wang, J. H.; Bush, P.; Siegal, M. P.; Provencio, P. N. Synthesis of Large Arrays of Well-Aligned Carbon Nanotubes on Glass. *Science* **1998**, 282 (5391), 1105-1107.
105. Bajpai, V.; Dai, L.; Ohashi, T. Large-Scale Synthesis of Perpendicularly Aligned Helical Carbon Nanotubes. *Journal of the American Chemical Society* **2004**, 126 (16), 5070-5071.
106. Sarkar, P.; Nicholson, P. S. Electrophoretic Deposition (EPD): Mechanisms, Kinetics, and Application to Ceramics. *Journal of the American Ceramic Society* **1996**, 79 (8), 1987-2002.
107. Kleinstreuer, C., *Modern fluid dynamics: basic theory and selected applications in macro- and micro-fluidics* Springer 2010; Vol. 87.
108. Yoda, S.; Ishihara, K. The advent of battery-based societies and the global environment in the 21st century. *Journal of Power Sources* **1999**, 81-82 (0), 162-169.
109. Kötz, R.; Carlen, M. Principles and applications of electrochemical capacitors. *Electrochimica Acta* **2000**, 45 (15-16), 2483-2498.

110. Sarangapani, S.; Tilak, B. V.; Chen, C. P. Materials for Electrochemical Capacitors. *Journal of The Electrochemical Society* **1996**, *143* (11), 3791-3799.
111. Reddy, R. N.; Reddy, R. G. Synthesis and electrochemical characterization of amorphous MnO₂ electrochemical capacitor electrode material. *Journal of Power Sources* **2004**, *132* (1-2), 315-320.
112. Burke, A. Ultracapacitors: why, how, and where is the technology. *Journal of Power Sources* **2000**, *91* (1), 37-50.
113. An, K. H.; Kim, W. S.; Park, Y. S.; Moon, J. M.; Bae, D. J.; Lim, S. C.; Lee, Y. S.; Lee, Y. H. Electrochemical Properties of High-Power Supercapacitors Using Single-Walled Carbon Nanotube Electrodes. *Advanced Functional Materials* **2001**, *11* (5), 387-392.
114. Frackowiak, E.; Béguin, F. Carbon materials for the electrochemical storage of energy in capacitors. *Carbon* **2001**, *39* (6), 937-950.
115. Malinauskas, A.; et al. Conducting polymer-based nanostructured materials: electrochemical aspects. *Nanotechnology* **2005**, *16* (10), R51.
116. Peng, C.; Jin, J.; Chen, G. Z. A comparative study on electrochemical co-deposition and capacitance of composite films of conducting polymers and carbon nanotubes. *Electrochimica Acta* **2007**, *53* (2), 525-537.
117. Sugimoto, W.; Yokoshima, K.; Murakami, Y.; Takasu, Y. Charge storage mechanism of nanostructured anhydrous and hydrous ruthenium-based oxides. *Electrochimica Acta* **2006**, *52* (4), 1742-1748.
118. Young Rack, A.; et al. Electrochemical capacitors based on electrodeposited ruthenium oxide on nanofibre substrates. *Nanotechnology* **2006**, *17* (12), 2865.
119. Jiang, J.; Kucernak, A. Electrochemical supercapacitor material based on manganese oxide: preparation and characterization. *Electrochimica Acta* **2002**, *47* (15), 2381-2386.
120. Nelson, P. A.; Owen, J. R. A High-Performance Supercapacitor/Battery Hybrid Incorporating Templated Mesoporous Electrodes. *Journal of The Electrochemical Society* **2003**, *150* (10), A1313-A1317.
121. Hibino, M.; Abe, K.; Mochizuki, M.; Miyayama, M. Amorphous titanium oxide electrode for high-rate discharge and charge. *Journal of Power Sources* **2004**, *126* (1-2), 139-143.
122. Hu, C.-C.; Huang, C.-M.; Chang, K.-H. Anodic deposition of porous vanadium oxide network with high power characteristics for pseudocapacitors. *Journal of Power Sources* **2008**, *185* (2), 1594-1597.

123. Wang, G.; Zhang, L.; Zhang, J. A review of electrode materials for electrochemical supercapacitors. *Chemical Society Reviews* **2012**, *41* (2), 797-828.
124. Xu, C.; Kang, F.; Li, B.; Du, H. Recent progress on manganese dioxide based supercapacitors. *Journal of Materials Research* **2010**, *25* (08), 1421-1432.
125. Babakhani, B.; Ivey, D. G. Anodic deposition of manganese oxide electrodes with rod-like structures for application as electrochemical capacitors. *Journal of Power Sources* **2010**, *195* (7), 2110-2117.
126. Zhao, X.; Sanchez, B. M.; Dobson, P. J.; Grant, P. S. The role of nanomaterials in redox-based supercapacitors for next generation energy storage devices. *Nanoscale* **2011**, *3* (3), 839-855.
127. Xia, H.; Feng, J.; Wang, H.; Lai, M. O.; Lu, L. MnO₂ nanotube and nanowire arrays by electrochemical deposition for supercapacitors. *Journal of Power Sources* **2010**, *195* (13), 4410-4413.
128. Devaraj, S.; Munichandraiah, N. Effect of Crystallographic Structure of MnO₂ on Its Electrochemical Capacitance Properties. *The Journal of Physical Chemistry C* **2008**, *112* (11), 4406-4417.
129. Jeyagowry, T. S.; Jian, D.; Gan Geok, J.; Effendi, W.; Low Qui Hui, E. Template-free low temperature hydrothermal synthesis and characterization of rod-shaped manganese oxyhydroxides and manganese oxides. *Nanotechnology* **2007**, *18* (2), 025601.
130. In, H. J.; Kumar, S.; Shao-Horn, Y.; Barbastathis, G. Origami fabrication of nanostructured, three-dimensional devices: Electrochemical capacitors with carbon electrodes. *Applied Physics Letters* **2006**, *88* (8), 083104-3.
131. Toupin, M.; Brousse, T.; Bélanger, D. Charge Storage Mechanism of MnO₂ Electrode Used in Aqueous Electrochemical Capacitor. *Chemistry of Materials* **2004**, *16* (16), 3184-3190.
132. Kim, H.; Popov, B. N. Synthesis and Characterization of MnO₂-Based Mixed Oxides as Supercapacitors. *Journal of The Electrochemical Society* **2003**, *150* (3), D56-D62.
133. Pang, S.-C.; Anderson, M. A. Novel electrode materials for electrochemical capacitors: Part II. Material characterization of sol-gel-derived and electrodeposited manganese dioxide thin films. *Journal of Materials Research* **2000**, *15* (10), 2096-2106.
134. Wang, X.; Wang, X.; Huang, W.; Sebastian, P. J.; Gamboa, S. Sol-gel template synthesis of highly ordered MnO₂ nanowire arrays. *Journal of Power Sources* **2005**, *140* (1), 211-215.

135. Xu, C.-L.; Bao, S.-J.; Kong, L.-B.; Li, H.; Li, H.-L. Highly ordered MnO₂ nanowire array thin films on Ti/Si substrate as an electrode for electrochemical capacitor. *Journal of Solid State Chemistry* **2006**, *179* (5), 1351-1355.
136. Xu, M.; Kong, L.; Zhou, W.; Li, H. Hydrothermal Synthesis and Pseudocapacitance Properties of α -MnO₂ Hollow Spheres and Hollow Urchins. *The Journal of Physical Chemistry C* **2007**, *111* (51), 19141-19147.
137. Subramanian, V.; Zhu, H.; Vajtai, R.; Ajayan, P. M.; Wei, B. Hydrothermal Synthesis and Pseudocapacitance Properties of MnO₂ Nanostructures. *The Journal of Physical Chemistry B* **2005**, *109* (43), 20207-20214.
138. Chen, X.; Li, X.; Jiang, Y.; Shi, C.; Li, X. Rational synthesis of [alpha]-MnO₂ and [gamma]-Mn₂O₃ nanowires with the electrochemical characterization of [alpha]-MnO₂ nanowires for supercapacitor. *Solid State Communications* **2005**, *136* (2), 94-96.
139. Yang, Y.; Xiao, L.; Zhao, Y.; Wang, F. Hydrothermal synthesis and electrochemical characterization of α -MnO₂ nanorods as cathode material for lithium batteries. *Int. J. Electrochem. Sci.* **2008**, *3* (1), 67-74.
140. Subramanian, V.; Zhu, H.; Wei, B. Nanostructured MnO₂: Hydrothermal synthesis and electrochemical properties as a supercapacitor electrode material. *Journal of Power Sources* **2006**, *159* (1), 361-364.
141. Brousse, T.; Toupin, M.; Dugas, R.; Athouel, L.; Crosnier, O.; Belanger, D. Crystalline MnO₂ as Possible Alternatives to Amorphous Compounds in Electrochemical Supercapacitors. *Journal of The Electrochemical Society* **2006**, *153* (12), A2171-A2180.
142. Wang, X.; Li, Y. Synthesis and Formation Mechanism of Manganese Dioxide Nanowires/Nanorods. *Chemistry – A European Journal* **2003**, *9* (1), 300-306.
143. Liang, S.; Teng, F.; Bulgan, G.; Zong, R.; Zhu, Y. Effect of Phase Structure of MnO₂ Nanorod Catalyst on the Activity for CO Oxidation. *The Journal of Physical Chemistry C* **2008**, *112* (14), 5307-5315.
144. Han, S. P.; Yang, S.-M. Orientation Distribution and Electrophoretic Motions of Rod-like Particles in a Capillary. *Journal of Colloid and Interface Science* **1996**, *177* (1), 132-142.
145. Dini, J. W., *Electrodeposition: The Materials Science of Coatings and Substrates*. Noyes Publications: 1993.
146. Stoller, M. D.; Ruoff, R. S. Best practice methods for determining an electrode material's performance for ultracapacitors. *Energy & Environmental Science* **2010**, *3* (9), 1294-1301.

147. Rajendra Prasad, K.; Miura, N. Electrochemically synthesized MnO₂-based mixed oxides for high performance redox supercapacitors. *Electrochemistry Communications* **2004**, *6* (10), 1004-1008.
148. Ye, Z. G.; Zhou, X. L.; Meng, H. M.; Hua, X. Z.; Dong, Y. H.; Zou, A. H. The Electrochemical Characterization of Electrochemically Synthesized MnO₂-Based Mixed Oxides for Supercapacitor Applications. *Advanced Materials Research* **2011**, 287-290, 1290-1298.
149. Lei, Y.; Daffos, B.; Taberna, P. L.; Simon, P.; Favier, F. MnO₂-coated Ni nanorods: Enhanced high rate behavior in pseudo-capacitive supercapacitor. *Electrochimica Acta* **2010**, *55* (25), 7454-7459.
150. Wei, W.; Cui, X.; Chen, W.; Ivey, D. G. Electrochemical cyclability mechanism for MnO₂ electrodes utilized as electrochemical supercapacitors. *Journal of Power Sources* **2009**, *186* (2), 543-550.
151. Yu, G.; Hu, L.; Vosgueritchian, M.; Wang, H.; Xie, X.; McDonough, J. R.; Cui, X.; Cui, Y.; Bao, Z. Solution-Processed Graphene/MnO₂ Nanostructured Textiles for High-Performance Electrochemical Capacitors. *Nano Letters* **2011**, *11* (7), 2905-2911.
152. Chen, S.; Zhu, J.; Wu, X.; Han, Q.; Wang, X. Graphene Oxide–MnO₂ Nanocomposites for Supercapacitors. *ACS Nano* **2010**, *4* (5), 2822-2830.
153. Wu, Z.-S.; Ren, W.; Wang, D.-W.; Li, F.; Liu, B.; Cheng, H.-M. High-Energy MnO₂ Nanowire/Graphene and Graphene Asymmetric Electrochemical Capacitors. *ACS Nano* **2010**, *4* (10), 5835-5842.
154. Hu, L.; Chen, W.; Xie, X.; Liu, N.; Yang, Y.; Wu, H.; Yao, Y.; Pasta, M.; Alshareef, H. N.; Cui, Y. Symmetrical MnO₂–Carbon Nanotube–Textile Nanostructures for Wearable Pseudocapacitors with High Mass Loading. *ACS Nano* **2011**, *5* (11), 8904-8913.
155. Yuan, L.; Lu, X.-H.; Xiao, X.; Zhai, T.; Dai, J.; Zhang, F.; Hu, B.; Wang, X.; Gong, L.; Chen, J.; Hu, C.; Tong, Y.; Zhou, J.; Wang, Z. L. Flexible Solid-State Supercapacitors Based on Carbon Nanoparticles/MnO₂ Nanorods Hybrid Structure. *ACS Nano* **2011**, *6* (1), 656-661.
156. Masarapu, C.; Zeng, H. F.; Hung, K. H.; Wei, B. Effect of Temperature on the Capacitance of Carbon Nanotube Supercapacitors. *ACS Nano* **2009**, *3* (8), 2199-2206.
157. Hu, C.-C.; Chang, K.-H.; Lin, M.-C.; Wu, Y.-T. Design and Tailoring of the Nanotubular Arrayed Architecture of Hydrous RuO₂ for Next Generation Supercapacitors. *Nano Letters* **2006**, *6* (12), 2690-2695.

158. Yu, Z.; Zinger, D.; Bose, A. An innovative optimal power allocation strategy for fuel cell, battery and supercapacitor hybrid electric vehicle. *Journal of Power Sources* **2011**, *196* (4), 2351-2359.
159. Thounthong, P.; Raël, S.; Davat, B. Energy management of fuel cell/battery/supercapacitor hybrid power source for vehicle applications. *Journal of Power Sources* **2009**, *193* (1), 376-385.
160. Sunand Santhanagopalan, A. B., Evan Lucas, Franco Marcano, Dennis Meng High Voltage Electrophoretic Deposition of Aligned Nanoforests for Scalable Nanomanufacturing of Electrochemical Energy Storage Devices. *Key Engineering Materials* **2012**, *507*, 67-72.
161. Bonard, J.-M.; Kind, H.; Stöckli, T.; Nilsson, L.-O. Field emission from carbon nanotubes: the first five years. *Solid-State Electronics* **2001**, *45* (6), 893-914.
162. Nakayama, Y.; Akita, S. Field-emission device with carbon nanotubes for a flat panel display. *Synthetic Metals* **2001**, *117* (1-3), 207-210.
163. Oh, S. J.; Zhang, J.; Cheng, Y.; Shimoda, H.; Zhou, O. Liquid-phase fabrication of patterned carbon nanotube field emission cathodes. *Applied Physics Letters* **2004**, *84* (19), 3738-3740.
164. Fan, S.; Chapline, M. G.; Franklin, N. R.; Tomblor, T. W.; Cassell, A. M.; Dai, H. Self-Oriented Regular Arrays of Carbon Nanotubes and Their Field Emission Properties. *Science* **1999**, *283* (5401), 512-514.
165. Ma, H.; Zhang, L.; Zhang, J.; Zhang, L.; Yao, N.; Zhang, B. Electron field emission properties of carbon nanotubes-deposited flexible film. *Applied Surface Science* **2005**, *251* (1-4), 258-261.
166. Wang, Z.; Liu, J.; Liang, Q.; Wang, Y.; Luo, G. Carbon nanotube-modified electrodes for the simultaneous determination of dopamine and ascorbic acid. *Analyst* **2002**, *127* (5), 653-658.
167. de Toledo, R. A.; Santos, M. C.; Cavaleiro, E. T.; Mazo, L. H. Determination of dopamine in synthetic cerebrospinal fluid by SWV with a graphite-polyurethane composite electrode. *Analytical and bioanalytical chemistry* **2005**, *381* (6), 1161-6.
168. Minnikanti, S.; Skeath, P.; Peixoto, N. Electrochemical characterization of multi-walled carbon nanotube coated electrodes for biological applications. *Carbon* **2009**, *47* (3), 884-893.
169. Minnikanti, S.; Peixoto, *Implantable Electrodes with Carbon Nanotube Coatings*. 2011.

170. Heim, M.; Yvert, B.; Kuhn, A. Nanostructuration strategies to enhance microelectrode array (MEA) performance for neuronal recording and stimulation. *Journal of physiology, Paris* **2012**, *106* (3-4), 137-45.
171. Rolison, D. R.; Long, J. W.; Lytle, J. C.; Fischer, A. E.; Rhodes, C. P.; McEvoy, T. M.; Bourg, M. E.; Lubers, A. M. Multifunctional 3D nanoarchitectures for energy storage and conversion. *Chem Soc Rev* **2009**, *38* (1), 226-52.
172. Sun, W.; Chen, X. Fabrication and tests of a novel three dimensional micro supercapacitor. *Microelectronic Engineering* **2009**, *86* (4-6), 1307-1310.
173. Sun, W.; Zheng, R.; Chen, X. Symmetric redox supercapacitor based on micro-fabrication with three-dimensional polypyrrole electrodes. *Journal of Power Sources* **2010**, *195* (20), 7120-7125.
174. Liang, S. H.; Teng, F.; Bulgan, G.; Zong, R. L.; Zhu, Y. F. Effect of phase structure of MnO₂ nanorod catalyst on the activity for CO oxidation. *J. Phys. Chem. C* **2008**, *112* (14), 5307-5315.
175. Du, C.; Pan, N. High power density supercapacitor electrodes of carbon nanotube films by electrophoretic deposition. *Nanotechnology* **2006**, *17* (21), 5314.

Appendix A: Water based HVEPD*

A1. Introduction

The advent of carbon nanotubes (CNTs) has brought forth new possibilities in the field of electronics and microelectromechanical systems (MEMS). The excellent electrical properties possessed by CNTs have made them attractive electrode materials for powerMEMS devices. Due to their anisotropic electrical conductivity, CNTs vertically-aligned on the substrate usually exhibit enhanced electrical properties. Traditionally, these VACNT forests are prepared by catalytic-chemical vapor deposition (CVD) method under a process temperature of 700-1000°C. Since such a high temperature is incompatible with the manufacturing process of integrated circuits (IC) and MEMS,⁴³ its on-chip integration capability and application in powerMEMS are seriously limited. Attempts have been carried out to align CNTs vertically using chemical techniques,⁴⁵ magnetic fields,⁴⁶ filtration through hydrophilic membrane,²⁴ and electrophoretic deposition (EPD) in nanopores.¹⁶² However, most of the methods have faced problems like bundle formation and/or lack of good alignment. There are still significant challenges to achieve well-separated, dense array of VACNTs with room-temperature post-growth deposition methods.

EPD is a simple, room-temperature deposition process, which uses an electric field to move charged particles in a suspension and deposit them as thin films.⁴⁴ While high voltage is shown to achieve such alignment, bundles instead of separated CNTs were obtained.⁷⁰ It has also been suggested that CNTs align themselves along the electric field

* The material contained in this chapter was previously published in the PowerMEMS 2009 conference Proceedings. (Reprinted with permission from Santhanagopalan, S.; Teng, F.; Meng, D. D. In *IC-Compatible Deposition of Vertically-Aligned CNT Forests for Micro-Supercapacitors*, Proceedings of the 9th Power MEMS International Workshop, Washington DC, USA, December 1-4; Washington DC, USA, 2009; pp 593-596. Copyright 2009, PowerMEMS.)

direction during the EPD process, but usually do not maintain the vertical orientation after removal of the field.⁷⁰

In this work, we demonstrate HVEPD to align individual MWCNTs while simultaneously forming a holding layer to preserve the vertical orientation. The goal is to find the appropriate concentrations of metallic salt and MWCNTs as well as suitable voltage and time of deposition such that a holding layer can be simultaneously deposited during the HVEPD process due to the disassociation of the metallic salt into ions. At the same time, the concentration of MWCNTs is appropriately lowered so that bundle formation can be avoided. The HVEPD-deposited VACNT forest is also employed as the electrodes of a micro-supercapacitor³⁶ to demonstrate its potential applications.

A2. Experimental Methods

In this study, vertically-aligned MWCNTs were obtained using a single-step process of HVEPD with the formation of a holding layer, which is schematically shown in Fig. 1.

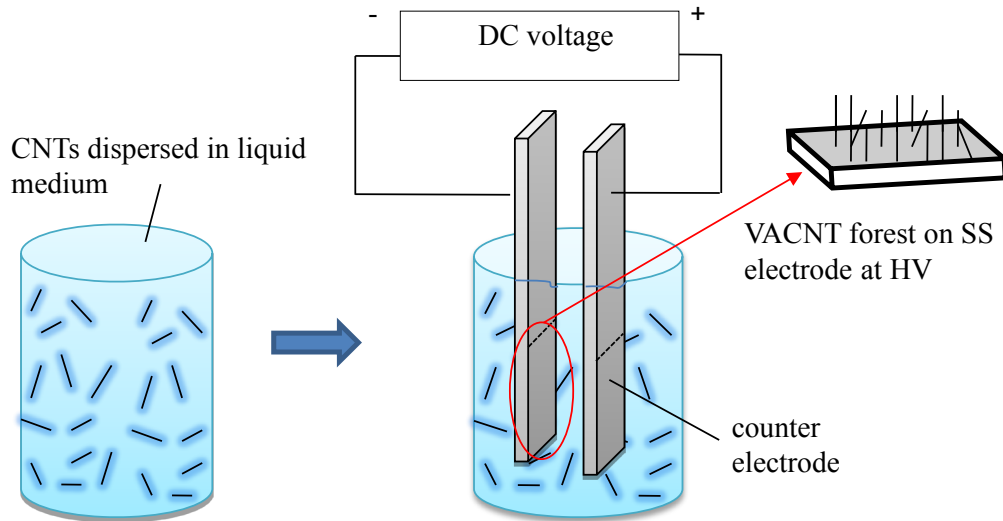


Figure A1. Schematic of HVEPD process for VACNT.

A stable dispersion of MWCNTs in distilled water was prepared by sonication for 30 minutes. $\text{Mg}(\text{NO}_3)_2$ salt was then added to this dispersion which was sonicated again

for 15 minutes. The salt will render positive charge to the dispersed MWCNTs and facilitate their deposition on the cathode under suitable voltage. Stainless steel electrodes with an exposed area of $2.54 \times 2.54 \text{ cm}^2$ were used in the electrodeposition cell with an electrode gap of 7 mm. Care was taken that the electrodes were parallel to each other. The DC voltage was then applied for specific times to deposit VACNT forests on the cathode. VACNT forests were obtained when a voltage of 150 V was applied for 1 min, with the concentrations for MWCNTs and Mg salt set at 0.125 mg/ml and 0.075 mg/ml respectively, which were maintained for the control experiments. A set of control experiments for different times of deposition, voltages and concentrations of Mg salt were performed and investigated to understand the deposition phenomena better. After deposition, the samples were dried under room temperature in a desiccator for 24 hrs.

The MWNTs were purchased from MER Corporation with a diameter of $140 \pm 30 \text{ nm}$ and a length of $7 \pm 5 \text{ }\mu\text{m}$. The sonication was carried out by a probe sonicator in pulse mode (30 sec. live and 10 sec. dead time). Scanning electron microscope (SEM) images were taken with a Hitachi S-4700 FESEM at 5 kV.

The contact resistance of the deposited films was also measured to ascertain that the MWCNTs were in contact with the steel substrate. A micro-supercapacitor, as shown in Fig. 2, is assembled by employing the VACNT samples as electrodes. Cyclic voltammetry was carried out for a two-electrode device with a $50 \text{ }\mu\text{m}$ spacer in a 2M KCl aqueous solution as the electrolyte.

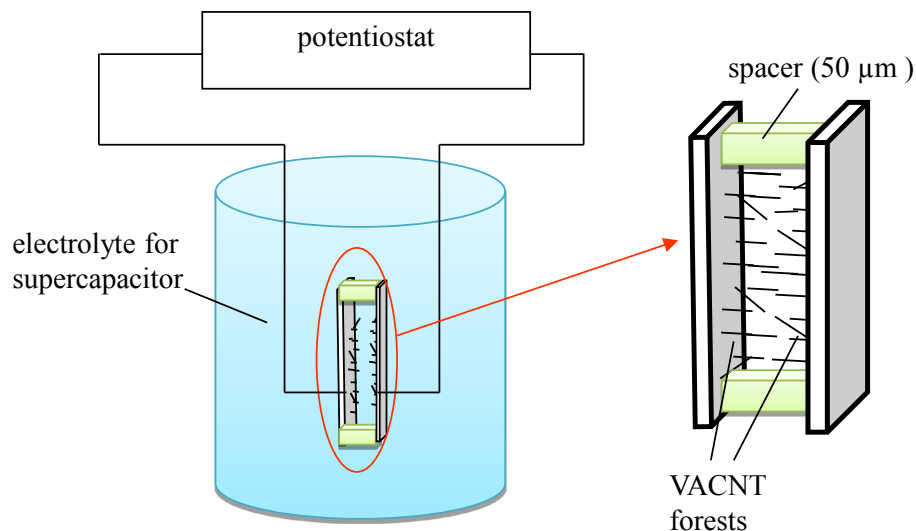


Figure A2. Setup to test the electrochemical properties of the obtained VACNT forest for its application in micro-supercapacitor.

A3. Results and Discussions

A key technology to hold the HVEPD-deposited VACNTs in the desired position/orientation is the simultaneous deposition of a holding layer. Usually, $\text{Mg}(\text{NO}_3)_2$ salt is added to the dispersion to render charges to the MWCNTs because the latter can adsorb Mg^+ ions to form an electric double layer around their surface so that they can be moved when a voltage is applied. However, this additive can also form a holding layer due to the reaction between the Mg^+ ions and the OH^- ions at the cathode. The simultaneous formation of a holding layer during the EPD process and its composition was determined by using the electron dispersive spectrum (EDS) of a JEOL, JSM-6400 SEM. Fig. 3 shows the EDS spectrum of such layer formed during the deposition of MWCNTs. The atomic percentage of magnesium and oxygen are in a 1:1 ratio which confirmed the formation of an MgO holding layer.

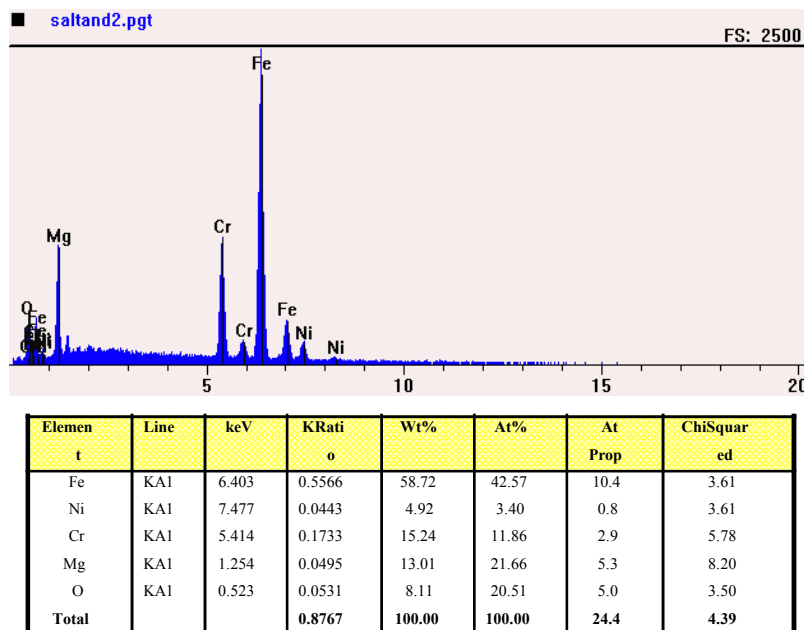


Figure A3. EDS spectrum of holding layer determining its composition to be MgO.

The dispersions formed with the salt being stable for a few days until settling-down of the CNTs was observed. The positive charges due to the absorption of Mg^+ ions cause cathodic deposition of the CNTs with the simultaneous deposition of $\text{Mg}(\text{OH})_2$ which on drying, forms a strong MgO holding layer. Alignment of the CNTs though, is only achieved at high voltages.

SEM images in Fig. 4 show the comparison between HVEPD (a-c), traditional EPD at 25 V for 2 mins (d-f) and a film formed by evaporating a drop of the dispersion placed on the SS substrate (g-i). Under high voltage of HVEPD, the VACNT forests show well-separated individual MWCNTs with fairly uniform, vertical orientation which has seldom been achieved by other post-growth techniques in earlier works. By contrast, the control experiments (d-i) did not yield any vertically aligned nanotubes, but instead displayed a film of laying-down CNTs. We thus ruled out the possibility that such VACNT forest can be formed in random deposition.

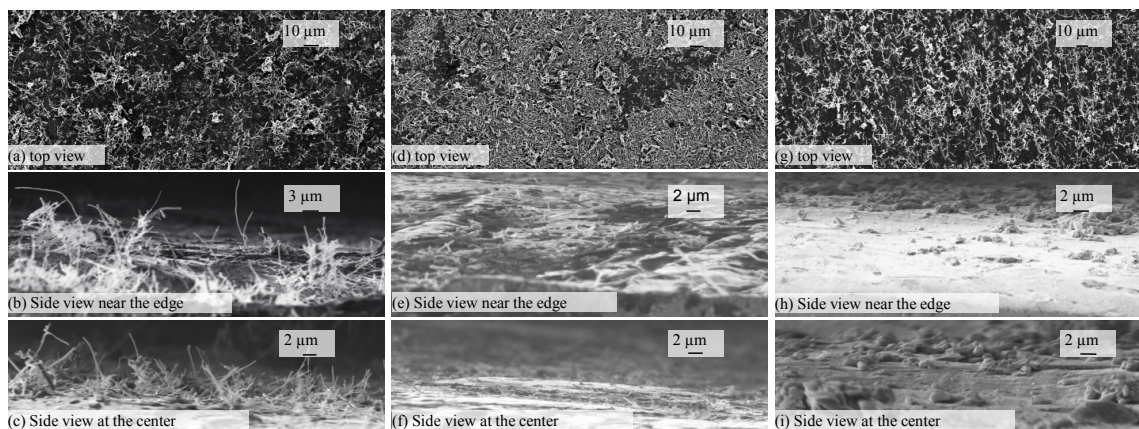


Figure A4. SEM images of the VACNT forests (a-c) and the control experiments (d-i).

A3.1. Effect of concentration of CNTs and salt

The effect of concentration of both CNTs and salt in the dispersion was investigated during this work. The use of highly-concentrated CNTs caused over-deposition, bundle formation and reduction in the possibility of alignment even under high voltages. During the EPD process, the speed in which the CNTs reach the electrode surface and their flux play important roles. With a higher concentration, more number of nanotubes may be accelerated towards the surface, with layers of CNTs pushing the layers before them. This may result in forming a film of randomly oriented nanotubes which are not vertically aligned. It was observed that reducing the concentration of nanotubes can lead to good separation and moderate density.

If the concentration of the salt is too high, a very thick MgO layer will be formed to bury the CNTs. On the other hand, if the concentration of the salt is too low, it cannot form a uniform MgO layer with enough thickness to hold the CNTs in their aligned position.

A3.2. Effect of voltage and time of deposition

During the trial experiments, it was observed that only high voltage can align the CNTs along the direction of electrical field. At lower voltages there was no alignment of CNTs observed. It was previously reported that CNTs can align themselves beyond a

threshold value of electric field ($> 200 \text{ V/cm}$),⁷⁰ below which no alignment had been found. Higher voltages caused too many nanotubes to deposit on the surface and initiate the formation of bundles instead of well-separated CNTs. However, bundle formation can be effectively oppressed by reducing the time of deposition and concentration of CNTs.

It will require further theoretical analysis and experimental confirmation to find out the exact time required for the nanotubes to get aligned and reach the surface as well as the conditions for the formation of a sufficient holding layer. However, it is indeed experimentally observed that neither very short nor very long deposition time can yield desirable VACNT forests with individual CNTs. In the sample after very short deposition time the CNTs didn't show significant amount of vertical CNTs, which can be attributed to the fact that they didn't get enough time to align themselves along the electrical field before reaching the SS substrate. On the other hand, much longer deposition times caused over-deposition to form additional layers of CNTs on top of existing nanotubes. More detailed investigation on the above-mentioned parameters is expected to reveal the optimum conditions under which the VACNTs can be obtained.

A3.3. Electrical and Electrochemical testing

In order to employ the VACNT forests as the electrodes of powerMEMS devices, the electrical conductivity between the VACNTs and the SS substrate is very important because contact resistance will negatively affect the performance of the device. Fig. 5 shows negligible electrical resistance till the distance between the VACNT forest and the testing electrode is smaller than several μm , which confirms the good electrical contact on the interface. Compared with the control samples, the VACNTs stay in contact with the substrate for much longer distance, which further confirmed the vertical alignment of MWCNTs over the whole sample surfaces. In order to further characterize the alignment of VACNT forests and explore their applications, a micro-supercapacitor was prepared with two VACNT-planted SS plates as the electrodes, as schematically shown in Fig. 2. The CV curves for the device are measured and shown in Fig. 6. The specific capacitances of the VACNT forests electrodes and the control samples are calculated

from these curves, by using the relation $C = I / ((dV/dt) \times A)$, where I is the current, dV/dt is the voltage scanning rate, and A is the effective area.

The specific capacitance for the device with VACNTs was found to be $93 \mu\text{F}/\text{cm}^2$, in contrast with the value $1.24 \mu\text{F}/\text{cm}^2$ found for the device with laying down MWCNTs and MgO holding layer deposited by traditional EPD.

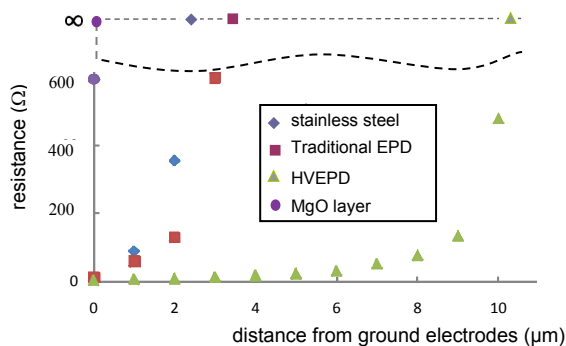


Figure A5. Electrical resistance vs distance from a reference steel plate.

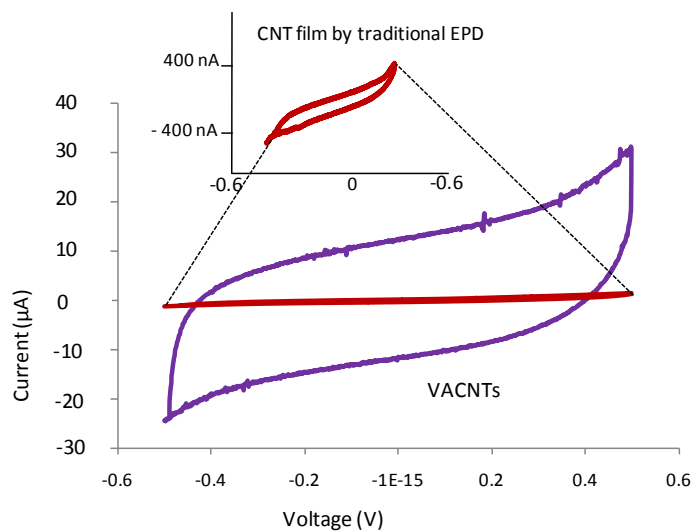


Figure A6. Cyclic Voltammetry (C-V) curves of devices prepared by the VACNT forest and control samples.

A4. Conclusions

HVEPD has been developed as a single-step, post-growth deposition method to form VACNT forests with well-separated, moderately-dense MWCNTs. The technique proposed herein is simple, economic, uniform and effective. Low contact resistance and high electrochemical capacitance were obtained, suggesting promising potential to use the obtained substrates for micro-supercapacitors and other powerMEMS devices.

Appendix B: Supporting Information for Chapter 3*

B1. Characterization of as-purchased multi-walled carbon nanotubes

The as-purchased multi-walled carbon nanotubes (MWCNTs) (MER Corporation, Arizona) were reported to have a diameter of 140 ± 30 nm and a length of 7 ± 5 μm . We checked these dimensions by visualizing the nanotubes using scanning electron microscopy. The as-purchased MWCNT were first dispersed in acetone by sonication. An adequate amount of the stable dispersion was then placed on a substrate and the acetone was left to evaporate. The dried substrate with MWCNTs was then observed under a Hitachi 6400 FESEM. Figure B1 shows the FESEM image of the as-purchased MWCNTs. The dimensions were verified to be as reported by the supplier. It was also observed that the CNTs were neither absolutely straight nor rigid.

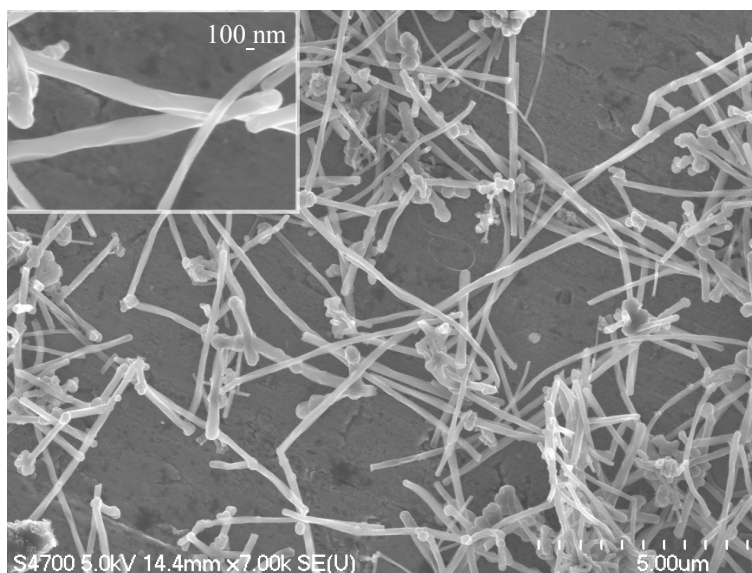


Figure B1. FESEM image of the as-purchased MWCNTs

* The material contained in this chapter was previously published in *Langmuir*. (Reprinted with permission from Santhanagopalan, S.; Teng, F.; Meng, D. D., *Langmuir* 2010, 27 (2), 561-569. Copyright 2010, American Chemical Society.)

B2. Preparation and characterization of β -MnO₂ nanorods

All the chemicals used in the experiments are analytic grade and used as purchased. The β -MnO₂ nanorods were prepared by a previously reported technique¹⁷⁴. Typically, 0.28 g of KMnO₄ and 0.45 g of MnSO₄·H₂O were dissolved in 40 mL deionized water and magnetically stirred for about 10 min to form a homogeneous solution. Then, the solution was transferred into a Teflon-lined stainless steel autoclave and kept at 160 °C for 12 h. The product was collected by centrifugation, washed and then dried at 80 °C overnight. FESEM images were taken to observe the morphology and size of the as-prepared nanorods, as shown in Figure B2a, the nanorods are estimated to have a length of 2-5 μ m and a diameter of about 50 nm. The phase compositions of the samples were characterized by an X-ray powder diffractometer (XRD, Rigaku D/MAX-RB), using graphite monochromatized Cu K α radiation (λ = 0.154 nm) and 50mA. The XRD patterns obtained in the range of 10-70° (2 θ) at a scanning rate of 5 ° min⁻¹, is shown in Figure B2b. All the diffraction peaks can be well indexed to pure β -MnO₂ crystals (JCPDS 24-0735). The sample is of high purity and in good crystallinity.

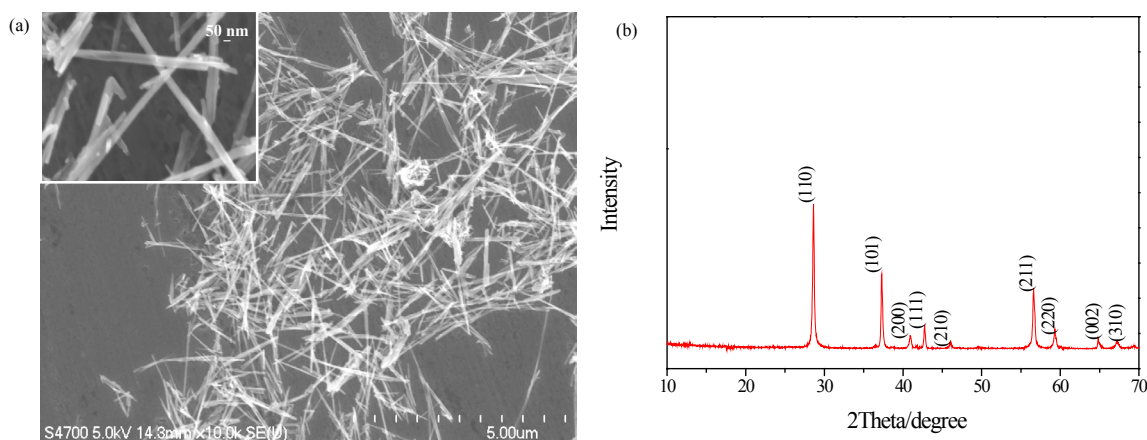


Figure B2. FESEM image (a) and XRD pattern of the as-prepared β -MnO₂ nanorods

B3. Variation of deposition voltage

The FESEM images for the deposition at the voltages of 30V, 60V, 120V and 180V are shown below. Alignment was first observed at 120V and there was cluster formation at 180V. Lower voltages of 30V and 60V did not produce the desired alignment.

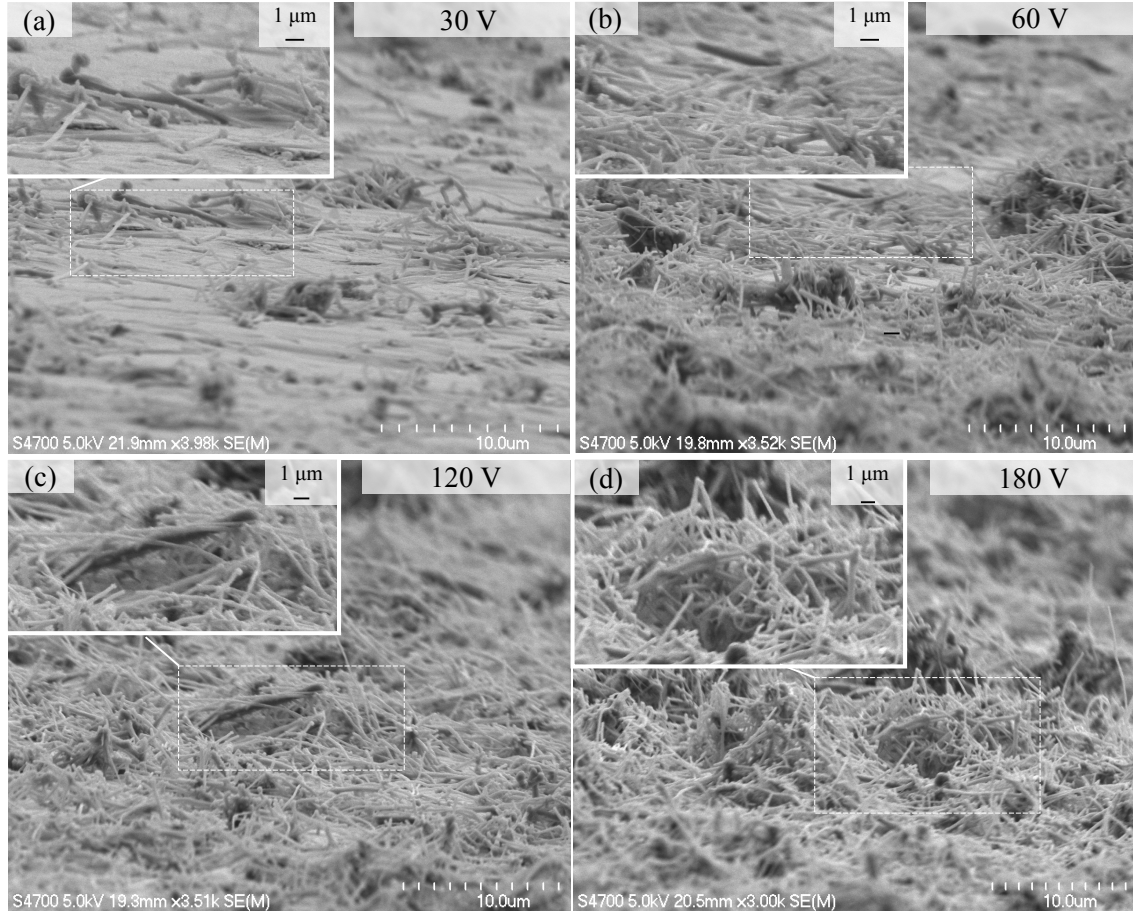


Figure B3. FESEM images of deposited sample under varied voltage

Calculation of critical alignment voltage: the voltage at which alignment of CNTs is achieved by overcoming the Brownian disturbance can be theoretically deduced by calculating the dimensionless ratio suggested by Han and Yang⁷¹:

$$m_i = \frac{\Delta\alpha \cdot E^2}{2k_B \cdot T} \quad (B1),$$

$$\text{where:} \quad \Delta\alpha = \alpha_T - \alpha_L = \frac{4\pi D_e L^3}{3} \chi^2 \quad (B2),$$

and E , k_B and T represent the electric field, the Boltzmann constant and the process temperature respectively. $\Delta\alpha$ is the difference between the transverse and longitudinal components of polarizability tensor, D_e is the dielectric constant of the solvent given by $\epsilon_0 \cdot \epsilon_r$ in which ϵ_0 and ϵ_r are the permittivity of free space and relative permittivity of solvent (IPA) respectively. L is half length and $\chi = r/L$ is the aspect ratio where r is the radius of particle. Since the dimensionless quantity m_i gives the ratio of the effect of electric field potential and the random distribution due to the Brownian motion, we assumed m_i as one to calculate the range of electric field (and voltage $V = dE$) at which the alignment of the CNTs would take place. Therefore, the critical alignment voltage is estimated as:

$$V_{cr} = d \cdot \sqrt{\frac{3K_B T}{2\pi\epsilon_0\epsilon_r} \cdot \frac{1}{L \cdot r^2}} \quad (3.4).$$

Following are the dimensional data of the MWCNTs given by the provider:

$$L=1\text{-}6 \mu\text{m}, r = 55\text{-}85 \text{ nm and } \chi = r/L = 0.055 - 0.014,$$

using physical constants:

$$D_e = \epsilon_0 \cdot \epsilon_r = 1.62 \times 10^{-10} \text{ F/m}, k_B = 1.38 \times 10^{-23} \text{ J/K and } T = 293 \text{ K},$$

the range of MWCNT alignment voltage can be calculated by equation 3 as 120 – 440 V.

Considering that the electrode gap is $d = 7 \text{ mm}$, the range of electric field is estimated as $E = 18 - 63 \text{ kV/m}$.

B4. Variation of deposition time

The FESEM images of the samples after being deposited for 35 seconds and 85 seconds are shown below. Little alignment can be seen when the deposition time was set as 35 seconds, indicating that the thickness of the $\text{Mg}(\text{OH})_2$ layer is not enough to hold nanotubes even if they are aligned to the desired orientation. Longer deposition time of 85 seconds showed distortion of alignment and cluster formation possibly caused by over deposition on top of an initial layer of aligned nanoforest.

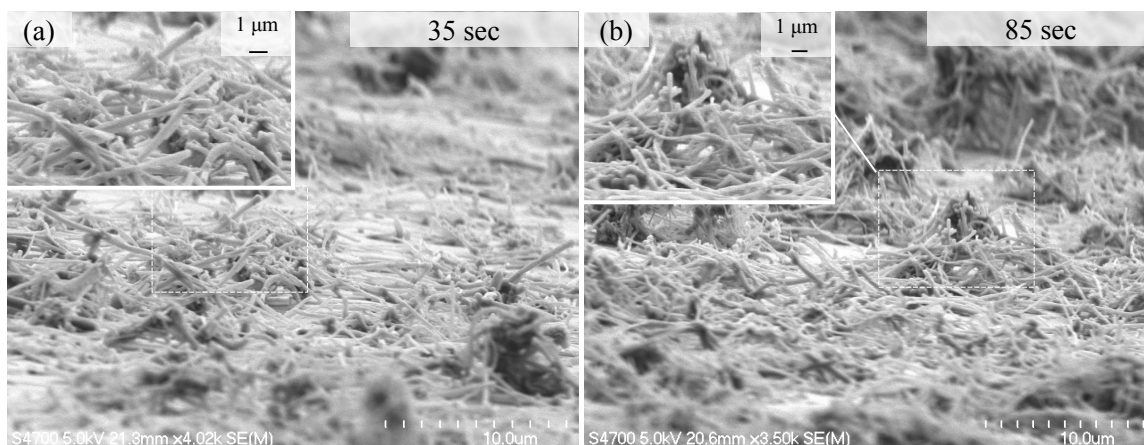


Figure B4. FESEM images of deposited sample with varied deposition time

B5. Variation of Mg salt concentration

The FESEM images below reveal the role of the holding layer which is determined by the concentration of its precursor. $\text{Mg}(\text{NO}_3)_2 \cdot 6\text{H}_2\text{O}$ was dispersed in IPA and electrochemically deposited on to stainless steel (SS) plate electrodes with same deposition parameters as used in the HVEPD process. The FESEM images show a continuous and relatively uniform layer being formed when the concentration used was 0.025 mg/ml (a). The thickness was measured as 300-400nm by a profilometer. In contrast, when a low concentration of 0.005 mg/ml was used, the layer formed did not cover the whole surface and had pores which could not have held the aligned nanotubes in their desired orientation (b). It is therefore confirmed that the layer formed with low-concentration Mg salt is not enough to hold the aligned nanoforests.

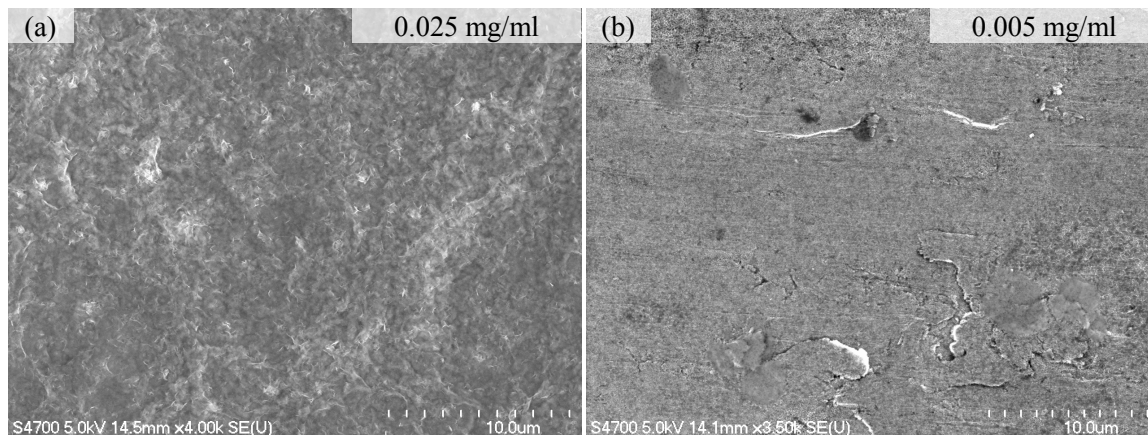


Figure B5. FESEM images shows the morphology of holding layer deposited with salt solution of different concentrations

B6. Electrical contact measurements - setup for electrical bridging method and results of linear sweep to measure electric resistance while contacting

Figure B6a shows the setup to measure the electrical contact to a parallel-plate reference electrode with increasing gap to confirm the alignment, a method named as electrical bridging. The substrates with the aligned CNT forest (ACNT forest) and horizontal CNT film were initially brought into contact with a bare SS plate as the reference electrode. They were then separated slowly in steps of 1 μm while measuring the electrical resistance until the measured value became infinity, indicating that the contact was completely lost.

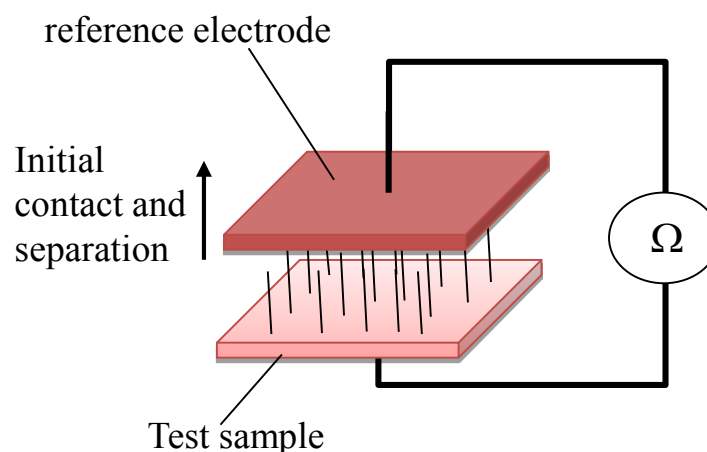


Figure B6a. The setup of electrical bridging method for verification of vertical alignment.

The current – potential (I-V) curves, shown in Figure B6b, were measured by using a potentiostat (Princeton Applied Research, Tennessee) while keeping the sample in complete contact with a reference electrode to check the contact resistance. A linear response was observed indicating ohmic contact between the CNTs and the conductive SS substrate. It can be confirmed that a significant amount of the CNTs are electrically connected to the substrate in both cases. Based on the slope of the curves, the resistance could be estimated to be about 6 Ω for the aligned CNT forest and about 12 Ω for the horizontal CNT film. Compared with the horizontal CNT film, the aligned CNT forest shows a lower resistance which can be understood as a result of the following factors: more intimate contact between the CNTs and the substrate under the effect of higher deposition voltage and less drag from the liquid and holding layer due to their aligned orientation; aligned CNTs tend to be connected to the substrate directly instead of through other CNTs laying beneath them and better electrical conductivity along the axis of CNTs.

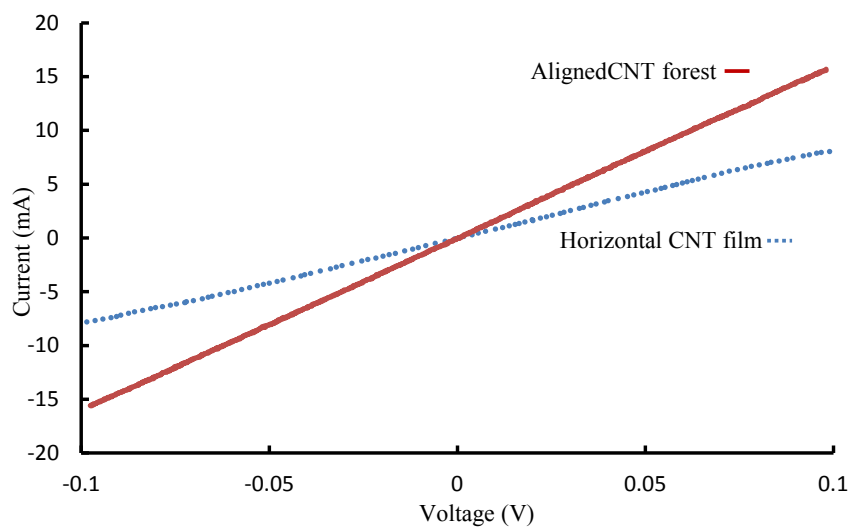


Figure B6b. I-V curves to characterize the electric resistance

B7. Setup for electrochemical characterization

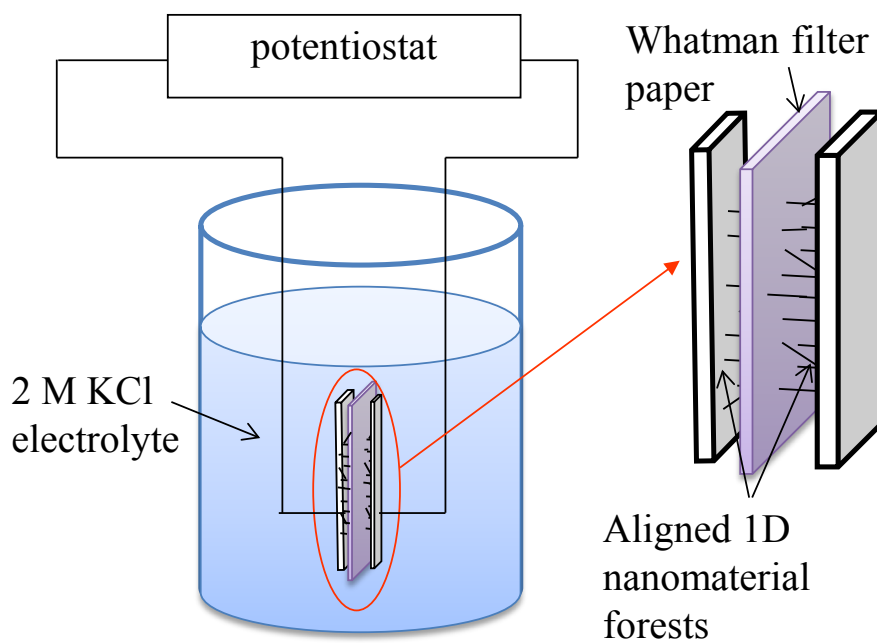


Figure B7. Schematic of the setup used for electrochemical characterization.

B8. Cyclic voltammograms of MWCNT-deposited samples

We used the same potentiostat as mentioned in SI 5 to perform CV on both the horizontal CNT film obtained by LVEPD and the aligned CNT forest obtained by HVEPD. The electrochemical cells were cycled for about 100 times to allow for stabilization before the final curves were taken. The deviation from rectangularity in the curves was mainly due to two reasons, *viz.* the contact resistance between the CNTs and the substrates which caused the slope in the central section of the curve and the impurity of the MWCNTs being used, which caused the excess current at the voltage extremities. It is understood that the use of refluxed CNTs would be more advisable for applications such as supercapacitors.¹⁷⁵ Processes like HVEPD with a conductive holding layer and annealing will be explored to reduce the contact resistance of the aligned CNT forest. The sample with the aligned CNT forest, though, displays a significantly higher capacitance than the horizontal CNT film which indicates the alignment over the surface. This shows that the HVEPD process can be used to achieve good alignment over the surface which opens up new possibilities for various applications.

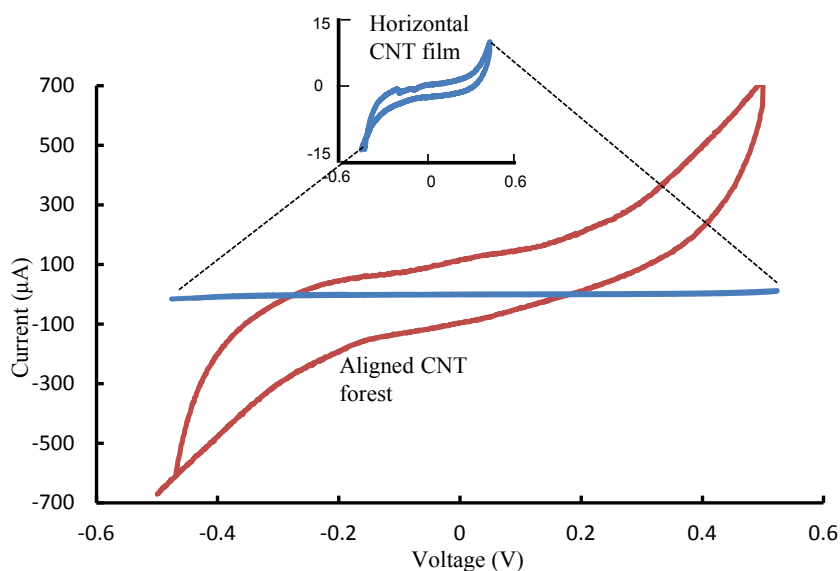


Figure B8. CV curves of horizontal CNT film obtained by LVEPD and the aligned CNT forest obtained by HVEPD

B9. Cyclic voltammograms of nanorod-deposited samples

A similar setup as used for the electrochemical testing of MWCNT-deposited samples, as mentioned in Appendix B6 was used to check the electrochemical characteristics of the deposited MnO₂ nanorod films. MnO₂ stores energy by means of redox reactions which can be characterized as pseudo-capacitance. Therefore, the curves obtained are not supposed to resemble a rectangle as in the case of the CNTs. The measured cyclic voltammograms were the stabilized readings taken after being cycled for about 200 times. The aligned MnO₂-nanorod forests showed a significantly higher capacitance than the horizontal MnO₂-nanorod film, indicating good alignment over the surface of the substrate and larger exposed area. This confirms that the proposed HVEPD method can be used to successfully align different kinds of nanomaterials.

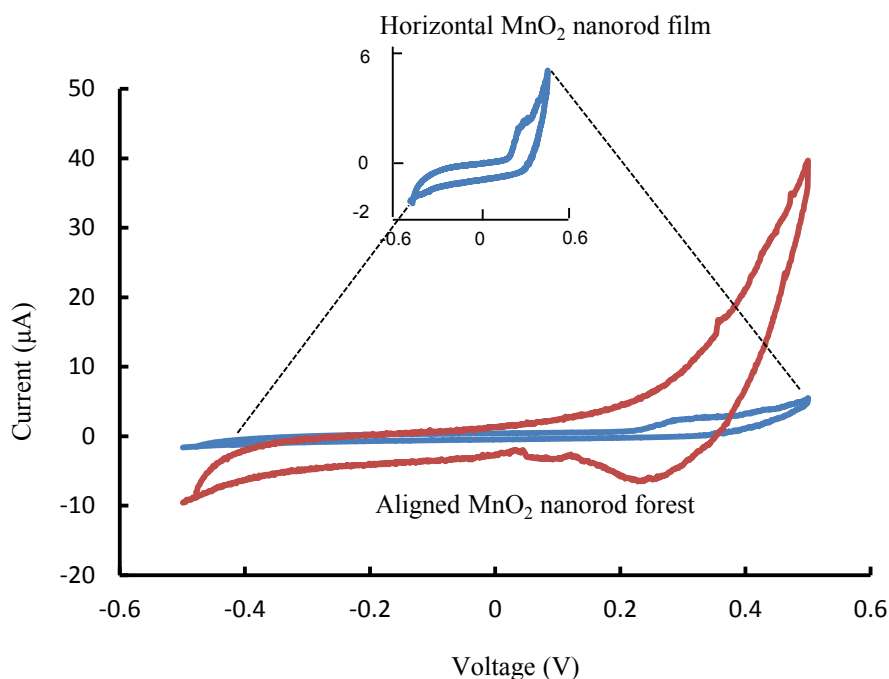


Figure B9. CV curves for EPD of MnO₂ nanorods

Appendix C. Continuous roll printing setup

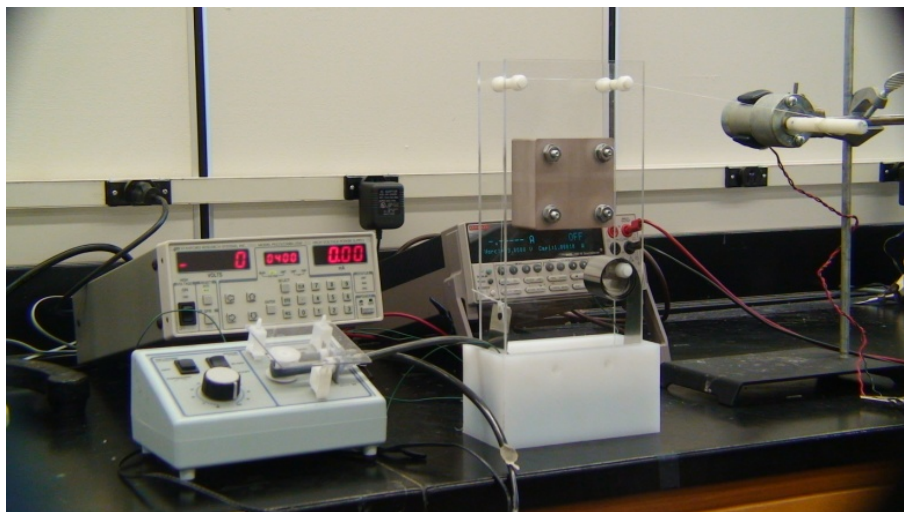


Figure C1. Setup for continuous HVEPD

Appendix D. Copyright Permissions

D1. Copyright Permission for Figure 1.1.

11/19/13

Michigan Technological University Mail - Copyright Permission Request



Sunand Santhanagopalan <ssanthan@mtu.edu>

Copyright Permission Request

2 messages

Sunand Santhanagopalan <ssanthan@mtu.edu>
To: office@woodbank.com

Tue, Nov 19, 2013 at 8:24 PM

Hello,

I am a doctoral candidate studying at Michigan Technological University, 1400 Townsend Drive Houghton, Michigan 49931-1295.

I would like to request copyright permissions for the figure labelled 'Ragone plot of electrochemical devices' as seen on the webpage "<http://www.mpoweruk.com/performance.htm>", for use in the introduction section of my dissertation.

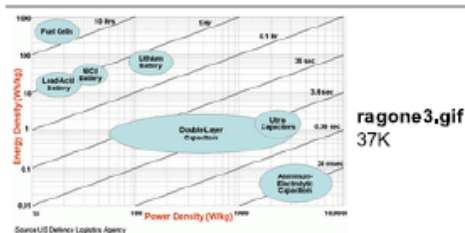
I have attached the figure with this email for your reference.

My dissertation is titled "High voltage electrophoretic deposition for electrochemical energy storage and other applications". As mentioned above, I would like to use the figure in the introduction section of the dissertation as part of a brief discussion on electrochemical devices.

I have referenced the figure using the link "<http://www.mpoweruk.com/performance.htm>" in the current draft of my dissertation. Please let me know if I could use the figure and would you like it to be referenced in any other way.

Thank you.

—
Sunand Santhanagopalan
Doctoral Candidate
MuSES lab, MEEM
Michigan Technological University



Barrie Lawson <bl@woodbank.com>
To: Sunand Santhanagopalan <ssanthan@mtu.edu>

Tue, Nov 19, 2013 at 9:22 PM

Sunand

Thank you for your email.

<https://mail.google.com/mail/u/0/?ui=2&ik=00ed451fe7&view=pt&search=inbox&th=142731b5719c21e>

1/2

11/19/13

Michigan Technological University Mail • Copyright Permission Request

Yes you may use any of the information you wish from the Electropaedia web site as indicated on the home page.

Your proposed acknowledgement is fine.

Thank you for your interest in the Electropaedia and good luck with your project.

Barrie Lawson

From: Sunand Santhanagopalan [mailto:ssanthan@mtu.edu]

Sent: 20 November 2013 01:24

To: office@woodbank.com

Subject: Copyright Permission Request

[Quoted text hidden]

Electropaedia

Battery and Energy Technologies

[Home](#)
[Help Lines](#)
[Energy Sources](#)
[Energy Storage](#)
[Applications](#)
[History](#)
[Search](#)
[About Us](#)
[Contacts](#)

Finding your Way Around

Smart Phone / Tablet Users
See [Alternative Navigation](#) Below

Sponsors



Battery Performance Improvement by Electronic Means

AdChoices

► [Battery Solar](#)
► [Energy Companies](#)
► [Battery Charge](#)
Free Report
[Buying Batteries in China](#)

Electropaedia Pages

Alphabetical Index

[About Us](#)
[AC Batteries](#)
[AC Motors](#)
[Alkaline Batteries](#)
[Alternative Energy Storage Methods](#)
[Authentication and Identification](#)
[Battery Applications](#)
[Battery Comparison Chart \(PDF\)](#)
[Battery Life \(and Death\)](#)
[Battery Management Systems \(BMS\)](#)

The Electropaedia

What is on this site ?

The site provides a comprehensive knowledge base about energy supply and battery technologies, battery applications, chargers and ancillary equipment.

It contains over 140 web pages of information and explanations, many of which are the equivalent of several A4 pages long.

It also contains a History of Technology (with a special mention of batteries of course) [Site Map](#)

Who is it for ?

It should be useful to educators, product designers, battery applications engineers, electric traction specialists and energy systems buyers and planners.

[Beginners Page](#) (For students)

This is not a trading site. We do not buy or sell anything on this web site.

Electrical Energy Sources

Sustainable Development ?
Electric power generation and energy supply technologies.

The engineering without the politics

[Energy Supply Overview](#)
[Energy Resources](#)
[Energy Consumption](#)
[Energy Efficiency](#)
[Energy from Fossil Fuels](#)
[Energy from Biofuels](#)
[Solar Energy](#)
[Wind Energy](#)
[Nuclear Energy](#)

Economics of some domestic energy capture systems. (The cost of green energy)

- [Solar Thermal](#) (Water heating)
- [Solar Photovoltaic \(PV\)](#) (Electricity generation)
- [Wind Turbines](#)

[Carbon Footprints](#) (A short story)

Electrical Energy Storage

Everything you ever wanted to know about batteries

[Battery Types](#)
[Battery Chemistries](#)
[Battery Performance](#)
[Battery Management Systems](#)
[Battery Manufacturing](#)
[Battery Failure Modes](#)
[Battery Reliability and Warranty Issues](#)
[Battery Chargers](#)
[Battery Glossary](#)
[New Cell Designs and Chemistries](#)

History of Technology

Heros and Villains

Some interesting little known, or long forgotten, facts as well as a few myths about technology developments, the context in which they occurred and the deeds of the many personalities, eccentrics and charlatans involved.

[Technology Timeline](#)
[History of Technology](#)
[Hall of Fame](#)
[Timeline of the Elements](#)

Technologies & Applications

[Energy Alternatives](#)
[Battery Technologies](#)
[Electric Machines](#)
[Semiconductors](#)

Finding Your Way

[Technology Search Engine](#) [Find it Fast](#)
[Frequently Asked Questions - \(FAQ\)](#)
[Site Map](#)

Who Provided the Information ?

The information on this site was made available by **Woodbank Communications** an independent, technology consulting company. The information provided by the company is given freely but limited to what is published here on the site. Hopefully you will find what you want here. More information is added regularly to the site and any contributions or suggestions for improvement you wish to make will be gratefully received. We hope you find it helpful.

This is not a trading site and the company does not solicit sales, nor offer services via this site.

Except for **CHEEV**, **Woodbank Communications** has no business relationship with, or financial interest in, any of the companies whose ads appear on the site. All such ads are selected and administered independently by **Google**.

Use of Information from the Electropaedia Web Site

The copyright of all the pages on the Electropaedia web site belongs to Woodbank Communications Ltd.

You may freely use extracts of the information published here in your own publications or Web sites but only if, in each instance, you prominently acknowledge **Electropaedia** as the source with a link to the web site as follows [www.electropaedia.com](#) or by means of a link directly to the relevant page on the [www.mpoweruk.com](#) domain. If you choose to take advantage of this opportunity we would also expect you to notify us at [admin@woodbank.com](#) where we can find the publication in which the information is used.

You may not use large sections of text or images and pass them off as your own.

D2. Copyright Permission for Chapter 3 and Appendix B

3/11/13

Rightslink® by Copyright Clearance Center



RightsLink®

Home

Create Account

Help



ACS Publications
High quality. High impact.

Title: High-Voltage Electrophoretic Deposition for Vertically Aligned Forests of One-Dimensional Nanoparticles

Author: Sunand Santhanagopalan, Fei Teng, and Dennis D. Meng

Publication: Langmuir

Publisher: American Chemical Society

Date: Jan 1, 2011

Copyright © 2011, American Chemical Society

User ID
Password
<input type="checkbox"/> Enable Auto Login
<input type="button" value="LOGIN"/>
Forgot Password/User ID?
If you're a copyright.com user, you can login to RightsLink using your copyright.com credentials. Already a RightsLink user or want to learn more?

PERMISSION/LICENSE IS GRANTED FOR YOUR ORDER AT NO CHARGE

This type of permission/license, instead of the standard Terms & Conditions, is sent to you because no fee is being charged for your order. Please note the following:

- Permission is granted for your request in both print and electronic formats, and translations.
- If figures and/or tables were requested, they may be adapted or used in part.
- Please print this page for your records and send a copy of it to your publisher/graduate school.
- Appropriate credit for the requested material should be given as follows: "Reprinted (adapted) with permission from (COMPLETE REFERENCE CITATION). Copyright (YEAR) American Chemical Society." Insert appropriate information in place of the capitalized words.
- One-time permission is granted only for the use specified in your request. No additional uses are granted (such as derivative works or other editions). For any other uses, please submit a new request.

BACK

CLOSE WINDOW

Copyright © 2013 [Copyright Clearance Center, Inc.](#) All Rights Reserved. [Privacy statement.](#)
Comments? We would like to hear from you. E-mail us at customer@copyright.com

D3. Copyright Permission for Chapter 4

11/21/13

Michigan Technological University Mail - Request for Copyright Permission for my published paper



Sunand Santhanagopalan <ssanthan@mtu.edu>

Request for Copyright Permission for my published paper

2 messages

Sunand Santhanagopalan <ssanthan@mtu.edu>

Thu, Nov 21, 2013 at 1:19 PM

To: t.wohlbier@ttp.net, info@ttp.net

Hello,

I am a doctoral candidate studying at Michigan Technological University, 1400 Townsend Drive Houghton, Michigan 49931-1295.

I would like to request copyright permissions for the paper titled 'High Voltage Electrophoretic Deposition of Aligned Nanoforests for Scalable Nanomanufacturing of Electrochemical Energy Storage Devices', for use as a chapter of my dissertation.

I am the lead author of the paper and the last author Dennis Desheng Meng is my graduate adviser. The paper was published in Volume 507 of Key Engineering Materials (ISSN1013-9826)

The doi for the paper is [10.4028/www.scientific.net/KEM.507.67](https://doi.org/10.4028/www.scientific.net/KEM.507.67).

The full citation of the paper is 'Sunand Santhanagopalan et al., 2012, Key Engineering Materials, 507, 67'

I conducted this work as part of my PhD research and am writing my dissertation as a collection of articles as is allowed by my university.

My dissertation is titled "High voltage electrophoretic deposition for electrochemical energy storage and other applications". As mentioned above, I would like to use the published article as a chapter in the dissertation as part of my work during my PhD.

Please let me know if this would be possible and if there is anything else required from my end.

Thank you

—

Sunand Santhanagopalan
Doctoral Candidate
MuSES lab, MEEM
Michigan Technological University

Thomas Wohlbiel <t.wohlbier@ttp.net>

Thu, Nov 21, 2013 at 2:27 PM

To: Sunand Santhanagopalan <ssanthan@mtu.edu>

Dear Sunand Santhanagopalan,

Thank you for your email. Yes, this is fine with us.

Best regards,
Thomas Wohlbiel

Thomas Wohlbiel
Director of Publications & CCO

11/21/13

Michigan Technological University Mail - Request for Copyright Permission for my published paper

Trans Tech Publications
105 Springdale Lane
Millersville, PA 17551
U.S.A.

Email: t.wohlbier@ttp.net
Fax: +1 717 872 4327

Trans Tech Publications
Kreuzstr. 10
8635 Zurich-Dumten.
Switzerland

Fax +41 44 922 1033
<http://www.ttp.net>
<http://www.scientific.net>

[Quoted text hidden]

D4. Copyright Permission for Chapter 5

3/11/13

Rightslink® by Copyright Clearance Center



RightsLink®

Home

Create Account

Help



ACS Publications
High quality. High impact.

Title: Scalable High-Power Redox Capacitors with Aligned Nanoforests of Crystalline MnO₂ Nanorods by High Voltage Electrophoretic Deposition

Author: Sunand Santhanagopalan, Anirudh Balram, and Dennis Desheng Meng

Publication: ACS Nano

Publisher: American Chemical Society

Date: Feb 1, 2013

Copyright © 2013, American Chemical Society

User ID
Password
<input type="checkbox"/> Enable Auto Login
<input type="button" value="LOGIN"/>
Forgot Password/User ID?
If you're a copyright.com user, you can login to RightsLink using your copyright.com credentials. Already a RightsLink user or want to learn more?

PERMISSION/LICENSE IS GRANTED FOR YOUR ORDER AT NO CHARGE

This type of permission/license, instead of the standard Terms & Conditions, is sent to you because no fee is being charged for your order. Please note the following:

- Permission is granted for your request in both print and electronic formats, and translations.
- If figures and/or tables were requested, they may be adapted or used in part.
- Please print this page for your records and send a copy of it to your publisher/graduate school.
- Appropriate credit for the requested material should be given as follows: "Reprinted (adapted) with permission from (COMPLETE REFERENCE CITATION). Copyright (YEAR) American Chemical Society." Insert appropriate information in place of the capitalized words.
- One-time permission is granted only for the use specified in your request. No additional uses are granted (such as derivative works or other editions). For any other uses, please submit a new request.

Copyright © 2013 [Copyright Clearance Center, Inc.](#) All Rights Reserved. [Privacy statement.](#)
Comments? We would like to hear from you. E-mail us at customercare@copyright.com

D5. Copyright Permission for Appendix A



Submission Date: 11/26/2013

TRF Permission Number: TR478321-13

Reprint Request Form

Submit by fax to 1-619-232-0799

I am preparing a manuscript that is to be published by: 12/20/2013

The estimated date of publication is 12/20/2013 and the approximate number of page(s): 138

I request permission of TRF to include the following material in this and in all subsequent editions of the publication listed above, including versions made by nonprofit organizations for use of physically handicapped persons, and in all foreign-language translations and other derivative works.

Requesting Publication's Author(s) and/or editor(s): SUNAND SANTHANAGOPALAN

Title of requesting publication: HIGH VOLTAGE ELECTROPHORETIC DEPOSITION FOR ELECTROCHEMICAL ENERGY STORAGE AND OTHER APPLICATIONS

Title, Author(s), Source and year of TRF publication material: IC-COMPATIBLE DEPOSITION OF VERTICALLY-ALIGNED CNT FORESTS FOR MICRO-SUPERCAPACITORS, PROCEEDINGS OF THE 9TH POWERMEMS INTERNATIONAL WORKSHOP; WASHINGTON DC, USA, DECEMBER 1-4; WASHINGTON DC, USA, 2009; pp 593-596. [0-9743611-5-1/PMEMS 2009] 2009.

Data Location:

- A. From page 593, line _____, beginning with the words ABSTRACT to page 596, line _____, ending with the words CONCLUSIONS: ... powerMEMS devices
- B. Figure number 1-6 on page 593-596, { FOR USE AS AN APPENDIX CHAPTER }
- C. Table number - on page -. If necessary, attach continuation sheets.

I have secured agreement for this requested permission from the author(s) of this material as indicated and have appended their approval letter with this form. I have read and accept the conditions for this permission and have attached copies of requested work as stated in the Policy for Grant of Reprint Permission by the Transducer Research Foundation dated August 2005.

Signature: _____ Date: 11/26/2013

Type or Print Name of Signator SUNAND SANTHANAGOPALAN

E-mail address: ssanthan@mtu.edu Fax#: _____

Agreed to, and accepted on behalf of The Transducer Research Foundation by:

TRF Representative: _____ Date: 11/26/13

Transducers Research Foundation
c/o Preferred Meeting Management
307 Laurel Street, San Diego, CA 92101-1630
Phone: 1-619-232-9499 Fax: 1-619-232-0799
info@transducer-research-foundation.org http://www.transducer-research-foundation.org